DYNAMICS OF POLYATOMIC MOLECULES

I. ENHANCEMENT OF VIBRATIONAL MODE MIXING DUE TO INTRAMOLECULAR CONVERSIONS

II. CHEMICAL REACTIONS IN CYCLIC NITRAMINES

CANDEE CAE CHAMBERS

Bachelor of Arts

Illinois College

Jacksonville, Illinois

1990

Submitted to the Faculty of the
Graduate College of the
Oklahoma State University
in partial fulfillment of
the requirements for
the Degree of
DOCTOR OF PHILOSOPHY
July, 1994

DYNAMICS OF POLYATOMIC MOLECULES

I. ENHANCEMENT OF VIBRATIONAL MODE MIXING DUE TO INTRAMOLECULAR CONVERSIONS

II. CHEMICAL REACTIONS IN CYCLIC NITRAMINES

Thesis Approved:

Donald L. Thompson
Thesis Adviser

Leonid M. Raff

Paul Westhaus

J Paul Devlin

Thomas C. Collins
Dean of the Graduate College

ACKNOWLEDGEMENTS

Many people are deserving of thanks for their guidance, advise, instruction, time, support, and encouragement in the last four years. Although I cannot completely express my gratitude, I wish to acknowledge those individuals that have made a difference in one way or another during my graduate study.

I wish to express my sincere appreciation to my research advisor, Professor Donald L. Thompson. He has provided ample resources, without which, this work could not have been conducted. More importantly, he has given me invaluable guidance, advise, and instruction. His methods of allowing the student scientific freedom while providing subtle guidance on occasion has permitted me to grow as much as possible scientifically in the last four years. I am grateful to have had the opportunity to study under him.

Thanks are also due to the members of my committee: Professors Lionel M. Raff, J. Paul Devlin, and Paul A. Westhaus. The time they have invested in my education is sincerely appreciated. Also, I consider myself quite fortunate to have been able to attend courses taught by each of them, as they all are very accomplished instructors.

I would like to extend a special thanks to Tommy Sewell. In the last four years he has been both an educator and, more recently, a collaborator. I have

benefited from many conversations with him concerning the studies of RDX. Additionally, he has provided friendship and advise as "someone who's been there."

There are also a number of postdocs and fellow graduate students with whom I am fortunate to have had the opportunity to interact. I would like to thank Karen Bintz for many scientific conversations and for friendship. I am thankful to have known and worked with Roger Petrin, Alison Marks, Qin Yue, Eric Wallis, Xiaoyan Chang, Marty Perry, and Paul Zahner.

Financial support during my graduate career came primarily from the Army Research Office. Other support has come from an EPSCOR-ARO grant. I would also like to acknowledge support in the form of fellowships from John W. Skinner and Conoco.

At this time I would also like to thank Drs. Don Filson and Robert Evans, members of the chemistry department at Illinois College. They did an excellent job of educating and preparing me for graduate school.

There are a number of others, without whose support, encouragement, laughter, and love, these last few years would have been much more difficult, if not impossible.

My parents, John and Wilma Chambers, cannot be thanked enough for all that they have done for me in the last quarter century. Their delicate balance of support and encouragement combined with being excellent role models in every facet of living has made an invaluable contribution to my education and my life. I am forever grateful for all that they have given me.

I would also like to thank a few other individuals who have enriched my life: Jason Chambers, Cheryl Rayot, Albert and Mary Fontaine, Christine Chambers, Jessica Sparks, and Elmo.

Finally, my deepest thanks go to my husband, Tom. His companionship, love, support, encouragement, and understanding are endless.

TABLE OF CONTENTS

LIST OF TABLES

LIST OF FIGURES

CHAPTER I

INTRODUCTION

The theories and methods of chemical dynamics have been evolving for nearly four centuries.[1] Yet only recently, with the rapidly increasing capabilities of computers have calculations of the magnitude currently being done been possible. This has contributed to the increasing interest in the study of dynamics of polyatomic molecules.

Experimental and theoretical studies are now at the point where intimate details of the dynamics can be observed and understood.[2] This has led to an increased understanding of both macroscopic chemical kinetics and the very basic processes which occur in chemical systems.

Our studies have two main thrusts. One is concerned with the development of theoretical methods for computational simulations and the other is of a more fundamental nature. The two different projects are bound by some common scientific threads.

One of our areas of interest is the study of chemical reactions in large molecules. We have constructed a new, realistic model of hexahydro-1,3,5-trinitro-1,3,5-triazine (RDX). We have compared branching ratios obtained from classical trajectory calculations with experimental observations of branching ratios between two different reaction paths, concerted ring fission and N-N bond fission, in a realistic model of RDX (Chapter VIII). We have also extended what we have

learned about RDX to octahydro-1,3,5,7-tetranitro-1,3,5,7-tetrazine (HMX, Chapter IX). While we have formulated these methods for RDX and HMX, we have also developed and demonstrated methods for treating reactions in complex molecules in general.

As a companion to this study, we computed power spectra of RDX at different energies and initial excitations (Chapter VII). This study includes the effects conformational changes have on intramolecular vibrational relaxation (IVR) on large, isomerizing systems (Chapter V). The power spectral study is what relates the two areas of our studies.

The more fundamental area of our research has several dimensions. This portion of our studies focuses on the fundamental behavior of vibrationally excited large molecules. Many things have been shown to cause mode mixing, the extent of which is important in reaction dynamics. We have come a long ways in our knowledge of IVR. We have studied an important aspect of IVR that has not been fully explored, namely, the influence of barrier crossings.

We show that isomerization barrier crossings lead to broadening of power spectral peaks and hence, an increase in IVR. Furthermore, we show that the broadening is due to two factors: an increase of time spent in the barrier region and mode mixing due to sampling multiple sets of normal modes (Chapters IV and V). As the system isomerizes, it samples intermediate frequencies between the two conformers--this leads to broadening of the spectral peaks. We also find, by making all other things equal (including the time in the barrier region) that there is mode

mixing that occurs due to the repeated sampling of the different sets of normal modes of the two conformers.

We have shown in these studies, as have other researchers, that the broadening of spectral peaks is related to the rate of reaction. We have also shown a quantitative relationship between the rate of reaction and the width of a power spectral peak (Chapter VI).

Intramolecular Vibrational Relaxation (IVR)

The study of intramolecular vibrational relaxation (IVR) has generated much interest in recent years.[3-80] Not only what does or does not lead to increases in the rate of IVR, but also what the consequences are of an enhanced rate of IVR.

It has been shown the greater the rate of intramolecular vibrational energy relaxation, the greater the rate at which phase space is sampled.[3] Additionally, the shape of the potential-energy surface (PES) has been shown to be related to the rate of IVR.[4] The shape of a power spectrum is also an indicator of the topology of the phase space which the trajectories experience.[5]

It has been shown that spectral lines broaden due to an increase in IVR. Hänsel[6] has studied a simple model of anharmonic oscillators using classical trajectories. His results showed "an intramolecular line broadening mechanism due to energy exchange between normal modes." In this study, he compared a stochastic parameter to spectral linewidths. While a quantitative relationship was not found, qualitative agreement was. In other words, the linewidth increased as the stochastic

parameter increased, but no further conclusions could be drawn.

Studies of Pollak and coworkers[36,37] give similar results. They have shown that the widths of spectral peaks are related to stability parameters,[36] but a direct correspondence cannot be drawn.[37] Additionally, they have shown that variations in the peak widths can be related to the regions of phase space which the trajectory visits. The more regular the portion of phase space, the narrower the peak.

Vibrational Bandshapes

Vibrational bandshapes can be affected by a large number of factors.[81-96] Our studies are designed to isolate particular factors which cause changes in the spectra. Factors which can influence the bandshapes and intensities, and methods of determining the true bandshape have been reviewed by Seshadri and Jones.[81] Since our studies focus on changes in vibrational spectra due to molecular isomerization, in this section we review only those studies that pertain to this topic.

In 1964 Eigen[82,83] suggested that very fast reactions may affect vibrational spectra. That is, if reaction is fast enough, vibrational line shapes can be related to reaction rates. Chemical reactions (e.g., conformational changes) are expected to increase broadening of vibrational bands and perhaps cause merging of certain bands in the spectra, much like the effects seen in NMR spectra. Although there is an analogy with NMR, there is a significant difference in time scales. Molecular vibrations times are on the order of subpicoseconds while NMR involves times on the order of 10^{-3} s. Since molecular vibrations are very fast, variations in the spectral

features might be useful for determining the rates for extremely fast chemical reactions. However, the extraction of reaction rates from vibrational spectra is complicated because there are several factors other than reaction (e.g., IVR, pressure broadening, etc.) that can cause spectral broadening, and the time scales for some of these can be on the order of reaction rates.

Wood and Strauss[84] argue that it is difficult to determine the rate of reaction from the broadening of vibrational spectral lines because the time spent in the region of the potential barrier is sufficiently long to cause complications in a simple interpretation of the broadening being due to the frequency of passage over the barrier. Stated differently, the time spent in a well must be greater than the time spent crossing the barrier for a simple, direct relationship between the reaction rate and line broadening. However, observed IR line broadening data have been ascribed to reactions. Kreevoy and coworkers[85-88] have determined reaction rates in this fashion. More recently, Cohen and Weiss[89-94] determined rate constants from broadened IR lines. Weiss[95] did a simulation of a picosecond, bimolecular exchange reaction in solution. He found that a distinction between natural width and exchange broadening is possible, and the chemical exchange can play a very important role in spectral broadening when the barrier is low.

Thus, while it seems reasonable to expect reactions to affect vibrational band widths, and some experiments suggest that rates can be derived from such data, there are obviously complicating factors that obscure the relationship of the rate of reaction and the line widths. It would be useful to have a better understanding of

the various causes of line broadening in polyatomic molecules. Classical trajectories offer an attractive means of doing so since they can be used to examine the various effects that can cause broadening. We have carried out some studies of the effects of transition-state crossings on mode mixing for realistic models of two isolated molecules, HONO and CH_3ONO, which undergo *cis-trans* isomerization.

There have been some previous theoretical studies which pertain to this topic. Jones, Holloway, and Gadzuk[96] used a model Hamiltonian to show that trajectories which cross a saddle-point many times produce broader vibrational spectral lines than trajectories with few crossings.

Internal Rotation and Conformational Analysis

The term "unimolecular chemical reaction" encompasses a wide range of processes from isomerization to unimolecular rearrangements to dissociation. Isomerizations could be thought of as a sort of intermediate between reversible excitations and dissociation,[97] which is usually irreversible. In a dissociation reaction, the energy of activation can be transformed into the kinetic energy of the products, thus usually preventing the return to reactants. The isomerization process, on the other hand, is such that products can return to the initial state. After passing over the isomerization barrier, the molecule still has enough energy to traverse it again. While energy may be transferred to other degrees of freedom, thus inhibiting isomerization, the energy is still present in the molecule and may return to the torsional mode again "activating" the molecule.

Since isomerization is such an important chemical process, the amount of published research on the topic is extensive. Two older, but good reviews on isomerization barriers and conformer energies are those by Mizushima[98,99] and Dykstra;[100] these are experimental and theoretical reviews, respectively.

Another source, which covers details on conformational changes and methods of studying these changes is a book by Orville-Thomas.[101] Included in the methods of analysis are IR and Raman, NMR and ESR, and microwave spectroscopy. Additionally, the calculation of barriers from both torsional frequencies and *ab initio* methods are discussed.

The rate of isomerization and the exploration of phase space in systems with double well potentials has been investigated by De Leon and coworkers[102-107] and Rice and Gray and coworkers.[108-110] Among their findings is when statistical theories are valid in isomerizing species and when they are not as well as characterization of the dynamics in various portions of phase space.

Molecular inversion can occur in any nonplanar molecule. The nature of a molecular inversion can be understood as a process which transforms any equilibrium configuration I into a symmetrically equivalent equilibrium configuration II which cannot be obtained from I by a rigid rotation in space. Configurations I and II are separated by a non-zero energy barrier. The height of the barrier can be determined by the path the molecule moves along during the inversion.

Molecular isomerization, on the other hand, refers to the transformation from any equilibrium configuration I into a non-symmetrically equivalent equilibrium

configuration II. In other words, a change in the molecular arrangement occurs which transforms the molecule from one potential minimum to another. In going from one conformer to another, the molecule must traverse a potential barrier. The energy required to cross the barrier varies greatly; it can be as little as tenths of a kcal/mol to 10^2 kcal/mol.

The isomerization reactions in this study have two minima; the isomerization occurs via the rotation about a bond. *Cis-trans* isomerizations involve two potential minima.

The "reaction" coordinate for a *cis-trans* isomerization, then, is the dihedral angle associated with the rotation about a bond. For instance, given a molecule ABCD, the dihedral angle (defined by the angle made by the normals to the two planes defined by atoms A, B, and C and B, C, and D[111]) allows for the determination of the conformation of the molecule and allows for the monitoring of the reaction from one conformer to the other.

Rings undergo an analogous process which involves interconversion among several configurations. Interconversion from one chair conformation to another chair conformation (for a six-membered ring) involves passage through a transition state, minima for boat and twist-boat conformations, and finally, another transition state.[112] The minimum-energy path involves: Bayer stain (bond angles), Pitzer strain (torsional angles), and interactions between atoms other than those described by the Pitzer and Bayer strains.[112] These three interactions are not always easily separated. By "barrier to ring inversion," what is usually meant is the free-energy difference between a chair

and a half-chair conformation.[112]

Description of RDX and HMX Reaction Studies

The challenge in modeling the chemical dynamics of RDX is the formulation of an accurate potential-energy surface (PES). *Ab initio* methods cannot be used to determine a global potential that includes the reaction channels because of the size of the molecule. Thus, we formulate a surface by making use of available experimental data for the equilibrium reactant and product molecules and by using *ab initio* results when experimental data are not available.

In an earlier study[113] of the unimolecular reaction dynamics of RDX, rates were computed for the ring fission reaction that gives 3 H_2CNNO_2 molecules and the simple N-N bond rupture reaction giving the radicals NO_2 and $C_2H_4N_4O_4$, and the product energy distributions, over the energy range 250-350 kcal/mol. These reaction channels were proposed by Zhao, Hintsa and Lee.[114] They used infrared multiphoton dissociation (IRMPD) in a molecular beam to study RDX. Their results indicate that the ratio of the rate of the molecular elimination reaction to that of the N-N bond rupture reaction is about 2 at a total energy estimated to be in the range 150-170 kcal/mol. That is, they found that the two channels are competitive.

In the earlier study,[113] potential-energy surfaces for which the barrier to N-N fission is 47.8 kcal/mol (the reaction endothermicity) and barrier heights of 35.7, 38.3, and 41.0 kcal/mol for the ring fission reaction (most of the calculations were done for the 38.3 kcal/mol barrier). The calculated branching ratios are in the range 1.0-

2.4. These results and the computed product energy distributions are in qualitative agreement with the molecular beam results of Zhao *et al.*[114] The calculations are for energies well in excess of those in the experiments and thus it is necessary to extrapolate the computed values to lower energies for the comparison. Because of the statistical error in calculated values of the branching ratio, it is not clear how quantitative the agreement is. Nevertheless, the comparison with experiment suggests that the PES are qualitatively correct. However, some *ab initio* calculations have given values on the order of 72 to 75 kcal/mol for the ring fission reaction.[115] This seems high in light of the Zhao *et al.*[114] conclusion that this channel is competitive with the N-N bond fission reaction, which has an energy requirement of about 46-50 kcal/mol.

In the present study we have carried out extensive classical trajectory calculations on similar but new potential-energy surfaces. The main reason for further study of the classical reaction dynamics of RDX is to help resolve the question of the barrier height for the ring fission reaction. That is, can a reasonable PES with a ring fission energy barrier on the order of 70 kcal/mol (as predicted by *ab initio* calculations) yield a branching ratio of 2:1 for ring fission to N-N bond fission (which has a barrier of less than 50 kcal/mol)? Most of the calculations reported here were done for surfaces with ring fission barrier heights of 37, 56, and 71 kcal/mol (PES I, II, and III). The energy required for N-N bond rupture is 47.8 kcal/mol for all three PES. Trajectories were calculated over the energy range 200-450 kcal/mol.

We also address problems in reconciling reported estimates of the RDX bond energies with the thermodynamics of the reaction to give the secondary products and the bond energies of the secondary product molecules.

We have preformed a small number of calculations to investigate changes in the reaction rates if the RDX well depths are adjusted to be in reasonable agreement with the thermodynamics of reaching the secondary reaction products.

RDX has been the subject of considerable interest and some controversy lately. For example, there has been a problem of reconciling the results of experiments on condensed-phase RDX with the Zhao *et al.*[114] results obtained by IRMPD of RDX in a molecular beam. The latter experiments indicate that the triple bond fission reaction is competitive with the simple N-N bond rupture channel. However, the results for liquid and solid RDX do not indicate reaction via the concerted molecular elimination channel. This difference may be due to the importance of the volume of activation, as recently pointed out by Wight and Botcher,[115] which may prohibit the ring fission reaction in the confines of a liquid or solid. (It should be noted that there have been difficulties with regard to interpreting different experiments for condensed-phase RDX reactions because of the observation of different sets of products.) Another controversy, which we address in this study, concerns the energy barrier to the ring fission reaction.

Some quite definitive experiments on the thermal decomposition of RDX (and HMX) have recently been reported by Behrens and Bulusu.[116] They used combined thermogravimetric analysis and time of flight mass spectrometry to measure the

products resulting from heated RDX samples. They determined the primary reaction pathways for the decomposition of RDX in the solid and liquid phases. They find that the initial reaction in solid RDX is the breaking of a N-N bond to form NO_2. Their data indicate that only about 10% of the decomposition could occur by the concerted molecular elimination mechanism, which has been observed in the gas phase;[114] however, their data are consistent with RDX→$H_2CN+NO_2+2H_2C=N-NO_2$ followed by the dissociation of the $H_2C=N-NO_2$ molecular fragments. Wight and Botcher[115] have reported data that show no evidence for the concerted molecular elimination of $H_2C=N-NO_2$.

The Behrens and Bulusu[116] data show that following the elimination of NO_2, 1-nitroso-3,5-dinitro-hexahydro-s-triazine (ONDNTA) is formed by reaction of the ring fragment with NO, which is postulated to come from either $CH_2O+NO_2→H_2O+CO+NO$ or the decomposition of HONO which is formed by a concerted mechanism involving H-atom migration (from a C to an O atom) followed by N-N bond fission in RDX. The CH_2O product disperses in the solid, leading to a weakening of the lattice structure and the formation of molten RDX, for which the decomposition reactions are much faster than in the solid.

Recently, Wight and Botcher[115] have reported a study of the photolysis (by a pulsed CO_2 laser) of thin films of RDX deposited on an infrared-transparent window. They also conclude that the N-N simple bond fission reaction to give NO_2 is the initial step in the thermal decomposition of RDX in the solid. Several other groups have reported relevant studies of RDX. Brill and coworkers[117] have studied the

surface region of energetic materials (RDX and HMX) heated by a T-jump method. They analyzed the product gases as functions of time by FTIR. Fifer and coworkers[118] pyrolyzed RDX and used chemi-ionization to produce ions which were then mass analyzed.

A summary statement of the experimental results for the decomposition of RDX in the solid and molten phases is that the mechanisms are relatively complicated. However, these experiments have provided a relatively clear picture of the mechanisms. The Zhao *et al.*[114] results provide strong evidence for the mechanism for the gas-phase decomposition. Adams and Shaw[119] have recently reviewed this subject. There is now enough experimental data with which to make comparisons and thus provide guidance for the development of models for realistic simulations of RDX.

CHAPTER II

METHODS

Classical Dynamics

Trajectory calculations serve as a means of exploring a potential-energy surface and relating experimental results with the topological features of the surface. The method of calculating classical trajectories is conceptually quite simple. The initial conditions for every atom are set and then Hamilton's equations of motion are integrated until some outcome, such as a reaction occurs or a predetermined time limit is reached. The final coordinates of each atom of every trajectory can then be analyzed. These methods have been described in detail elsewhere.[120-123]

A general classical trajectory code, GenDyn,[124] was used to calculate the trajectories. Hamilton's equations of motion are integrated by using a fourth-order Runge-Kutta-Gill routine in a space-fixed Cartesian coordinate system. The trajectories were calculated for preset periods of time or until reaction occurred, depending on the study (details are given in Chapters IV-IX). Normal mode frequencies were computed using analytical second derivatives of the potential.

Potential-Energy Surfaces

Potential-energy surfaces are essential in our understanding a number of problems, including molecular stability, vibrational spectroscopy, conformational changes, reaction dynamics, and evaluating vibrational averaging effects on observed

molecular properties.

A potential-energy surface of a molecule gives the interaction energy as a function of the configuration of the system. A potential-energy surface can describe the rearrangement of the atoms or dissociation of the system from reactants to products. Molecules consisting of N atoms which are nonlinear require 3N-6 independent coordinates to describe their potential-energy surfaces.

The potential-energy surfaces used in these calculations are sums of bond stretching terms, bond angle bending terms, wag angle bending terms, and torsional motion terms. Of course, for some surfaces it was not necessary to use all of the aforementioned types of terms. For instance, wag angle bending terms are not needed for a potential-energy surface with only four atoms. Two different functions were used for the bond stretches. In some cases, harmonic oscillator functions were used to approximate the bonds

$$V_{bonds}(R) = (1/2)\ K\ (R - R_e)^2, \tag{1}$$

where K is the force constant and R_e is the equilibrium bond length. For more realistic representation of the bonds, Morse functions were used

$$V_{bonds}(R) = D_e \{ 1 - \exp [-\alpha\ (R - R_e)]\}^2 - D_e , \tag{2}$$

where D_e is the bond dissociation energy and α is chosen to fit the harmonic vibrational frequency. The parameters α and D_e are related to the harmonic force constant by

$$K = 2\ D_e\ \alpha^2 . \tag{3}$$

Bond (θ) and wag angle (γ) bending motions were approximated by harmonic

oscillator functions

$$V_{\text{bond angles}}(\theta) = (1/2)\ K\ (\theta - \theta_e)^2 \tag{4}$$

$$V_{\text{wag angles}}(\gamma) = (1/2)\ K\ (\gamma - \gamma_e)^2 \tag{5}$$

where K is the harmonic force constant and θ_e and γ_e are the equilibrium bond and wag angles, respectively. The torsional modes were represented by six-term cosine series

$$V_{\text{torsions}}(\tau) = \Sigma_{\ i=0,5}\ a_i \cos(i\tau) \tag{6}$$

where the coefficients a_i are adjusted to fit known geometries, barrier heights, and frequencies.

General Form of the Potential-Energy Surfaces

As mentioned in the previous section, we have used potential-energy surfaces for HONO, CH_3ONO, RDX, and HMX based on anharmonic stretches (Morse functions), harmonic bends and wags, and truncated cosine series for the torsional modes. Some of the calculations were done on a modified methyl nitrite potential-energy surface in which Eq. 1 was used to represent the bonds rather than Eq. 2. Not only does this simplify the dynamics for the analysis, but as has been shown with a series of studies,[9-23] this form of potentials suffices to realistically describe the important aspects of IVR.

The potential-energy surfaces for HONO and CH_3ONO have the analytical form,

$$V = \Sigma_{\ \text{stretches}} [\ D_e \{\ 1 - \exp[\ -\alpha\ (R - R_e)]\}^2 - D_e] + \Sigma_{\ \text{bends}}\ (1/2)\ K\ (\theta - \theta_e)^2$$

$$+ \Sigma_{\text{torsions}} [\Sigma_{i=1,6} a_i \cos (i\tau)]. \quad (7)$$

For HONO, it is the sum of 3 Morse functions for the bonds, 2 harmonic oscillators for the angles, and a six-term cosine series for the dihedral angle, ONOH. For methyl nitrite, it is the sum of 6 Morse functions for the bonds, 8 harmonic oscillators for the angles, and 2 six-term cosine series for two of the dihedral angles. We constructed the global potentials based on the force fields for the two isomers.

The RDX and HMX potential-energy surfaces will be described in detail in Chapters VIII and IX, respectively. The analytical form, based on a valence force field, is

$$V = \Sigma_{\text{stretches}} [D_e \{ 1 - \exp [-\alpha (R - R_e)]\}^2 - D_e] + \Sigma_{\text{bends}} (1/2) K (\theta - \theta_e)^2$$
$$+ \Sigma_{\text{wags}} (1/2) K (\gamma - \gamma_e)^2 + \Sigma_{\text{torsions}} [\Sigma_{i=1,6} a_i \cos (i\tau)]. \quad (8)$$

For RDX, it is the sum of Morse functions for the 21 bonds, harmonic oscillators for the 36 bond and 3 wag angles, and six-term cosine series for 12 torsional angles. For HMX, it is the sum of Morse functions for the 28 bonds, harmonic oscillators for the 48 bond and 4 wag angles, and six-term cosine series for 16 torsional angles.

Modeling a Torsional Potential

The torsional mode generally does not interact with other vibrational modes of the molecule, thus simplifying its treatment.[101] There are several components involved in the proper modeling of the torsional motion. The most basic component is obtaining a function with the proper periodicity which is determined by the symmetry of the group which is rotating. The other components require some

experimentally or theoretically obtained information on the torsional potential shape (such as the barrier height and/or frequency of vibration of the torsional mode), or, if none exists, a similar molecule upon which to base the fit.

If one part of a molecule possesses N-fold symmetry, the potential function used to model the torsional motion (associated with the N-fold symmetry portion of the molecule) must have N-fold periodicity. For example, the MX_3 group of a MX_3ABC molecule contains 3-fold symmetry. The rotation about the AB bond should then have 3-fold periodicity. This can be modeled with the series

$$V = \Sigma_{K=1,\infty} (V_{KN}/2) [1 - \cos(KN\tau)] \quad (9)$$

where τ is the dihedral angle and V_{kN} is proportional to the barrier heights between potential wells.[101]

Additional information, such as the dihedral angle values at which minima and maxima (barriers) occur and the frequencies of vibrations at the minima and maxima allow one to more realistically model the torsional motion. A six-term cosine series (see Eq. 6) was used to model all of the torsional motions in our studies. To fit the coefficients, a_i, we used Eq. 6 and its first and second derivatives, evaluated at a variety of dihedral angles.

For example, consider the molecule ABCD with rotation about the BC bond. The function used to model the rotation should have two minima. Suppose we know that the minima occur at the dihedral angles 0° and 180° and the barriers are at, say, 87° and 273°. We can then write the equations

$$V'(0°) = 0 \quad (10)$$

$$V'(180°) = 0 \tag{11}$$

$$V'(87°) = 0 \tag{12}$$

$$V'(273°) = 0. \tag{13}$$

Equations 10 and 11 are not useful, of course, since the derivative of Eq. 6 evaluated at 0° and 180° is trivial.

If we also know information about the relative energies of the minima and maxima, we can write a few more equations. If the conformation with an ABCD dihedral angle of 0° is more stable than the conformation with an ABCD dihedral angle of 180° by 1.09 kcal/mol (the seemingly arbitrary values given in this section are the values used in fitting the ONOC dihedral angle in methyl nitrite), we can write

$$V(0°) = 0 \tag{14}$$

$$V(180°) = 1.09. \tag{15}$$

Knowledge of the barrier height, of say, 9.84 kcal/mol, allows for two more equations

$$V(87°) = 9.84 \tag{16}$$

$$V(273°) = 9.84. \tag{17}$$

Finally, if the frequency of the torsional motion is known in either, or both of the wells, this too can be used in fitting the coefficients by using the equations

$$V''(0°) = K_{cis} \tag{18}$$

$$V''(180°) = K_{trans} \tag{19}$$

where K_{cis} and K_{trans} are the force constants which correspond to the frequencies of vibration in the *cis* and *trans* conformers, respectively. If the torsional vibrational frequencies at the barriers are known, equations similar to 18 and 19 could also be

used to model the torsional potential.

Only six of the above equations are needed, of course, in solving for the six coefficients, a_i, in Eq. 6. However, sometimes data are not available to determine even six coefficeints. One must then use fewer terms in the cosine series.

Switching Functions Used for Molecular Isomerization

Switching functions that depend on the dihedral angle, or the reaction coordinate, were used to attenuate certain potential parameters as the system undergoes the *cis-trans* conversion. For potential-energy surfaces based on the *cis* conformer, the potential parameters (which were dramatically different in the *cis* and *trans* wells--over 10% change) were attenuated using

$$K(\tau) = K_{trans} - (1/2)(K_{trans}-K_{cis})[1+\cos(\tau)], \quad (20)$$

where K_{cis} and K_{trans} are the force constants for the *cis* and *trans* conformations, respectively, and τ is the dihedral angle which is the reaction coordinate.

For similar potential-energy surfaces, based on the *trans* minima, the switching function (Eq. 20) was rearranged

$$K(\tau) = K_{cis} - (1/2)(K_{cis}-K_{trans})[1-\cos(\tau)]. \quad (21)$$

Equations 20 and 21 are identical, but written so as to emphasize the fact that the reactants and products are different for the potential-energy surfaces which are based on different minima.

Switching Functions Used for Reactive PES (RDX and HMX)

The forms of the switching functions used to connect the reactant and product wells are the same for all RDX and HMX surfaces studied. The parameters of the switching functions were adjusted so as to give the desired barrier height to concerted ring fission. Thus, these values vary for the four RDX surfaces (and hence, four barrier heights) studied.

The switching functions used are the forms given in Eqs. 18 and 19 in Ref. 113,

$$S1(r)=\exp[-\beta(r-r^R)^n] \tag{22}$$

$$S2(r)=1+a(r,q^R,q^P)\tanh[\beta(r-r^R)^n]. \tag{23}$$

Equations 22 and 23 are used when $r>r^R$, when $r<r^R$ S1(r) and S2(r) are unity. The coefficients denoted $a(r,q^R,q^P)$ are used to define the asymptotic limits of the parameters they attenuate. The parameters used to define the switching functions for the surfaces studied are given in Chapters VII and VIII.

The rate at which a parameter such as a well depth, force constant, bond length, or angle attenuates is dependent upon the shape of the switching functions used to smoothly connect reactant and product parameters. To incorporate the reaction channels in RDX, we used 198 switching functions. A different set of switching function parameters was used give barriers of 37, 56, and 71 kcal/mol for the ring fission reaction (with products $3CH_2NNO_2$). The fitting of the barrier will be discussed in greater detail in Chapter VIII.

Initial Condition Selection

Two different methods have been employed for intial condition selection in our studies. Both methods, quasiclassical projection techniques[120] and the Efficient Microcanonical Sampling (EMS) Metropolis alogorithm,[125,126] have been described in depth elsewhere. Therefore, only a brief description accompanied by the necessary equations will be presented here.

The total angular momentum in all of our calculations is zero and both of the following schemes are offered as options in GenDyn.[124]

The Monte Carlo quasiclassical methods consist of projecting the energy onto the normal modes.[120] This allows for phase-averaged, mode-selective excitation of the equilibrium vibrational normal modes. (For a definition of normal modes and a description of a normal mode analysis, see Ref. 111.) The initial phases of the normal coordinates are[120]

$$Q_i = Q_i^\circ - (Q_i^\circ - \rho_i) \sin[(\pi/2) + \pi\xi], \tag{24}$$

where Q_i° is the equilibrium value of the normal coordinate, ρ_i is the classical inner turning point and ξ is a random number between zero and one. The classical inner turning point, ρ, is given by

$$\rho_i = \pm (2\epsilon_i/\lambda_i)^{1/2} \tag{25}$$

where ϵ_i is the energy of the normal mode and λ_i is the force constant obtained from the fundamental frequencies.[120]

The velocity of the normal mode Q_i is

$$\partial Q_i/\partial t = \pm (2T)^{1/2} \tag{26}$$

where T is the kinetic energy of normal mode Q_i (obtained from the difference between the desired normal mode energy and the potential energy). The sign is determined by using a random number.

The normal mode coordinates and velocities (Eqs. 24 and 25) are then transformed to Cartesian coordinates and momenta for use as the initial conditions of the trajectory.

The classical microcanonical methods used consisted of generating classical initial conditions with a proceedure developed by Nordholm and coworkers.[125,126] This method yields a microcanonical distribution of points in phase space.

The proceedure begins with the equilibrium configuration and 10^6 warm-up random walk steps (described in the following text) are sampled to allow the system to lose "memory" of the initial configuration. Every 10^5 random walk steps, a set of momenta are selected and a trajectory computed.

A random walk is executed in the following manner.[125,126] Starting with the configuration q_k, all 21 coordinates are moved to a trial configuration q_{k+1}. This configuration is accepted or rejected based on the following criteria. (1) The configuration q_{k+1} is rejected if it is not a "reactant" configuration. (2) If the statistical weight of the trial configuration (see Refs. 125 and 126 for the form of the weight function) q_{k+1} is greater than that of q_k then the trial configuration q_{k+1} is accepted. (3) If (1) or (2) do not result in acceptance or rejection, the ratio of the trial weight function to the q_{k+1} weight function is compared to a random number between zero and one. If the ratio is greater than the random number, the trial

configuration q_{k+1} is accepted. (4) Finally, if steps 1-3 have not resulted in acceptance or rejection of the trial configuration q_{k+1}, then it is rejected.

If q_{k+1} is rejected (steps 1-4) then the configuration for state k+1 is taken to be the same as that for state k.

Defining End Tests for Isomerizing Trajectories

The *cis-trans* isomerizations were identified by monitoring the relevant dihedral angle. For instance, for methyl nitrite, the ONOC angle was used to calculate the number of isomerizations and the amounts of time spent in the two conformers. The value of the dihedral angle for each trajectory was saved every 4 fs. After the calculation of an ensemble of trajectories, "statistics" were gathered for each trajectory. An isomerization consisted of crossing the barrier from one conformer to another. Occasionally, a trajectory would recross, back to the recently visited conformer, and then recross again to the second well. In these instances, we counted this as multiple isomerizations. In other words, if the barrier was crossed, we counted it as an isomerization. If a trajectory recrossed the barrier, before truly sampling the second well (conformationally) it was counted as multiple isomerizations. Many (hundreds) of dihedral angles were plotted, and very few exhibited this recrossing behavior.

Power Spectra

Power spectra are a valuable tool which can provide a wide variety of

information about a molecule.[1, 7-9, 25-26, 127-151] At low energy, a power spectrum contains sharp peaks at the fundamental frequencies of vibration of the molecule. At higher energies there are peaks in the spectra from overtones and shifting of peaks due to anharmonicity of the PES. Also, broadening of the spectral peaks occurs due to different factors such as anharmonicity, increased rate of IVR (as discussed in Chapter 1) and isomerization (which is discussed in more detail in the Vibrational Bandshapes section of Chapter I and is the focus of Chapters IV and V).

It has been shown that Fourier transforms of the dipole moment and the polarizability tensor calculated from classical trajectories accurately reproduce experimental IR and Raman spectra, respectively.[127,129] Since the dipole moments and the polarizability tensor of the molecules studied here have not been well characterized, calculations of the IR and Raman spectra were not done. Our calculations correspond to what the IR and Raman spectra would be if the dipole moments and the polarizability tensor were linearly related to the internal coordinates.[133] A number of studies[134-136] have shown non-linear fits to be better representations of the dipole moment. However, data are not available for such fits. Thus, by transforming the internal coordinates, we are assuming linear dipole moments. Since linear fits have been shown to be reasonable approximations to the dipole moment,[133] we can justify our methods in light of the fact that at this point in time, the necessary data for improving the modeling of the dipole moments is not available (see Chapter X for more on this topic).

Power spectra were calculated by Fourier transforming[127,128,130,131] ensemble-

averaged autocorrelation functions of internal coordinates. Composite spectra were calculated by summing the individual internal coordinate spectra.

Time-Delay Plots

Time-delay mappings were plotted for methyl nitrite in order to further understand the changes in phase space samplings due to the effects of isomerization. A time-delay map[152-154] demonstrates the "memory" of a trajectory. An internal coordinate is plotted against itself at some later point in time. A periodic system yields a closed curve while a quasi-periodic system produces one that is not quite closed. The computed time-delay mappings are for a total time of 0.499 ps and time-gaps of 3 fs. The time-gap and mapping time length were selected to yield easily analyzable (clean) plots. For these calculations we used a harmonic potential-energy surface to reduce the effects of anharmonicity (there is still anharmonicity present in the surface due to the switching functions). The Morse functions representing the bonds were replaced with harmonic oscillators; the force constants used were calculated from the Morse function parameters α and D_e using Eq. 3. Equal amounts of energy were inserted into each normal mode initially for a total energy of 65.5 kcal/mol.

Time-delay mappings calculated from a harmonic PES of methyl nitrite are shown and discussed in Chapter V.

CHAPTER III

CLASSIFICATION OF VARIOUS DYNAMICAL BEHAVIORS IN ISOMERIZING SYSTEMS

Motivation of Study

Power spectra of large molecules are complicated and often not easily interpreted. Since there are several factors which can affect the spectra, such as anharmonicity and other couplings which induce "ordinary" IVR. An isomerizing molecule is further complicated by additional factors, such as a second set of peaks, relating to the second conformer, time spent in the barrier region, and mode mixing induced by sampling more than one set of normal modes.

In an effort to delineate these differences, we computed large ensembles of classical trajectories for a particular set of initial conditions, then, based on characteristics which we wished to isolate, we designed "definitions" for ensembles and sorted the large ensemble of trajectories into the smaller "defined" ensembles. Power spectra calculated from these ensembles of trajectories with specific behaviors illustrate the relationships between trajectoral behavior and the spectra.

Since we wished to study the effects of isomerization, our ensemble definitions were based on the behavior of the isomerization coordinate. Individual trajectories from the large ensemble were sorted and placed into various smaller ensembles in order to isolate some of the various effects that complicate the spectra and cause line broadening.

This is unusual, in that most studies consist of the calculation of an ensemble of trajectories followed by some form of analysis and then comparison to another ensemble which had a different set of initial conditions. If we were to follow this procedure with the goal of studying the effects of isomerization, we might study one ensemble with the energy initially imparted so as to induce isomerization in most trajectories and another ensemble in which the energy was initially imparted so as to not induce isomerization in most trajectories. This procedure would lead to difficult data interpretation. For instance, it would be difficult to conclusively state whether differences seen in the power spectra were due to the isomerization, or the manner (and consequent dynamical behaviors) in which the energy was initially imparted to the molecule. By calculating a large ensemble for a particular set of initial conditions, and then subdividing this large ensemble into smaller ensembles based on the isomerization *history* of the trajectories, we can draw firmer conclusions based on the differences in the power spectra.

Definitions

As stated in the previous section, the "smaller ensembles" (hereafter referred to as cases) are defined based on the isomerization coordinate. The trajectories in the HONO ensembles are separated into 5 different cases and those in the CH_3ONO ensembles into 4 cases. The different types of ensembles are illustrated in Figs. 1 and 2, HONO and CH_3ONO, respectively. The average percentage of time spent in each well is shown in the circles, and the average number of isomerizations of the 10

ps trajectories are shown above the arrows. Case 1 trajectories sample only one well, *cis* in the case of CH_3ONO and *trans* for HONO. Cases 2 and 3 undergo a few barrier crossings and the difference in the two is mainly in the amount of time spent in the other well. The amounts of time spent in the two wells in Case 4 is about the same as in Case 3, but the number of barrier crossings is significantly larger in Case 4. An additional type of ensemble was constructed for HONO (Case 5) which was designed to probe the influence of the "time spent in the transition-state region." For HONO, Case 4 trajectories spend at most 3 ps in a well before recrossing the barrier while Case 5 trajectories undergo about the same number of crossings as Case 4 trajectories and spend at least 5 ps in a well before recrossing. We excluded from Cases 4 and 5 those trajectories which spent periods of 3 to 5 ps in a well before recrossing in order to make the spectral distinctions sharper.

Ensemble parameters for the HONO and CH_3ONO studies are given in Table I and discussed in Chapter IV.

The Types of Information Sorting Can Provide

Even with the careful selection of the ensembles, the spectra are still complicated and comparisons of them are not easy to interpret. For example, the comparison of a power spectrum of a trajectory which spends all of its time in one well with that of a trajectory which spends half of the time in each of two potential wells shows changes in the intensities of peaks as well as the appearance of additional peaks for the second well at frequencies which do not match those in the first well.

Comparison of Cases 1, 2, and 3 illustrates the changes in the spectra due merely to the effects of sampling an additional set of motions since their definitions are for sampling only the phase space of the original well (*cis* for CH_3ONO and *trans* for HONO), sampling mainly the original well, and sampling approximately equally the two wells, respectively.

The repeated barrier crossings lead to mixing of the motions due to sampling different sets of normal modes. The cases were designed to illustrate other spectral characteristics and isolate spectral broadening due to isomerizations. To study the effects due mainly to the frequencies of the second well (*trans* for CH_3ONO and *cis* for HONO), we use Cases 2 and 3 which involve very few crossings (this makes the "barrier crossing effects" negligible in comparison to Cases 4 and 5) and different percentages of time spent in the two wells (see Figs. 1 and 2). The effects of multiple crossings are illustrated by Case 4. Cases 3 and 4 are for nearly identical percentages of time spent in the two wells, but different isomerization rates.

We studied an additional type of behavior in HONO (Case 5; see Fig. 1) in order to differentiate between broadening of spectral peaks caused by sampling time spent near the saddle point and that due to the repeated sampling of more than one set of normal modes. The trajectories in Cases 4 and 5 spend roughly the same amount of time in the barrier region, which must be defined somewhat arbitrarily (see Chapter IV for more detail). This provides a comparison between spectra for an ensemble in which the trajectories spend roughly equal amounts of time in the barrier region but experience more of less regular multiple-mode sampling (Case 4)

with one in which the trajectories experience multiple-mode sampling in a shorter period of time and dwell in one of the wells for most of the time.

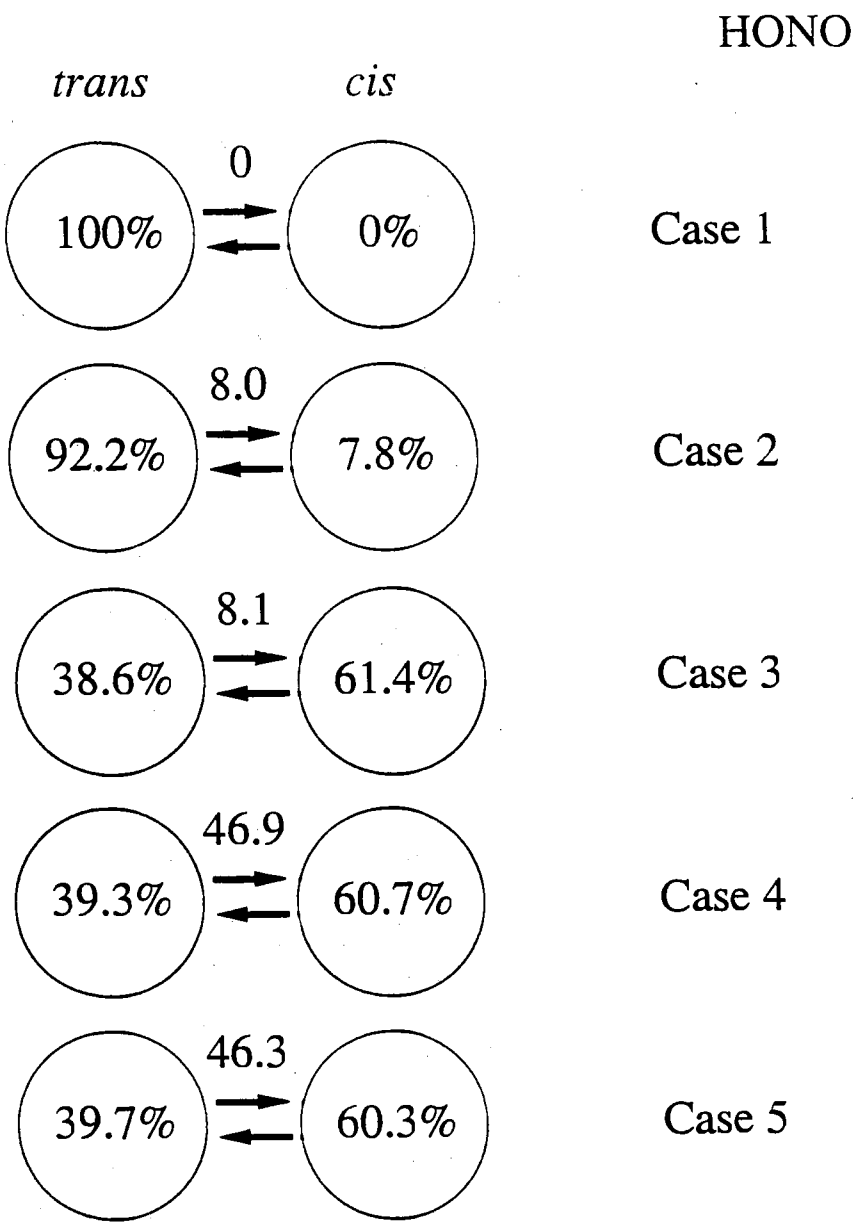

Figure 1. Illustration of the various types of ensembles considered in the HONO study. The numbers above the arrows are the average number of isomerizations experienced in ensembles of 40 trajectories of 10 ps lengths.

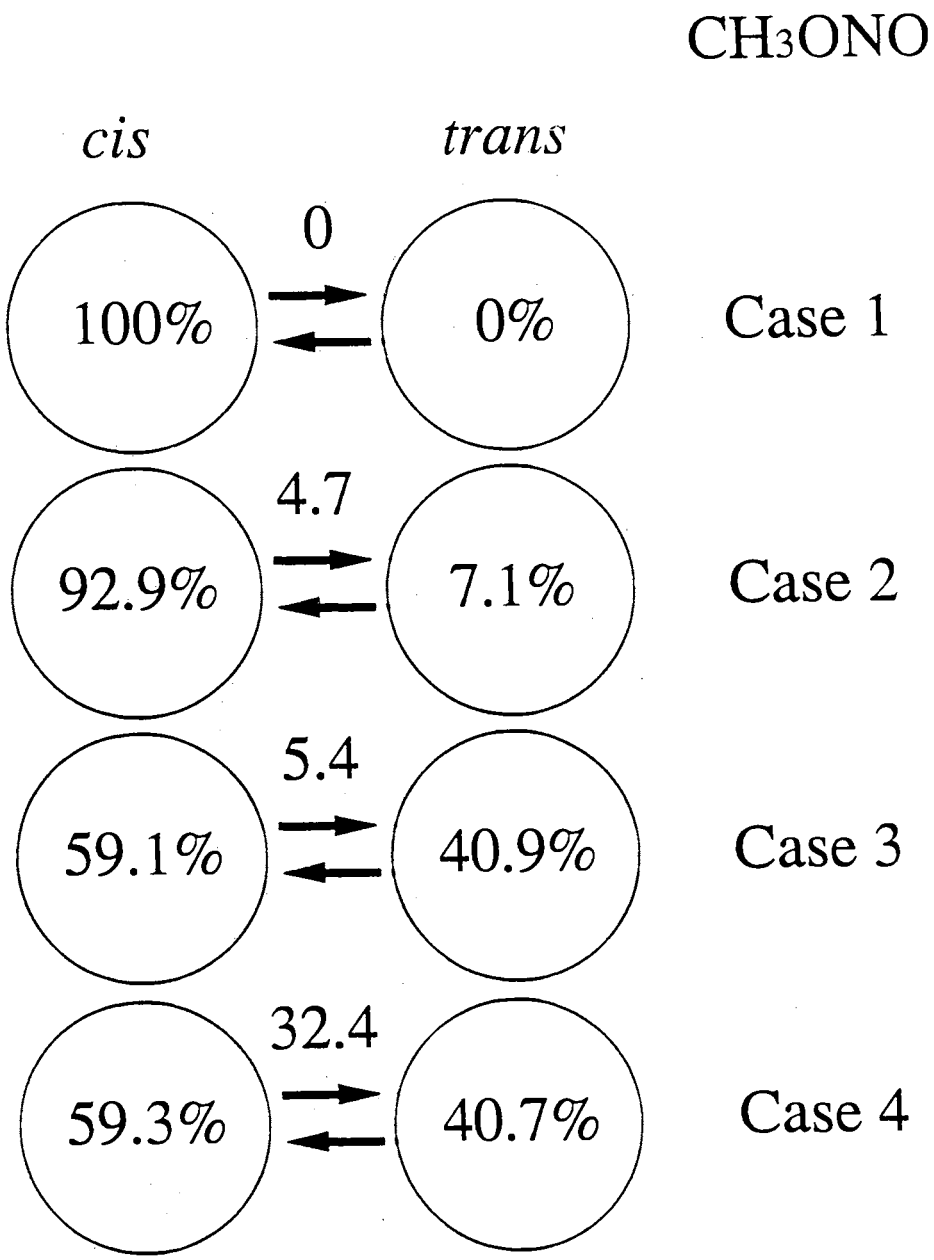

Figure 2. Illustration of the various types of ensembles considered in the CH_3ONO study. The numbers above the arrows are the average number of isomerizations experienced in ensembles of 40 trajectories of 10 ps lengths.

CHAPTER IV

ENHANCEMENT OF VIBRATIONAL MODE MIXING DUE TO BARRIER CROSSINGS: HONO AND CH_3ONO

Introduction

In 1964 Eigen[82,83] suggested that very fast reactions may affect vibrational spectra. That is, if reaction is fast enough, vibrational line shapes can be related to reaction rates. Chemical reactions (e.g., conformational changes) are expected to increase broadening of vibrational bands and perhaps cause merging of certain bands in the spectra, much like the effects seen in NMR spectra. Although there is an analogy with NMR, there is a significant difference in time scales. Molecular vibrations times are on the order of subpicoseconds while NMR involves times on the order of 10^{-3} s. Since molecular vibrations are very fast, variations in the spectral features might be useful for determining the rates for extremely fast chemical reactions. However, the extraction of reaction rates from vibrational spectra is complicated because there are several factors other than reaction (e.g., IVR, pressure broadening, etc.) that can cause spectral broadening, and the time scales for some of these can be on the order of reaction rates.

Wood and Strauss[84] argue that it is difficult to determine the rate of reaction from the broadening of vibrational spectral lines because the time spent in the region of the potential barrier is sufficiently long to cause complications in a simple interpretation of the broadening being due to the frequency of passage over the

barrier. Stated differently, the time spent in a well must be greater than the time spent crossing the barrier for a simple, direct relationship between the reaction rate and line broadening. However, observed IR line broadening data have been ascribed to reactions. Kreevoy and coworkers[85-88] have determined reaction rates in this fashion. More recently, Cohen and Weiss[89-94] determined rate constants for the broadening of IR lines. Weiss[95] did a simulation of a picosecond, bimolecular exchange reaction in solution. He found that a distinction between natural width and exchange broadening is possible, and the chemical exchange can play a very important role in spectral broadening when the barrier is low.

Thus, while it seems reasonable to expect reactions to affect vibrational band widths, and some experiments suggest that rates can be derived from such data, there are obviously complicating factors that obscure the relationship of the rate of reaction and the line widths. It would be useful to have a better understanding of the various causes of line broadening in polyatomic molecules. Classical trajectories offer an attractive means of doing so since they can be used to examine the various effects that can cause broadening. We have carried out some studies of the effects of transition-state crossings on mode mixing for realistic models of two isolated molecules, HONO and CH_3ONO, which undergo *cis-trans* isomerization. We report here some preliminary results of this work; a full account of our studies will be published elsewhere.

There have been some previous theoretical studies which pertain to this topic. Jones, Holloway, and Gadzuk[96] used a model Hamiltonian to show that trajectories

which cross a saddle-point many times produce broader vibrational spectral lines than trajectories with few crossings. Other studies[155-157] have shown that models which undergo transitions between sets of normal modes experience enhanced IVR (as manifested in autocorrelation functions, power spectra, and other results). The basic idea involved here was discussed, in a different context, by Hougen and Watson[158] in 1965; they refer to the process as "axis-switching." Heller[159] has illustrated how electronic nonadiabatic transitions between two stable wells can lead to mode mixing. The model treated by Heller represents a limiting case of the transition-state crossing problem in that essentially no time is spent in the "transition-state" in the surface hopping model.

Methods

We begin by calculating large ensembles of classical trajectories for a particular set of initial conditions. These ensembles are then divided into smaller ensembles based on the behavior of the individual trajectories in order to isolate some of the various effects that can cause line broadening. Power spectra are computed for these ensembles by Fourier transforming the internal coordinates.

There are several factors, such as anharmonicity and other couplings which induce "ordinary" IVR, time spent in the barrier region, and mode mixing induced by sampling more than one set of normal modes (like that illustrated by Heller's model), which can affect the spectra. Thus, we computed power spectra for ensembles comprised of trajectories with specific behaviors to illustrate the effects

of various factors. The trajectories in the HONO ensembles are separated into 5 cases and those in the CH_3ONO ensembles into 4 cases. The different types of ensembles are illustrated in Fig. 1. Case 1 trajectories sample only one well, *cis* in the case of CH_3ONO and *trans* for HONO. Cases 2 and 3 undergo a few barrier crossings and the difference in the two is mainly in the amount of time spent in the other well. The amounts of time spent in the two wells in Case 4 is about the same as in Case 3, but the number of barrier crossings is significantly larger in Case 4. An additional type of ensemble was constructed for HONO (Case 5) which, as discussed below, was designed to probe the influence of the "time spent in the transition-state region."

It is worthwhile to consider some of the basic aspects of the spectra since even with the careful selection of the ensembles the spectra are still complicated and the comparisons of them are not easy to interpret. For instance, the comparison of a power spectrum of a trajectory which spends all of its time in one well with that of a trajectory which spends half of the time in each of the two potential wells shows changes in the intensities of peaks as well as the appearance of additional peaks for the second trajectory at frequencies which do not match those in the first well. To illustrate the changes in the spectra due merely to the effects of sampling an additional set of motions, we have assembled ensembles for various times spent in the two wells: Cases 1 through 3 are for sampling only the phase space of the first well (Case 1), sampling mainly the first well (Case 2), and sampling approximately equally the two wells (Case 3). The details of the ensembles are given in Table I.

The barrier crossings lead to frequency sampling at and near the barrier top and, due to repeated crossings, mixing of the motions due to sampling different sets of normal modes. To see the effects due mainly to the frequencies of the second well, Cases 2 and 3 involve very few crossings (this makes the "barrier crossing effects" negligible in comparison to Cases 4 and 5) and different percentages of time spent in the two wells (see Table I). The effects of multiple crossings are illustrated by Case 4. Cases 3 and 4 are for nearly identical percentages of time spent in the first well (*cis* for CH_3ONO and *trans* for HONO).

We studied an additional type of behavior in HONO (Cases 5; see Fig. 1 and Table I) in order to differentiate between broadening of spectral peaks caused by sampling time spent near the saddle point and that due to the repeated sampling of more than one set of normal modes. Case 4 trajectories spend at most 3 ps in a well before recrossing the barrier while Case 5 trajectories undergo about the same number of crossings as Case 4 trajectories and spend at least 5 ps in a well before recrossing. We excluded from Case 4 and 5 those trajectories which spent periods of 3 to 5 ps in a well before recrossing in order to make the spectral distinctions sharper. The trajectories in Cases 4 and 5 spend roughly the same amount of time in the barrier region, which must be defined somewhat arbitrarily. For example, if we define the "barrier region" as extending 5° on either side of the top of the barrier, the average times spent in that region for Cases 4 and 5 are 0.62 and 0.50 ps, respectively; thus, the difference is only 0.12 ps (for 10 ps trajectories). Note that we expect Case 4 trajectories to sample slightly more of the barrier region since they

undergo more crossings. For comparison, if we define the barrier region to be 60° in width, the difference in times for the two cases is still less than 0.4 ps. This provides a comparison between spectra for an ensemble in which the trajectories spend roughly equal amounts of time in the barrier region but experience more of less regular multiple-mode sampling (Case 4) with one in which the trajectories experience multiple-mode sampling in a shorter period of time and dwell in one of the wells for most of the time.

Potential-Energy Surfaces

We have used potential-energy surfaces based on anharmonic stretches (Morse functions), harmonic bends, and a truncated cosine series for the torsional mode. Not only does this simplify the dynamics for the analysis, but it has been previously shown with a series of studies that this simple form for potentials suffices to realistically describe the important aspects of IVR.[9-23] The form of the potentials is the same for both CH_3ONO and HONO and is given by Eq. 7.

We constructed a global potential for methyl nitrite which is based on the force fields for the two isomers. The equilibrium geometries[160] and frequencies[161] (see Tables II and III) from experiment were used in fitting the *cis* and *trans* minima. The constants a_i for the torsional potential about the NO bond are those calculated by Darsey and Thompson.[162] The coefficients for the torsion about the CO bond were adjusted to fit the geometries and barrier height.[160,163] The barriers for methyl rotation are approximately 1.9[163] and 0.03 kcal/mol[160] for the *cis* and *trans*

conformations, respectively. We did not attempt to fit these values, but instead used the same value, 0.88 kcal/mol, for the two conformers. Only the torsion about the CO bond involving the in-plane hydrogen is used in the potential, but all three NOCH dihedral angles are defined. The values of the potential parameters are given in Table IV.

The experimental[161] normal mode frequencies are compared in Table II with those computed from our potential. The *cis* potential frequencies deviate an average of 11.2 cm^{-1} from the experimental values, whereas the *trans* potential frequencies deviate an average of 8.8 cm^{-1}. The greatest difference in the computed and experimental frequencies is 46.8 cm^{-1}.

Switching functions that depend on the ONOC angle were used to attenuate certain potential parameters as the system undergoes the *cis-trans* conversion. The force constants for the NO and OC bonds and the ONO, NOC, ONH, and HCH angles were attenuated by using Eq. 20, where τ is the ONOC dihedral angle.

The potential-energy surface used in the calculations involving HONO was taken from previous studies.[14,16,22] The form of the potential is that of Eq. 7 with a dihedral angle switching function of the form of Eq. 21. The equilibrium geometries,[14] frequencies,[164] and potential parameters[14,16] are given in Tables II, III, and IV, respectively.

Calculations

The general classical trajectory code, GenDyn,[124] was used to calculate the

trajectories. Hamilton's equations of motion are integrated by using a fourth-order Runge-Kutta-Gill routine in a space-fixed Cartesian coordinate system. Integration step sizes of 1.5 x 10^{-16} and 1.0 x 10^{-16} s were used for CH_3ONO and HONO, respectively. The trajectories were calculated for 10 ps. The normal mode frequencies (Table II) were computed by using analytic second derivatives of the potential.

Initially two quanta of energy were placed in each of the three CH normal modes and zero-point energy in all other modes, using the method described by Bintz *et al.*,[11a,120] for a total energy of 80.4 kcal/mol for the methyl nitrite calculations. For the HONO trajectories, 9 quanta of energy were initially placed in the torsional mode and zero-point energy in all other modes for a total energy of 25.93 kcal/mol.

The trajectories were sorted into 4 different cases for methyl nitrite and 5 for HONO as described in Section 2. Each ensembles consists of 40 trajectories. Power spectra were calculated by Fourier transforming[127,128] ensemble-averaged autocorrelation functions of internal coordinates. Composite spectra were calculated by summing the individual internal coordinate spectra.

Results and Discussion

Composite power spectra were computed for the various cases (see Fig. 1 and Table I) for CH_3ONO and HONO to investigate the various effects due to passages through a transition-state (*cis-trans* isomerization in this case). We can illustrate these effects by using selected frequency ranges.

Figure 2 shows spectra of all four cases for CH_3ONO for the range 250-700 cm^{-1}; this spectral range corresponds to normal modes comprised of ONO and NOC bends and NO, N=O, and CO stretches.[161] Figure 2 shows that as the time spent in the *cis* configuration decreases and the time spent in the *trans* configuration increases (going form Case 1 to 3), there are decreases in the intensities of the flanking *cis* peaks and the appearance of the *trans* peaks. This pattern is expected since the trajectories in Case 1 sample only *cis*-space; for Case 2 the ensemble average for the time spent in the *cis* well is 92.9% and for Case 3 that average is 59.1% (see Table I). The trajectories making up the ensemble for Case 4, Fig. 2, on the other hand, spend on average nearly the same amount of time in *cis*-space as Case 3 trajectories do, 59.3%, but the peaks are broader. We conclude that much of the observed broadening of the power spectral peaks is related to an increase in the rate of exploration of space due to repeated crossings of the transition state.

Figure 3 shows HONO composite spectra for the frequency range 1500-1800 cm^{-1}, which is the region of the N=O normal modes; Cases 1, 2, and 3 are compared in frame a and Cases 3, 4, and 5 in frame b.

Spectral differences due to varying amounts of time spent in a particular well are illustrated by comparing the spectra for Cases 1, 2, and 3 shown in panel a of Fig. 3. The spectrum for Case 1, for sampling only the *trans* well, has a peak just below 1700 cm^{-1}. Case 3, on the other hand, has a strong peak at around 1600 cm^{-1}, corresponding to the *cis* N=O mode and a low shoulder in the *trans* peak region. (There is some red shift from the fundamentals in the peaks due to the

anharmonicity, induced mainly by the switching functions in the potential.) The shoulder to the right of the strong *cis* peak for Case 3 in frame b is probably due to motion in the *trans* well, a comparison to Case 4 shows that both the *cis* peak is much broader and the *trans* peak is nearly faded into the baseline.

As mentioned above, comparison of Case 5 to Case 3 should show differences due to sampling the barrier region. The *cis* peak in Case 5 is broader, but the *trans* peak is actually more distinguished.

A comparison of Cases 4 and 5 illustrates the effects of mixing due to two-well, multiple-mode sampling. Since the trajectories in both ensembles spend nearly the same amount of time in the barrier region the differences should be due to other factors. In panel b of Fig. 3 the Case 4 *cis* peak is notably broader compared to that of Case 5, and while the *trans* peaks is still distinguishable in Case 5, it is not in Case 4. Case 4, the ensembles which we assert experiences the most mixing due to sampling multiple sets of normal modes, has broader peaks (in the frequency range shown here) than Cases 1-3 or 5.

Figure 4 shows composite power spectra of all five cases for HONO for the complete frequency range. Since the Case 1 ensemble only samples the *trans* well, it serves as a reference spectrum for the other four cases. It illustrates the broadening and shifting of the peaks which occur at this particular energy and initial conditions for the anharmonic potential-energy surface.

The peaks below 500 cm^{-1} are due to the torsional motion, and the sharp peak just above 500 cm^{-1} is the ONO bending motion. Note that going from Cases 1

through 5, the torsional peaks decrease in intensity and become broader. These changes in the spectrum are expected for Cases 1 through 3 because of the changes in the amounts of time spent in the two wells (see Table I). The broader peak in Case 4, compared to Case 3, is due to the increase in the reaction rate. The rate for Case 5 is nearly the same as for Case 4, but all Case 5 trajectories undergo a period of rapid isomerizations (essentially hindered rotor motion); we attribute the slightly broader peak in Case 5 compared to Case 4 to this behavior.

The power spectral peak due to the ONO angle bending motion decreases in intensity in going from Case 1 to 3. Again, the decrease in intensity is due to sampling more of the second well. The peak due to this motion in Case 4 and 5 is notably broader than in Case 3.

The peak around 800 cm^{-1} is due to the ON bond stretching motion. That peak in Case 2 is slightly broader and lower in intensity than in Case 1; this is the result of less time spent in the *trans* well. No notable broadening occurs going from Case 2 to 3, but there is a decrease in intensity due to the increase in the time spent in the *cis* well. In Case 4 there appears to be a single broader peak rather than the two resolved peaks as in Case 3. The repeated sampling of the two sets of normal modes broadens the ON *cis* and *trans* spectral peaks into one in Case 4. There appears to be two peaks in Case 5, although not as well resolved as in Case 3. These comparisons illustrate that both barrier region sampling (Case 5) and repeated sampling of multiple sets of normal modes (Case 4) contribute to the broadening of spectral peaks and hence, an increase in the rate of sampling of phase space.

The spectral region around 1300 cm^{-1} is due to the HON angle bending motion. Going from Case 1 to Case 2 results in some decreases in intensity and slight broadening with respect to the Case 1 peak, yet does not notably broaden. There is significantly more broadening in Case 3 and then sharpening of the peak for Cases 4 and 5. In Case 5 the "peak" appears to be split. What may be occurring is to very close peaks coalescing into one--showing up as a single sharp peak at an intermediate frequency (Cases 3 and 4), and Case 5 being too similar to Case 4 to discern differences. This apparent sharpening of the peaks may be due to sampling more of the intermediate frequencies (at the transition state) relative to the frequencies of the two wells, as Wood and Strauss[84] have suggested. Another possible explanation could lie in the fact that we initially deposited all of the excitation energy in the torsional mode, which is strongly coupled to the HON angle mode.[22] In any case, it is clear that different modes are affected differently by transition state crossings.

The N=O bond mode has been described in the above text and is shown in detail in Fig. 3.

The peaks at the far right if the spectra are due to the OH bond stretching motion. Other than Case 1, the peaks are very broad and the *cis* and *trans* peaks (with fundamental frequencies of 3426 and 3589.2 cm^{-1}, respectively) are not resolved. Close inspection of the spectra reveals that the Case 4 peak is broader than the others. Also, we note that the extensive broadening of the OH band is different from the behavior of the other bands. There is dramatic broadening caused by

sampling of the phase space of the second well (see Case 2).

Similar results were obtained at other energies, initial excitations, and in other portions of the spectra for both molecules. A full report of the methyl nitrite study is presented in the next chapter.

Conclusions

The effects of mode mixing, due to crossings of a transition state, have been studied by Fourier transforming classical trajectories of HONO and CH_3ONO undergoing *cis-trans* isomerizations. The various causes of changes in power spectra has been investigated by the careful construction of special ensembles which illustrate particular types of dynamical behavior. We have shown that several factors, such as differing amounts of time spent in each conformation and the number of barrier crossings, contribute to power spectral broadening. The broadening due to and increase in the number of barrier crossings can be attributed to two factors, one of which is simply the increase in the number of times the barrier is crossed (perhaps due to an increase in time spent in the barrier region coupled), the other is the repeated sampling of multiple sets of normal modes which, in a simple picture, can be viewed as the jumping back and forth between two sets of "Slater-type" trajectories. The latter is akin to the effects described by Heller for nonadiabatic transitions.

The spectral peaks due to different types of normal modes are affected differently by the isomerizations, that is, the shifting and broadening are not the same

for all peaks. This suggests that the determination of reaction rates from spectra may not be simple. We are currently examining the relationship of the reaction rates and spectra to see if the rates can be quantitatively determined from the changes in the spectra.

Table I. Ensemble Parameters for HONO and CH_3ONO

	HONO			
	Crossings		Percent time in *trans* well	
	Average	Range	Average	Range
Case 1	0.0	0	100	100
Case 2	8.0	1-15	92.2	80-99
Case 3	8.1	1-15	38.6	1-79
Case 4	46.9	25-65	39.3	1-79
Case 5	46.3	25-65	39.7	1-79
	CH_3ONO			
	Crossings		Percent time in *cis* well	
	Average	Range	Average	Range
Case 1	0.0	0	100	100
Case 2	4.7	1-9	92.9	80-99
Case 3	5.4	1-9	59.1	35-85
Case 4	32.4	25-50	59.3	35-85

Table II. Equilibrium Geometries of CH_3ONO and HONO

		cis	*trans*
Bonds (Å)			
CH_3ONO[a]			
	O=N	1.164	1.64
	N-O	1.395	1.415
	O-C	1.437	1.436
	$C-H_i$	1.09	1.09
	$C-H_o$	1.10	1.09
HONO[b]			
	O=N	1.1773	1.665
	N-O	1.3776	1.3996
	O-H	0.9646	0.9539
Angles (degrees)			
CH_3ONO[a]			
	ONO	114.8	111.8
	NOC	114.7	109.9
	OCH_i	101.8	109.44424
	OCH_o	109.9	109.44424
	H_iCH_o	113.485	109.5
	H_oCH_o	108.113	109.5
	ONOC	0.0	180.0
HONO[b]			
	ONO	113.94	111.38
	HON	111.61	107.89
	HONO	0.0	180.0

[a] Turner *et al.* Ref. 160.
[b] Guan *et al.* Ref. 14.

Table III. Normal Mode Frequencies[a] of CH_3ONO and HONO

Cis		*Trans*	
CH_3ONO			
experiment[b]	calculated	experiment[b]	calculated
118.1	120.3	136.0	137.8
333.7	301.9	196.3	176.4
351	344.8	370	370.3
625	640.1	565	542.4
838	836.3	807	814.4
985	987.1	1031	1031.5
994	1003.5	1043	1040.1
1231	1232.0	1180	1186.3
1408	1396.7	1424	1423.7
1438	1438.2	1447	1437.5
1455	1456.7	1467	1469.1
1613	1611.6	1665	1667.4
2952	2905.2	2823	2794.9
3002	3020.3	2883	2899.3
3031	3049.0	2913	2925.4
HONO			
experiment[c]	calculated	experiment[c]	calculated
639.8	647.5	543.9	537.3
609	540	595.6	540.7
851.9	907.4	790.1	884.7
1302.0	1301.4	1263.2	1262.9
1640.5	1639.6	1699.8	1698.9
3426.2	3426	3590.7	3589.2

a Units are cm-1. The normal mode frequencies were obtained by using analytical second derivatives of the potential.
b P.N. Ghosh and H.H. Günthard Ref. 161.
c J. Murto *et al.* Ref. 164.

Table IV. Potential Parameters of CH_3ONO and HONO

Morse Parameters

Coordinate[b]		D_e[a] (kcal/mol)	*cis* α ($Å^{-1}$)	*trans* α ($Å^{-1}$)
CH_3ONO	$r_{O=N}$	115.0	2.528631	2.653267
	r_{NO}	41.1	3.403016	2.3611352
	r_{OC}	56.9	2.187235	1.786939
	r_{CHi}	102.7	1.860	1.791
	r_{CHo}	102.7	1.845725	1.77
HONO	$r_{N=O}$	115.0195	2.6228	2.7553
	r_{NO}	40.7985	2.1364	2.1027
	r_{OH}	78.8310	2.4459	2.5629

Harmonic Force Constants

Coordinate[b]		k_θ[kcal/(mol rad^2)] *cis*	*trans*
CH_3ONO	θ_{ONO}	184.269840	486.710671
	θ_{NOC}	253.424749	176.096657
	θ_{OCHi}	79.144297	101.941916
	θ_{OCHo}	85.726096	99.612315
	θ_{HiCHo}	76.773461	73.430016
	θ_{HoCHo}	71.618535	72.328566
HONO	θ_{ONO}	277.9544	249.179
	θ_{HON}	120.4446	107.2161

Cosine Series Coefficients [kcal/mol]

		a_o	a_1	a_2	a_3	a_4	a_5
CH_3ONO	ONOC[b]	5.099403	-0.045548	-4.43329	-0.431542	-0.169819	-0.520258
	NOCH	0.4397	0.0	0.0	0.4403	0.0	0.0
HONO[c]	HONO	4.8567	0.5745	-4.4298	-0.2544	-0.1185	-0.0129

[a] A. Preiskorn and D.L. Thompson Ref. 23.
[b] The subscripts i and o denote in- and out-of-plane hydrogen atoms.
[c] Y. Guan *et al.* Refs. 14 and 16.
[d] J.A. Darsey and D.L. Thompson Ref. 162.

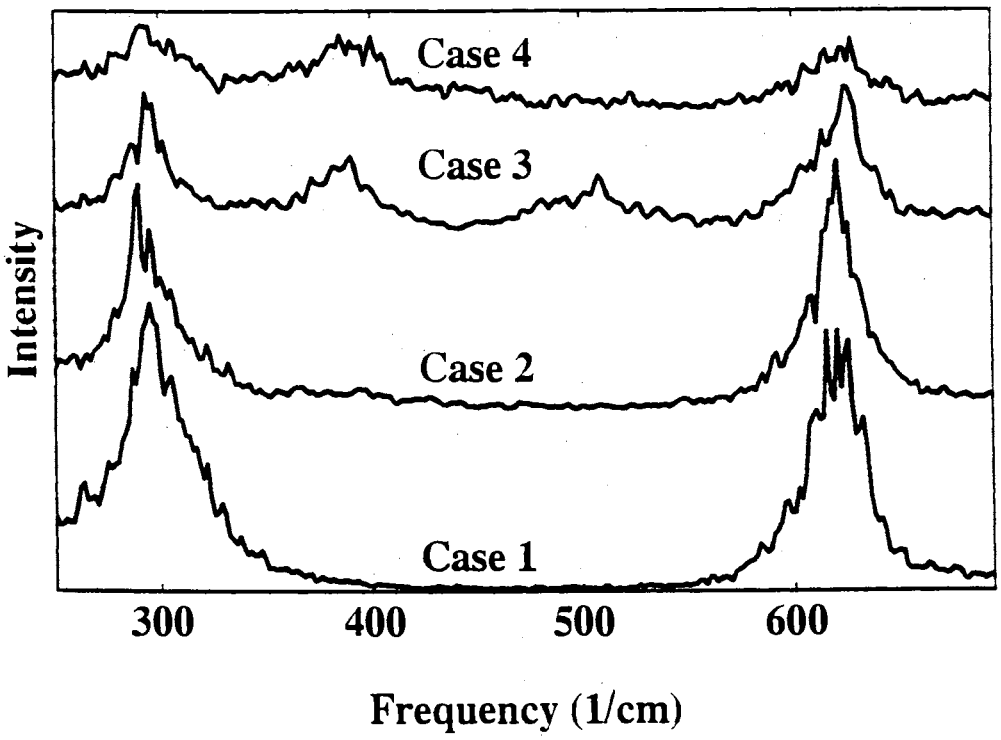

Figure 3. Composite power spectra for methyl nitrite for the frequency range 250-700 cm^{-1} , which comprises two normal modes for both the *cis* and *trans* conformers. Spectra for the four different types of ensembles (see Fig. 1 and Table I); the spectra are shifted for clarity. Case 1-3 illustrate the spectral changes due to increasing time spent in the *trans* well of the potential. Case 4 trajectories spend about the same amounts of time in the two wells as do the trajectories in Case 3.

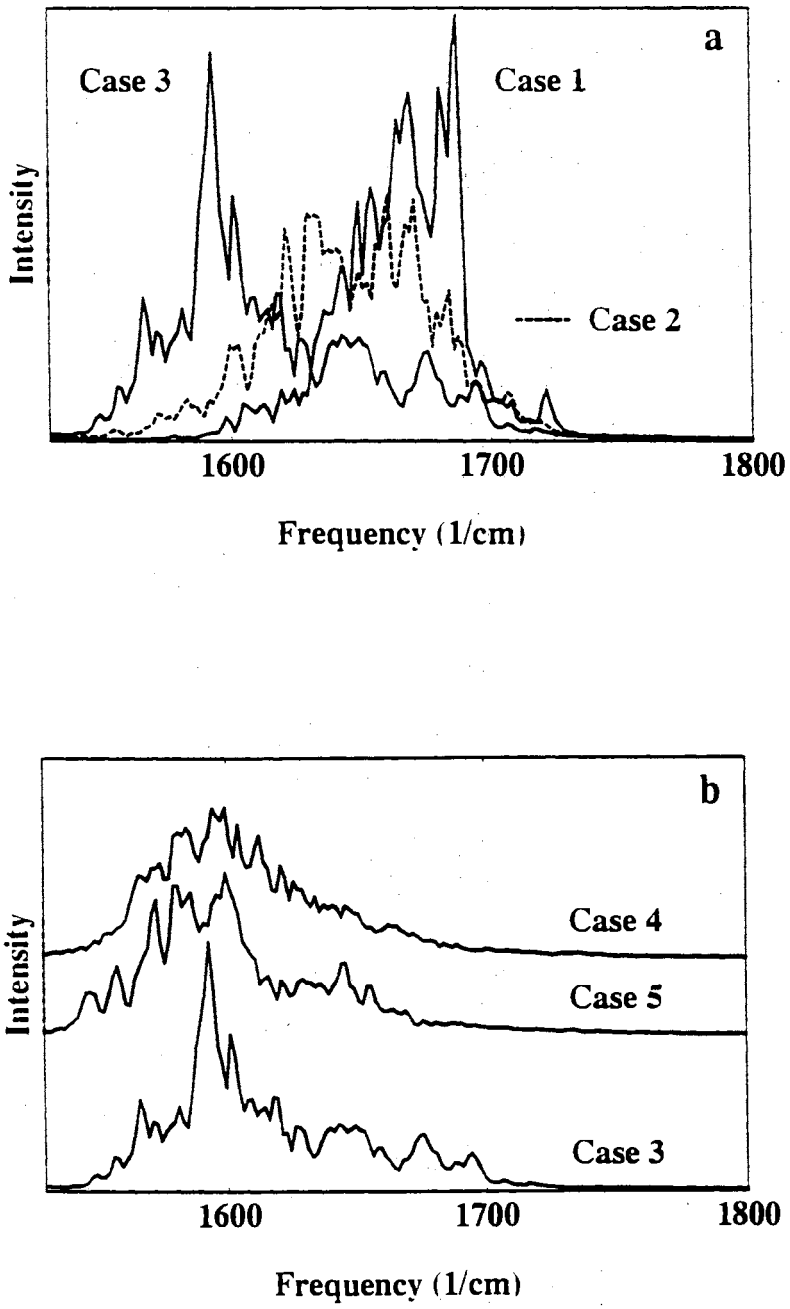

Figure 4. Composite power spectra for HONO for the frequency range 1500-1600 cm^{-1}. The structure in the spectra are due to the N=O normal mode in the *cis* and *trans* conformers. Power spectra Case 1-3 are shown in frame a and Cases 3-5 in frame b; see Fig. 1 for the ensemble characteristics for the various cases.

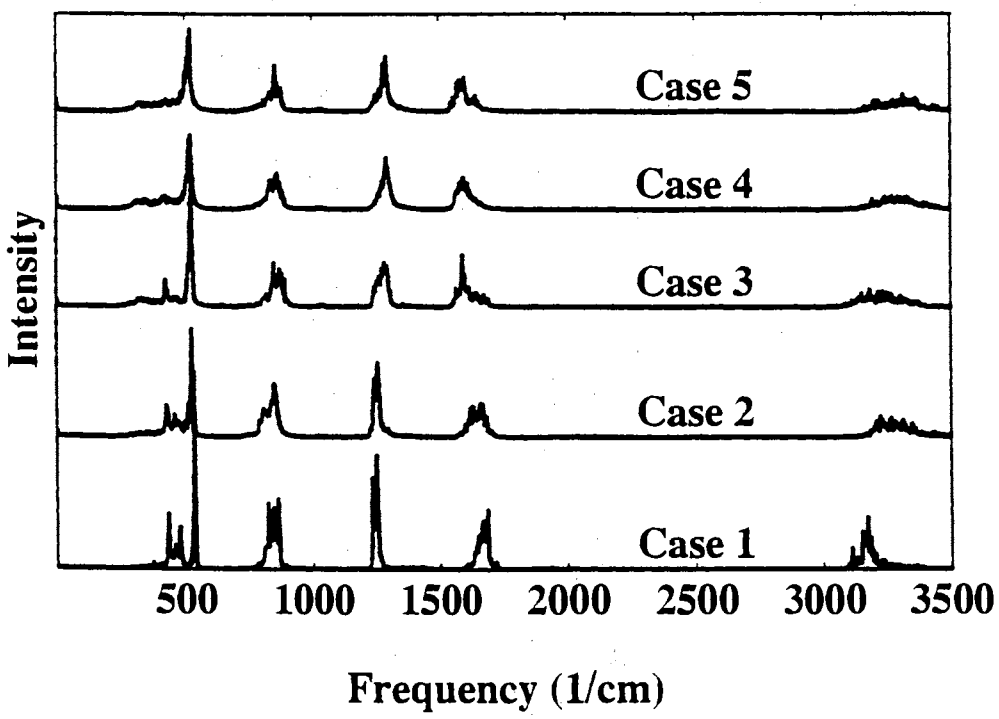

Figure 5. Composite power spectra for HONO.

CHAPTER V

EFFECTS OF MULTIPLE CROSSINGS OF A POTENTIAL-ENERGY BARRIER ON VIBRATIONAL MODE MIXING: CH_3ONO AND RDX

Introduction

Much has been written about the ramifications of chaotic dynamics for the statistical behavior of unimolecular reactions. While this may be a consideration for small polyatomics (e.g., triatomics), it is not clear that chaotic behavior is likely at the energies at which most reactions occur in "large" molecules. A more accurate picture for larger molecules is probably one of quasiperiodic behavior with sufficient "mode mixing" to cause statistical behavior in chemical reactions under ordinary conditions.[25] Therefore, it is important to understand the extent and causes of mode mixing in molecules that undergo unimolecular reactions.

Thompson and coworkers[9-23] have been trying to develop a better understanding of how intramolecular vibrational energy redistribution (IVR) relates to basic molecular structure and various features of the potential-energy surface by using classical trajectories to investigate IVR pathways and rates in various molecules. Here we extend these studies by exploring the effects of barrier crossings on mode mixing. We describe in Chapter IV some results of a classical trajectory study of vibrational mode mixing in polyatomic molecules due to passages through a transition state.[27] In this chapter, we report more extensive results on methyl nitrite and new

results on RDX.

Figure 6 is a schematic illustration of the basic idea we explore here. (Although our discussions, as well as our calculations, are classical, we have for the sake of illustration shown discrete contour levels in Fig. 6.) The two ovals represent two normal modes, each in a different conformation. For example, in our study one is a mode in the *cis* well and the other a mode in the *trans* well. We are interested in the question of whether a trajectory that begins in one well and then samples the other well for an equal period of time experiences as rapid IVR as does a trajectory that hops back and forth between the two conformations. Obviously, a trajectory that remains only one well will sample less phase space than a trajectory that samples both wells. But does a trajectory that samples both wells regularly sample more phase space than one that merely samples one well, isomerizes, and then samples the other well? Figure 6 illustrates a trajectory (in bold) which starts in one well, undergoes isomerization, samples the second well for a period of time, and then isomerizes back to the original conformation. Our premise is that the trajectory will not reenter the wells in the same regions of phase space from which it left, that is, it will "lose some memory" of where it was in phase space when it traverses the barrier. This leads to enhanced mode mixing.

A similar dynamical effect has been seen in other contexts. The Rössler[165] slow-manifold description of trajectorial flow might be another way of pictorially describing mode mixing due to sampling more than one set of normal modes. It has been used in describing the transition to chaos in the Belousov-Zhabotinskii

reaction.[166] The manifold is pictorially represented (see for example Fig. 1 in Ref. 165) as a plane with two stable branches folded into an "S" shape. One manifold is on the top part of the "S" and the other on the bottom. The two branches have different flowing orientations, analogous to different sets of normal modes. The "chaos-generation" is experienced when the flow is "reinjected" onto one of the branches after having spent a period of time flowing (at a different orientation) on the other branch. There is a direct analogy to the case considered here. We have studied *cis-trans* isomerization in methyl nitrite. The ONOC torsional angle is the reinjection variable. Reinjection of a trajectory repeatedly between two different potential-energy surfaces leads to a more rapid rate of IVR; the reinjection is a smooth transition between two different sets of normal modes. Similar to the Rössler[165] dynamics, classical trajectories experience "flow" with a particular orientation in the *cis* well and then are injected into the *trans* well where the flow is oriented differently.

Heller[159] has illustrated how electronic nonadiabatic transitions between two stable wells can lead to mode mixing. The idea can be understood in terms of Slater theory[167] since the "mode mixing" in the harmonic approximation results from hops between two Slater (i.e., normal mode) systems. Therefore, one can imagine a Slater trajectory with a fixed amount of energy in each normal mode. The trajectory is then interrupted by a transition at the crossing seam of the potentials. Now the trajectory evolves on the second potential, on which some (or all) of the normal mode vectors do not correspond to those on the first (ground-state) potential, until undergoing

another transition which puts it back on the first potential. Each time that the system returns to the ground-state potential following an "excursion" into a somewhat unrelated part of phase-space, a new Slater trajectory is initiated. This process causes "mode mixing." We are interested in examining the effect of recrossings on an adiabatic potential for which the transitions are not as abrupt as in the nonadiabatic case. Nevertheless, the basic effect on mode mixing should be quite similar to that discussed by Heller.

A number of studies have, at least indirectly, presented results that suggest the enhancement of mode mixing by passages through transition states. Cho *et al.*[155] studied HCN-HNC isomerization while searching for conditions leading to the transition to more rapid IVR, not just the threshold at which it occurs. They found not only that chaotic motion is associated with the hydrogen atom orbiting the CN radical (by alternating bonding to the carbon and the nitrogen atoms), but that chaotic behavior was not displayed without an associated orbiting motion occurring. Furthermore, they found that the energy redistribution is much faster when inserted directly into the bending (isomerization) mode. This study differs from ours in that the orbiting motion would be analogous to "hopping" (Heller's[159] description) at every crossing, or, in the case of a *cis-trans* system, being a free-rotor.

Zuhrt *et al.*[157] have studied IVR in HO_2, which undergoes isomerization, using a Fourier transformed dynamical variable. The resulting spectra showed that excitation of the isomerization mode above the isomerization threshold leads to broadened spectral peaks. This suggests that isomerization may enhance IVR, but

not conclusively, as the broadening could be due to greater IVR at the higher energy, rather than isomerization, or some combination of the two.

Ohmine and Tanaka[156] found a similar behavior in a system[168] of 64 nonvibrating water molecules. They examined the nature of the potential-energy surface at different "inherent" structures by using trajectory calculations. What they found could be interpreted as a correlation between mode mixing and "inherent" structures transitions. They concluded that the phase space covered by the trajectory expands significantly when an inherent structure transition occurs. It is obvious that if two different "inherent" structures, consisting of different sets of normal modes, are sampled, that the amounts of phase space covered by the trajectory would increase. While Heller's[159] study shows that mode mixing is enhanced by transitions between structures, the Ohmine and Tanaka[156] study illustrates an increase in the amount of phase space sampled but not an enhancement of mode mixing. In other words, this study is analogous to Heller's, but neither confirms nor denies that mode mixing is enhanced by transitions between different sets of normal modes--since repeated transitions between two different inherent structures was not the point of the study. In the present study, we show that the amount of phase space sampled in a system that undergoes transitions between two sets of normal modes is even greater than if both sets were sampled independently.

Remacle and Levine[69] have also discussed the concept of increasing the volume of phase space sampled by undergoing transitions. The context in which they discuss the phenomenon is when a molecule experiences "healing" (a bond breaking

and then reforming). They say that when a molecule crosses the transition state to the product region, and then recrosses back to the reactant region, it can reenter in a different region of phase space.

These studies suggest that IVR may be enhanced by isomerization, but do not conclusively illustrate it. They were not designed to do so. That is, they do not determine the causes of the IVR to be the repeated sampling of more than one set of normal modes. For example, in some of the studies the increased sampling of phase space, or "onset of chaotic motion," could be due to factors other than isomerization or the sampling of two sets of normal modes.

Eigen[82,83] suggested that if a reaction is fast enough, the vibrational line shape can be related to the reaction rate. However, Strauss and coworkers[84,169,170] have argued that it is difficult to determine the rate of reaction from the broadening of spectral lines because the rate of reaction is not fast enough (too much time is spent in the region of the barrier). On the other hand, Kreevoy and coworkers[85-88] and Cohen and Weiss[89-95] have reported rate constants determined from spectral lines.

Chapter IV contains the results of some trajectory calculations for HONO *cis-trans* isomerization which show that the time spent in the barrier region does contribute some to the broadening of spectral lines, but that the effect of mode mixing due to the repeated sampling of two different conformations causes power spectral broadening[27] (see Chapter IV). Here we present a more detailed study of the enhancement of mode mixing in methyl nitrite and RDX due to isomerization barrier crossings.

Molecular isomerization is discussed in Chapter I. Methyl nitrite undergoes *cis-trans* isomerization via rotation about the NO single bond. RDX, being a six-membered ring, undergoes an analogous process which involves interconversion among several configurations from one chair conformation to a another chair conformation.

Potential-Energy Surfaces

We have used potential-energy surfaces (described in greater detail in Chapters IV and VIII) for CH_3ONO and RDX based on anharmonic stretches (Morse functions), harmonic bends and wags, and truncated cosine series for the torsional modes.

The potential-energy surface for CH_3ONO has the analytical form of Eq. 7. It is the sum of 6 Morse functions for the bonds, 8 harmonic oscillators for the angles, and 2 six-term cosine series for two of the dihedral angles. The coefficients for the torsional potential about the NO bond are those calculated by Darsey and Thompson.[162] The barrier to rotation is 9.84 kcal/mol.

Since we initiate trajectories in the *cis* conformation, we constructed the global potential-energy surface based on the *cis* conformer. In other words, equilibrium geometries, frequencies, and normal mode compositions were used in fitting the *cis* and *trans* minima[27] (see Chapter IV), then we constructed the global potential-energy surface by basing it on the *cis* minima and attenuating those potential parameters which differ by more than 5% in the *trans* well.

Switching functions that depend on the ONOC angle were used to attenuate certain potential parameters as the system undergoes the *cis-trans* conversion. The force constants of the NO and OC bonds and the ONO, NOC, OCH, and HCH angles were attenuated using Eq. 20, where τ is the ONOC dihedral angle.

We constructed another, similar, potential-energy surface based on the *trans* minimum and attenuated the same parameters as in the "*cis*" surface. For this surface, Eq. 21 was used to smoothly connect the *trans* and *cis* parameters.

The RDX potential-energy surface will be described in detail in Chapter VIII, thus, we give only a brief description here. The analytical form, based on a valence force field, is that of Eq. 8. It is the sum of Morse functions for the 21 bonds, harmonic oscillators for the 36 bond and 3 wag angles, and six-term cosine series for 12 torsional angles. The barrier to ring inversion in RDX is not known, and estimating based on other ring systems would not necessarily be very accurate.[171] Therefore, we have used information available in the literature[171-174] on the modeling of the forces which are the main contributors to the barrier to ring inversion, mainly the angle and torsional strains. We obtained the force constants relating to these strains by fitting to experimental[173] and *ab initio*[174] vibrational frequencies.

The decomposition of RDX in the gas phase has two main reaction channels, simple NN bond rupture and concerted ring fission.[114] The ring fission reaction yields 3 CH_2NNO_2 molecules; this reaction channel was incorporated by using switching functions, which resulted in a barrier of 71 kcal/mol for concerted ring fission.[175] At the energies used in this study, decomposition of RDX did not occur. The forms

of the switching functions, parameters, and product potential-energy surface will be described in Chapter VIII. Although we have used a potential-energy surface with a 71 kcal/mol barrier to the ring fission reaction, it is not clear that this is realistic. We address this point in Chapter VIII. Computed reaction dynamics results on this surface indicate that this barrier is probably too high, but it is well suited for the purposes of this study. We find that a barrier height of 37 kcal/mol for the concerted ring fission yields branching ratios more reconcilable with experiment,[114] but the zero-point energy power spectrum is considerably broadened compared to both the spectrum generated from the surface with a barrier to concerted ring fission of 71 kcal/mol and a spectrum from a surface with all switching functions removed (see Chapter VII). Since the results will be in the form of power spectra, we have elected to use the surface which yields the "cleanest" (least band broadening) zero-point energy power spectrum.

The approach used to study the effects on power spectra of barrier crossings in RDX was slightly different from that for CH_3ONO and HONO[27] (see Chapter IV). Since RDX is so large, running hundreds of trajectories and saving all of the data necessary to sort the trajectories into cases and then computing fast Fourier transforms, as we did with CH_3ONO and HONO, would be computationally expensive, as well as require a prohibitive amount of disk space. Instead, we use the global potential-energy surface which includes the reaction channels and compare the results for this surface to those for a surface with higher ring torsional barriers. We ran an ensemble of 40 trajectories at the zero-point energy with a barrier of 0.36

kcal/mol for the CNCN and NCNC torsions and computed power spectra. Then, we ran a second ensemble of 40 trajectories, again at the zero-point energy, with a barrier of 10.69 kcal/mol for the ring torsions and calculated power spectra for this ensemble. The values of the cosine series coefficients for the two different torsional barriers are given in Table V. The higher barrier for the CNCN and NCNC torsional potentials leads to fewer conformational transitions. We plotted the Cremer-Pople[172,176] coordinates for several trajectories from each ensemble in order to ascertain that the higher torsional barrier inhibits ring inversion.

Of course, changing the torsional barrier changes the normal mode frequencies. Table IV contains the values of frequencies computed for the two surfaces as well as the experimental[173] and *ab initio*[174] frequencies. The higher torsional barrier is aphysical and results in dramatic shifts of some of the frequencies. Most are raised only a few or 50 to 60 cm^{-1}. The large shift in the frequency of one mode (ring) to 1869 cm^{-1} on the surface with the higher barrier is due to a much higher force constant. Usually one expects the torsional motion to be a normal mode.[101] Thus, usually changing the shape (and here, the frequency) of the torsional potential does not affect the other modes. RDX, however, is quite complex and thus the composition of a normal mode usually involves a number of the internal coordinates.[174] This causes most of the frequencies to be affected by a change in the shape of the torsional potential. The resulting difference in the zero-point energies is small, 81.1 and 84.0 kcal/mol for the low and high barriers, respectively.

Calculations

The general classical trajectory code GenDyn[124] was used to calculate the trajectories. Hamilton's equations of motion are integrated by using a fourth-order Runge-Kutta-Gill routine in a space-fixed Cartesian coordinate system. Integration step sizes of 1.5×10^{-16} and 1.0×10^{-16} s were used for CH_3ONO and RDX, respectively. The trajectories were calculated for 10 ps. Normal mode frequencies for CH_3ONO and RDX (see Chapters IV and VIII) were computed using analytical second derivatives of the potential.

Initially two quanta of energy were placed in each of the three C-H normal modes and zero-point energy in all other modes, using the method described by Bintz *et al.*,[11a,120] for a total energy of 80.4 kcal/mol for the methyl nitrite calculations. This choice of initial conditions is arbitrary. Excitation of the three C-H normal modes to this energy produces a satisfactory range of dihedral angle time histories for 10 ps trajectories. In other words, we get a reasonable number of trajectories which do not isomerize, a reasonable number which isomerize often, and a reasonable number in between. Other kinds of initial conditions were used and gave similar results. The RDX calculations were run with the zero-point energy in all modes, for a total energy of 81.1 and 84.0 kcal/mol of total energy for the torsional barrier heights of 0.36 and 10.69 kcal/mol, respectively.

We began the CH_3ONO study by calculating a large ensemble of classical trajectories for a particular set of initial conditions. This ensemble was then divided into smaller ensembles based on the behavior of the isomerization coordinate of the

individual trajectories in order to isolate some of the various effects that complicate the spectra and cause line broadening. Power spectra were computed for these ensembles by Fourier transforming ensemble-averaged autocorrelation functions of the internal coordinates.

Since there are several factors which can affect the spectra, such as anharmonicity and other couplings which induce "ordinary" IVR, time spent in the barrier region, and mode mixing induced by sampling more than one set of normal modes, we computed spectra for ensembles of trajectories with specific behaviors to illustrate the relationships between trajectoral behavior and the spectra. The parameters used to define the different types of ensembles are given Table I. Case 1 trajectories sample only the *cis* well. Cases 2 and 3 undergo a few barrier crossings. The difference in the two is that Case 3 trajectories spend more time in the *trans* well. The amounts of time spent in the two wells in Case 4 is about the same as in Case 3, but the number of barrier crossings is significantly larger in Case 4. See Chapter III for more discussion of the types of information that ensemble sorting can provide.

Power spectra were calculated by Fourier transforming[127,128] ensemble-averaged autocorrelation functions of internal coordinates. Composite spectra were calculated by summing the individual internal coordinate spectra. Time histories of the isomerization coordinate were stored and the trajectories sorted into different cases as defined in Table I. Power spectra were computed for ensembles consisting of 40 trajectories of each case.

Time-delay mappings were plotted for methyl nitrite in order to further elucidate the changes in phase space samplings due to the effects of isomerization. See the Methods chapter for more details on time-delay maps.

RDX is a much larger system, 21 atoms, hence a similar procedure to that used for CH_3ONO would be far more computationally expensive. Instead, we used two different barriers heights for the ring (CNCN and NCNC) torsions, one which is reasonable for RDX (see PES discussion in Chapter VIII) and another much larger, so as to inhibit isomerization and therefore conformational interconversion.

Results and Discussion

We have examined the dynamics of methyl nitrite and RDX as they undergo barrier crossings by using power spectra. First, we will present and discuss the results for *cis-trans* isomerization of methyl nitrite since they are simpler. The conformational changes in RDX are much more complicated and the number of normal modes greater (57 in RDX, compared to only 15 in methyl nitrite), thus the power spectra are more complicated. While the methods of our studies for the two systems differ (case sorting for CH_3ONO and varying the stiffness of the ring for RDX), the conclusions are similar, and the different designs of the studies compliment each other (e.g., the values force constants change as the system crosses the barrier in CH_3ONO , whereas they do not in RDX).

A. Methyl Nitrite

By using plots of the isomerization coordinate (the torsional mode in CH_3ONO) as a function of time we can illustrate the barrier crossings which the molecule undergoes. Thus, these plots are examples of time histories of typical trajectories used in the various kinds of ensembles (see Table I).

Figure 7 contains time histories of the ONOC angle for some of the individual trajectories. The histories vary in both time spent in each conformation and in the number of isomerizations. They are arranged in Fig. 7 such that going left to right the number of crossings increases, and going top to bottom the time spent in the *trans* configuration increases. Since moving down the columns corresponds to increasing the amount of time spent in the *trans* well, power spectra would be expected to have increasing intensities of *trans* peaks and decreasing intensities of *cis* peaks. The trajectory in panel a, for instance, does not spend any time in the *trans* conformation, whereas the trajectory in panel d spends a small amount of time in the *trans* well. (Power spectra of these trajectories were calculated but are not shown here; however, we discuss the spectral trends which are observed.) Therefore, the power spectrum of the trajectory in panel d is "grassier" than that of the trajectory in panel a. While this might appear to be due to an increase in IVR (and it is to some extent) the spectrum of (d) will appear "messier" because the number of frequencies sampled is doubled and the intensities of the *cis* peaks will decrease in comparison to those in (a). If the peaks do not broaden, then IVR has not notably increased. The intensity of a peak is proportional to the time that mode is sampled,

that is, the time spent in the conformation with that mode.

A distinction should be made between broadening and intensity changes in the power spectra. If a peak broadens (comparing half-widths at half-height) the rate of IVR has increased. Intensity changes, on the other hand, should not be taken to indicate changes in the rate of IVR, since changes in the amounts of time spent sampling the two sets of normal modes will affect the intensities of the peaks. (*Id est*, if 80% of the ensemble time is spent in well I and 20% in well II, peaks corresponding to well I will have greater intensity than those for well II. Now, if 30% of the ensemble time is spent in well I, the peaks corresponding to well I will have decreased in intensity, as compared to the spectrum from the ensemble with 80% of the time spent in well I. This sort of intensity change does not indicate a change in the rate of IVR.)

Moving across Fig. 7 the corresponding power spectra broaden, since this corresponds to keeping the relative time in the two wells constant and increasing the number of isomerizations. It is this effect in which we are interested. Yet we must be aware of both effects upon the spectra so as not to confuse an increase in the number of peaks (and decreases in intensities) with spectral broadening. The "cases" defined in Table I are designed to differentiate between variations in the spectra due to the time spent in the two wells and spectral broadening due to barrier crossings. Examples of isomerization time histories of Cases 1, 2, 3, and 4 trajectories are shown in Fig. 7, panels a, d, g, and i, respectively. Comparing power spectra of Cases 1, 2, and 3 should show changes in peak intensity due to variations in the ratio of

time spent in the two wells. Comparison of Cases 3 and 4 should illustrate spectral changes (broadening due to enhanced IVR) from an increased rate of isomerization.

Internal coordinate and composite power spectra for Cases 1 through 4 (see Table I) are shown in Figs. 8-12; Figs. 8, 9, and 10 contain the N=O, O-N, and O-C bond spectra, respectively, Fig. 11 contains the NOC angle spectra, and Fig. 12 contains the composite power spectra. Since these spectra are for 80.4 kcal/mol total energy the frequencies are shifted from the fundamentals. The arbitrarily assigned normal mode numbers and internal coordinate compositions,[37] the frequencies calculated by using analytical second derivatives of our potential,[3] and the frequencies obtained from the power spectra at 80.4 kcal/mol (Figs. 8-12) are listed in Table VII. In the following discussions when we refer to frequency values, they are the approximate values obtained from the power spectra.

We are interested in the general trends in intensity changes and spectral broadening going from case to case (see Table I). Going from Cases 1 to 2 shows a slight decrease in intensity of the *cis* peaks and the appearance of *trans* peaks (see Figs. 8-12). At some frequencies the intensity changes are very small, however, the changes become more apparent in the Case 3 spectra where there is less difference in the *cis* and *trans* sampling times than in Case 2. The trajectory times in the *trans* well are on average 0, 7.1, and 40.9% for Cases 1, 2, and 3. Thus, we expect that in going from Case 1 to 2 to 3, a progressive increase in the intensities of the *trans* conformation peaks and a corresponding decrease in the intensities of the *cis* peaks. For some modes this effect is quite clear, while for others it is less so because the *cis*

and *trans* peaks are very close in frequency and because of the "ordinary" broadening (which occurs without isomerization) that exists at this energy.

Of course the differences in the Cases 1 and 2 spectra could be attributed to both the differences in well sampling times and the fact that Case 1 does not isomerize while Case 2 does. Spectra for Case 3, for which the trajectories isomerize nearly the same number of times as those in Case 2, illustrate changes due to different amounts of time spent in the two wells. Results for Case 4, which spends the same percentage of time in the two wells as Case 3 but isomerizes many more times should show spectral broadening caused by traversing the barrier. In other words, Case 1 provides useful reference spectra where broadening is not due to isomerizations, but merely to "ordinary" IVR. Cases 2 and 3 illustrate the changes in the spectra due to differing percentages of time in the two wells since they are for about the same number of crossings. Finally, comparison of Cases 3 and 4 show the changes in the spectra due only to barrier crossings since the sampling times of the two wells are about the same in both cases.

We now examine the spectra for the individual coordinates (Figs. 8-11). We present spectra from all four cases in a single panel for easy comparison; they are shifted for clarity. The various bands in the power spectra behave differently for the different ensembles. For example, some are hardly affected by isomerization, while others are strongly affected. This is to be expected because of the different couplings and symmetries of the various modes.

We can see the effects from the sorting of trajectories into cases as we have

described by examining power spectra calculated for the four ensembles. Reference to Table VII is necessary to interpret the spectra. It contains arbitrarily assigned mode numbers and the experimentally derived normal mode compositions.[161] In Table VII we also list the approximate peak locations (frequencies) obtained from the computed power spectra shown in Figs. 8-11 (peaks are slightly shifted due to anharmonicities) and the frequencies obtained by performing a normal mode analysis on our potential, (which matched a low energy power spectrum). We only list those modes which pertain to our discussion of Figs. 8-11 in Table VII; the reader is referred to Table III for a full listing of the frequencies computed on our potential-energy surface and to Ref. 161 for a listing of all of the normal mode compositions.

We begin by looking at the power spectra for the N=O bonds shown in Fig. 8. This peak is about the same for the four ensembles. The *cis* and *trans* frequencies (see Table VII) for this mode are separated by only about 50 cm^{-1}. From the normal mode compositions,[161] (see Table VII) we can see that the N=O bond participates in mode number 12 (which comprises ν(N-O), ν(N=O), and δ(NOC) motions[161]) and the N=O normal mode (not listed in Table VII) in the *cis* well, and only in the N=O normal mode (not listed in Table VII) in the *trans* well. The very short peak at approximately 620 cm^{-1} corresponding to the *cis* mode decreases in intensity going from Case 1 to Case 4. This series illustrates that some modes are not significantly affected by the differences in the behavior of the ensembles.

On the other hand, the spectra shown in panel b of Fig. 9 (N-O bond spectra) illustrate the trends discussed above (intensity changes as sampling time varies and

enhanced IVR due to the repeated sampling of more than one set of normal modes). A comparison of Cases 1 and 2 shows decreases in the peaks centered at approximately 295, 620, and 770 cm^{-1}. There is also the appearance of *trans* peaks in the Case 2 spectrum at 390, 510, and 745 cm^{-1}, however, they are very weak because the time spent in the *trans* well is only 7% of the total ensemble time. For instance, the "peak" at 510 cm^{-1} could be interpreted as a raising of the baseline in Case 2, but in Case 3 has become a distinguishable peak. The "raising" of the baseline in Case 2 (in the region between the two tall peaks), would usually be interpreted as due to increased irregular motion. However, in this case the entire baseline is not raising, rather a peak with very low intensity (nearly negligible when compared to the baseline "noise") is present due to sampling the *trans* well. In the spectrum for Case 3 the peak intensity has greatly increased. The peaks at 390 and 745 cm^{-1} have become more intense as well. There is dramatically greater broadening of the peaks in Case 4 compared to Case 3. These spectra are for the same initial conditions. The difference is that the Case 4 spectrum is for trajectories that undergo more isomerizations on average than those in Case 3.

Interesting behavior is displayed by the peaks in the range 745-770 cm^{-1}. It appears that there is a single peak which broadens, narrows, and then significantly broadens as it slightly red shifts. However, this is misleading. The *trans* peak is red shifted by 25 cm^{-1} from the *cis* peak. The apparent broadening in the Case 2 spectrum is due mainly to the lowering of intensity of the *cis* peak and the appearance of the (lower frequency) *trans* peak since the trajectory spends time in

both conformers. Since the two peaks are so close in frequency, they are not well resolved. The *trans* peak is more intense than the *cis* peak (which we know from individual spectral studies of each conformer). Thus, in Case 3, which samples the two wells more equitably, the *trans* peak essentially washes out the *cis* peak (seen in Case 1 approximately 25 cm^{-1} higher in frequency). The changes seen here are due to varying the ratio of the trajectory times in the two wells. In the Case 4 spectrum this peak is not much more than a grassy band that almost blends into the baseline.

The power spectra of the OC bond are shown in Fig. 10. Strong peaks appear at 620, 770, and 865 cm^{-1}; little, if any, intensity is lost in going from 100% to 93% *cis* sampling, Cases 1 and 2, respectively. These correspond to modes 12, 11, and 10, respectively, in the normal mode assignments (compositions of 11 and 10 include the CO bond). The trajectories in Case 3 spend 59% of the time in the *cis* well resulting in a noticeable decrease in the peak intensities but no significant broadening compared with Cases 1 and 2. In Case 3 there is the appearance of two *trans* conformation peaks at 390 and 510 cm^{-1}.

Case 4 of Fig. 10 shows broadening in all of the peaks, *cis* and *trans*, as compared with Case 3. The peaks centered at 390, 620, and 745-770 cm^{-1} are still discernable, but have broadened. The *trans* peak at approximately 510 cm^{-1} is lost in the noise at the baseline. The time spent in the two wells is the same as in Case 3, but the Case 4 trajectories isomerize more, thus, mixing the motions more rapidly than in Case 3 trajectories. The result is broader power spectrum peaks. This qualitatively illustrates that increasing the "reaction" rates increase the widths of the

peaks.

Figure 10 shows the same effect seen in the NO spectra (Fig. 9) in the 745-770 cm^{-1} region. What might seem to be a single peak that is red shifted in the region 745-770 cm^{-1} is really the two, unresolved, modes in the *cis* and *trans* wells. The "shifting" is due to the fact that the *trans* peak, which increases in spectral representation, is at a lower frequency that the *cis* peak. Also, note that both the NO and the OC bonds are involved in the normal modes 11 (Table VII) in the two conformations.

From the normal mode compositions in Table VII, it can be seen that the NOC angle "participates" in modes with power spectral peaks at 295 and 620 cm^{-1} in the *cis* well. NOC angle power spectra, shown in Fig. 11, contain clean *cis* peaks at 295 and 620 cm^{-1} which decrease in intensity in going from Cases 1 through 3. However, they do not broaden. There are three, broader peaks in the range 770-1000 cm^{-1} which decrease in intensity going from Case 1 to 3 and are lost in the baseline in Case 4. Since these three peaks are broader initially (as seen in the reference spectrum of Case 1) the effects which we describe, while they can be seen, are not nearly as clear as those seen in the peaks which are cleaner initially.

A "raising of the baseline" is seen in Case 2 between the two *cis* peaks, similar to what was seen in the NO spectra (panel b). This is caused by the sampling of two *trans* modes which becomes more evident in Case 3. The relatively clean *trans* peaks are centered at approximately 390 and 510 cm^{-1}. Case 3 has four distinguishable peaks from 295 to 620 cm^{-1}--two *trans* peaks are flanked by two *cis* peaks. In Case

4, all four of these peaks are broadened considerably. In fact, the 510 cm^{-1} peak loses all structure and becomes part of the grassy baseline in Case 4.

The composite power spectra, which are sums of all of the bond, angle, and torsional coordinates (which comprise 15 modes), illustrate the same trends. Composite power spectra for all four cases are shown in Fig. 12. Since these spectra are sums of all of the coordinate spectra, they are more complicated to analyze than are the individual coordinate spectra. For example, if an individual coordinate spectrum has structure in a particular region and another is very grassy in the same region, then in the composite the grassiness may wash out the structure of the first. This, of course, depends on the relative intensities of the structured and "unstructured" portions of the overlying spectra.

To simplify the discussion of the composite spectra, we break them up into four regions: Regions I: 0-280 cm^{-1}, II: 280-650 cm^{-1}, III: 700-830 cm^{-1}, IV: 1250-3050 cm^{-1}. The composites are considerably more complicated than the internal coordinate spectra; at first glance, even Case 1 (the ensemble which samples only one of the conformers) looks quite grassy. Yet closer inspection of all the composite spectra of the cases reveals that the trends seen in the internal coordinate spectra can also be seen in them; for example, it is clear that spectral broadening is enhanced by isomerizations.

Region I initially (Case 1) has a single *cis* peak. A *trans* peak at a slightly higher frequency has emerged in Case 2; these two peaks (the *cis* peak, originally identified in Case 1, and the *trans* peak, identified in Case 2) are barely resolvable.

In Case 3, the intensities of the peaks are nearly equal to each other and they do not appear to have broadened compared to those in Case 2. In the Case 4 spectra the peaks have broadened enough so that they are no longer distinguishable.

Region II consists of two peaks due to each conformer (see Fig. 3, Chapter IV for an expanded plot of this region). Case 1 serves to show the two *cis* peaks. In Case 2 the baseline between them *appears* to raise a bit. This is not truly a raising of the baseline, but rather is from the two *trans* peaks which emerge more fully in Case 3. The *cis* peaks decrease in intensity, without significant broadening, in going from Case 1 to 2 to 3. This is expected since less time is spent sampling these frequencies as the case number increases, correspondingly the *trans* peaks increase in intensity as the percent of time in that well increases. Case 4 peaks are broader than the Case 3 peaks even though the two cases spend approximately equivalent amounts of time in the two wells. Again, the power spectra indicate an increase in the rate of IVR due to an increase in isomerization.

Region III contains the peaks at 745 and 770 cm^{-1}. Changes in the peak (the two are not resolved) from Case 1 to 3 consist of a slight decrease in intensity and slight red shifting. The slight intensity decrease can be attributed to the peak intensity being split between two modes (separated by only approximately 25 cm^{-1}). Since the peaks are close in frequency and rather broad, they appear as one. The apparent slight "red shifting" is due to the fact that peaks are close in frequency, and changes in the intensities (due to changes in the times spent in the two wells) lead to a shifting of the center of the peak. This gradual addition (as the cases change)

of lower frequency *trans* intensity in the spectrum causes the single peak to "shift" to a slightly lower frequency. The bands in Cases 2 and 3 are broader than in Case 1, showing that the "single peak" in Cases 2 and 3 is really two very close peaks. What appears to be a broad peak is really two peaks which are close in frequency.

Region IV is virtually unchanged in all four cases. These modes, numbered 1-7,[161] consisting mainly of methyl motions (and the N=O local mode), do not show mixing effects due to isomerization. The internal coordinate spectra of the CH bonds, HCH and OCH angles, and NOCH torsions (not shown) change less than those presented here. This is evident in the composite power spectra.

Similar results were observed at other energies and initial excitations. For instance, we computed some spectra for ensembles in which the energy was directly inserted into modes which are affected by isomerization. For example, we equally partitioned an equivalent amount of energy into *cis* modes 8 and 12 (see Table VII). The results lead to the same conclusions as those presented above.

We also performed a few calculations at the zero-point energy (29.08 kcal/mol). If the zero-point energy is correctly distributed among the modes, the number of isomerizations is negligible. Thus, we inserted all of the zero-point energy into the torsional mode and essentially no energy into all the other modes (n=-0.49999). While we realize that it is aphysical to partition nearly all of the zero-point energy initially in a single mode, it leads to much cleaner spectra since the low energies among the other modes results in negligible mode mixing. The results of these calculations show the same trends and conclusions as discussed above.

Since it is known that energy transfer in the *trans* configuration is slower than in the *cis* conformer,[14] we also calculated trajectories similar to those used to generate the spectra in Figs. 8-12 but by starting the trajectories in the *trans* geometry. For these calculations, we altered the potential-energy surface as well. Since our intention was to initiate the trajectories from the *trans* conformation, we used the "*trans*" potential-energy surface as described in Sect. II. These spectra were *slightly* cleaner than those in Figs. 8-12. This is expected since the IVR is less in the *trans* well than the *cis* well,[23] and if the ratios of the time spent in each conformer favor the *trans* well, cleaner spectra should result. The *trans*→*cis* results confirm the conclusions reached on the basis of the *cis*→*trans* results.

It could be argued that the observed effects are due to potential couplings resulting from the switching functions in the potential. Yet a comparison of the coordinates and the percentage change in the corresponding force constants demonstrate that switching is not as big a factor as the crossing of the transition state. The power spectra of the NO, OC, ONO, and NOC internal coordinates all show broadening that is proportional to isomerization. The N=O (see Fig. 8) and ONO (not shown) coordinate spectra of Cases 3 and 4 show less dramatic broadening than the other internal coordinate spectra. If the grassiness and broadening seen in the power spectra were due to changes in the force constants (i.e., by the switching functions), then one would expect the force constants of these two coordinates to change less than the others. This is not the case. The N=O bond experiences no switching, and the ONO angle changes by 164%. Whereas the NO, OC, and NOC

coordinates switch by 31, 18, and 30%, respectively. Therefore, it does not appear that the changes in force constants is a significant factor in the mode mixing that results from isomerization.

Thus, we have illustrated that several factors contribute to broadening in power spectra of an isomerizing molecule. The power spectra show that barrier crossings increase the volume of phase space sampled. This is further illustrated by time-delay mappings of several of the internal coordinates of CH_3ONO.

The top two panels (a and e) of Fig. 13 contain the time histories of the isomerization coordinate, the ONOC dihedral angle, for methyl nitrite. The time history in panel a shows that this trajectory does not isomerize in the 5 ps calculation time, whereas the one in panel e undergoes 17 isomerizations. In order for the IVR due to factors other than those related to barrier crossings to be roughly equivalent we select sampling times from only the *cis* well for making the plots. For the time-delay mappings we plotted an internal coordinate verses itself 3 fs later for the time ranges of 3.94-4.14, 4.346-4.446, and 4.56-4.76 ps; all the points for these three sampling times are included in the same mapping. The plots for both trajectories are for times in *cis* conformer space, the difference in the two is that for the three sampling time-periods the isomerizing trajectory (panel e) has just entered the *cis* space, whereas the other trajectory (panel a) remains in the *cis* well throughout. Mappings for these two trajectories are shown below the dihedral angle time histories; panels b-d and f-h correspond to the trajectories with the time histories shown in panels a and e, respectively.

The mappings in Fig. 13 are for the N=O (panels b and f) and N-O (panels c and g) bonds and ONO (panels d and h) angles. In comparing the mappings of the trajectory that undergoes isomerizations to those for the trajectory which does not, it is quite apparent that the former samples a greater volume of phase space than the trajectory which never visited the second well. In general, isomerization produces mappings with less structure in the elliptical curves.

Consider the N=O bond mapping, shown in Fig. 13 b and f. The power spectra of this coordinate (Fig. 8) show the least deterioration of structure compared to the other internal coordinate power spectra. Both mappings are elliptical, but the trajectory which undergoes barrier crossings produces a time-delay mapping (panel f) which shows that it covers more coordinate space than the trajectory which never leaves *cis* space (panel b). There is more structure (elliptical shape) in the mappings of the N=O bond generated from *both* trajectories than in any of the other internal coordinate mappings. This is in accord with the power spectral results for this coordinate which show less change upon isomerization than the other internal coordinate spectra. However, the mapping in panel f is less dense than that in panel b, illustrating a more rapid exploration of space when the molecule undergoes barrier crossings.

The next four panels in Fig. 13 illustrate the deterioration of structure more vividly. Panels c and g contain mappings of the NO bond for the non-isomerizing and isomerizing trajectories, respectively. As in the N=O comparisons, the NO bond mapping from the non-isomerizing trajectory is more dense than the mapping from

the isomerizing trajectory. There is, in this case, also less structure as well. The elliptical paths are not retained as well in the NO mapping comparisons as well as they are in the N=O mappings; notice how the center of the mapping in panel g is "filled in," whereas it is not in the mapping in panel f. The N=O mapping shows a retention of regularity, with increases in the values of the maximum and decreases in the values of the minimum bond lengths sampled. On the other hand, the NO mapping of the isomerizing trajectory samples a broader range of bond lengths and loses structure as well compared with the mapping of the non-isomerizing trajectory.

The ONO angle mappings, panels d and h, show similar behavior. The mapping for the trajectory which did not isomerize, panel d, is elliptical in shape, whereas the mapping from the isomerizing trajectory, panel h, is more irregular (less elliptical).

The other internal coordinate mappings show similar trends. Mappings from the *cis* well of the trajectory which had previously spent time in the *trans* well contain less structure and sample more space than those mappings produced from the trajectory which resided in the *cis* well for the entire time.

B. RDX

As discussed in Sect. II of this Chapter, the potential-energy surface of RDX and its processes (conformational changes and chemical reactions) are rather complicated. The molecule undergoes reaction through two main reaction channels, simple NN bond rupture and concerted ring fission. (Although reaction does not

occur at the energies used in the present study.) Adding to the complexity of this molecule is the fact that it can undergo conformational changes; the six-membered carbon and nitrogen ring can interconvert between chair and boat and all of the conformations in between. See Wallis and Thompson[172,177] for more details on the conformational changes of RDX. Cremer and Pople[176] give a description of the coordinates that can be used to monitor ring inversion.

The RDX calculations complement those for methyl nitrite and HONO. The conformational changes in RDX do not involve switching functions which are dependent on the isomerization coordinate. In other words, there is no anharmonicity introduced into the potential-energy surface with switching functions that are dependent on the CNCN torsional motion. There are switching functions associated with the reactions in the potential-energy surface, but we have shown elsewhere that they have very little effect on IVR at the energy used in this study (see Chapter VII).

The ensembles were calculated at the zero-point energy. Since the calculations are classical, isomerizations occur at the zero-point energy on the surface with the low barrier to ring inversion.

Figure 14 contains power spectra computed from the ensembles for the low and high barriers to ring inversion. Panels a, c, e, and g are for the low barrier. At this energy (81 kcal/mol) ring isomerizations occur frequently. Panels b, d, f, and h contain spectra obtained from the ensemble calculated on the surface with the higher torsional barrier. When the barrier is higher, and isomerization hindered, the power

spectra are notably cleaner (indicated by a lower baseline and sharper peaks) than when the system is more readily allowed to isomerize.

As noted in Section III, the zero-point energies of the two surfaces are close, but not identical. The total energies of the trajectories in the ensemble calculated on the surface with the higher barrier is 84.0 kcal/mol while that for the lower barrier potential is 81.1 kcal/mol. Thus, it is interesting to note that while the energies are about the same, the spectra for the trajectories which do not isomerize are significantly cleaner.

Effects due to barrier crossings similar to those seen in the CH_3ONO and HONO spectra (see Chapter IV) can be seen in the RDX composite power spectra. Panels a and b of Fig. 14 show the composite spectra from the low and high barriers, respectively. There are several very important points to note when comparing these two power spectra. The peaks in the spectrum in panel b (for the higher barrier) are slightly higher in frequency than those in the panel a spectrum. The ensemble which readily isomerized has a higher baseline, which indicates more energy transfer is occurring at the zero-point energy than in the ensemble in which isomerization is hindered. The peaks of the spectra in panel b are sharper (comparing half-width at half-height) than those in panel a, again, indicating that spectral broadening is enhanced when the system isomerizes more often. Note that in the region of the high frequency CH modes (around 3000 cm^{-1}) more definition can be seen in the panel b spectrum than in the one in panel a. This illustrates that ring inversion enhances the broadening of the CH modes, with cleaner modes being produced from

the ensemble in which ring inversion is hindered. (Differences due to X-H stretching motions were not observed in the CH_3ONO or HONO spectra, see Chapter IV.) There is a peak around 1850 cm^{-1} which appears in the panel b spectrum, but not in the panel a spectrum; it is due to the large torsional frequency shift. The peaks from 500-750 cm^{-1} are significantly more resolved for the ensemble computed on the surface with the higher barrier where isomerization is hindered. Many of the peaks from 900-1600 cm^{-1} are sharper (comparing half-widths at half-height) in the spectrum for the higher barrier ensemble (panel b) than the one for the lower barrier (panel a).

The comparison of the two ensembles is easier if we use internal coordinate spectra rather than the composite spectra. Thus, we will consider some related modes. Panels c and d show summed NCN angle spectra, (the 3 NCN internal coordinate power spectra were summed). The most dramatic differences in these spectra are the two peaks centered at approximately 600 and 975-1000 cm^{-1}. These two peaks are the most intense in both spectra, indicating the modes with the strongest NCN angle participation. Both of these peaks are sharper when isomerization is hindered. This illustrates that there is a decrease in spectral broadening when the ring is not allowed to readily isomerize. The differences in the spectra are quite similar to those in the Case 3 and 4 spectra in CH_3ONO and HONO, see Chapter IV, where the *cis-trans* isomerization rate is varied.

The C_2N-N wag spectra (obtained by summing the spectra of the 3 wags) shown in panels e and f of Fig. 14 (for the low and high barrier potentials,

respectively) contain similar features to those described for the NCN angle spectra (panels c and d), as well as a highly shifted peak at approximately 1850 cm^{-1}. The baseline of the spectrum for the ensemble in which isomerization readily occurs (panel e) is much higher than that in the other spectrum (panel f), and the peaks are sharper in the panel f spectrum than in the one in panel e. As mentioned briefly in the discussion of the composite spectra, there is a peak around 1850 cm^{-1} which appears in the spectrum in panel f, but not in the panel e spectrum.

Even the low frequency CNNO torsional spectra (which contain less structure to start with due to "ordinary" IVR) show differences based upon the barrier crossings. The CNNO summed torsional spectra for the low and high barriers are shown in panels g and h, respectively. At first glance, this pair of spectra might seem to show effects opposite to those seen in the other internal coordinates. The peak centered at approximately 200 cm^{-1} in the spectrum in panel g is less intense than the one in panel h. What is important to note, though, is that the half-width at half-height of this peak is actually smaller in the panel h spectrum than in that in panel g, which indicates less IVR in the predominately CNNO modes with essentially frozen ring torsions.

As discussed at the end of Sect. II of this Chapter, there is some shifting of the bands due to the change in the torsional potential. The dihedral angle spectrum (τ_{CNCN} and τ_{NCNC}), not shown, reveals sharp peaks at many of the frequencies seen in the composite. We attribute this to resonances. Some of the sharpening of peaks seen in the spectra from the inversion-hindered surface may be due to these sharp

resonant peaks. However, this is not the sole cause of spectral line sharpening because there are peaks which sharpen which do not appear (as resonances) in the CNCN torsional spectrum.

An important factor to note in the RDX study, is that, unlike the CH_3ONO and HONO studies, the force constants do not vary as the isomerization barrier is crossed. The switching functions in this surface are not dependant upon the dihedral angles, but only those coordinates associated with chemical reactions (decomposition). Thus, the observed broadening in the RDX power spectra cannot be caused by anharmonicity of the potential due to switching functions.

Conclusions

We have investigated the effects of repeated crossings of a potential energy barrier on power spectra of classical trajectories. We examined the causes of broadening and shifting of peaks in the power spectra of CH_3ONO and RDX. We also plotted time-delay maps of methyl nitrite trajectories to investigate the extent of phase space exploration in CH_3ONO.

We selected four different kinds of ensembles of CH_3ONO trajectories based on the number of barrier crossings and the times spent in the *cis* and *trans* conformations and then computed power spectra of these ensembles. The results show that broadening of power spectral bands increases with an increase in the number of passages through the transition state. We interpret this as evidence that repeated barrier crossings enhance vibrational mode mixing and IVR. The time-

delay mappings of selected trajectories illustrate that repeated barrier crossings leads to greater phase space exploration in a given potential well.

Some studies were also done for RDX, a 21-atom molecule, which undergoes ring conformation changes (which are more complicated than the *cis-trans* isomerization in CH_3ONO). Different barrier heights for the CNCN and NCNC isomerization were used to control the number of transitions between conformations. These results confirm the conclusions of the CH_3ONO study.

The results presented here show that there is a qualitative relationship between power spectral line widths and the number of times a molecule passes through a transition state between two conformations. These results do not definitively illustrate that the crossing of a barrier leads to an enhanced rate of IVR. For instance, other dynamical factors related to isomerization (which our study has not precluded) may lead to the broadening of the power spectral lines.[84] Furthermore, as we have discussed, there are differing points of view about whether it is possible to obtain quantitative reaction rates from infrared line broadening. The results of our calculations suggest that it should be possible, although it may not be easy. In Chapter VI we present the results of a study to see if rates of isomerization can be calculated from line broadening.

Table V. Cosine Series Coefficients for Ring Torsions in RDX

Coefficient	Barrier of 0.36 (kcal/mol)	Barrier of 10.69 (kcal/mol)
a_o	0.425221	12.7567
a_1	0.0	0.0
a_2	-0.430135	-12.9041
a_3	0.0	0.0
a_4	0.361213	10.8364
a_5	0.0	0.0

Table VI. RDX Normal Mode Frequencies[a]

I[b]	II[c]	Expt.[d]	*Ab Initio*[e]	I[b]	II[c]	Expt.[d]	*Ab Initio*[e]
36 (2)	44 (2)		22 (2)	889 (2)	931 (2)	910	995 (2)
39	45		52	931	931	885	912
46	47		64	972	1014	935	1053
49 (2)	59 (2)		87 (2)	1023 (2)	1128 (2)	1015	1070 (2)
104 (2)	167 (2)		198 (2)	1018	1018	1045	1117
138	211		291	1098	1869		1215
280 (2)	302 (2)		346 (2)	1137 (2)	1209 (2)		1121 (2)
302	305		415	1257	1253	1230	1238
328 (2)	365 (2)		380 (2)	1251 (2)	1265 (2)	1270	1309 (2)
360	389		426	1323 (2)	1373 (2)	1320	1348 (2)
508	522		535	1339	1340	1392	1274
525 (2)	530 (2)		537 (2)	1444	1374	1435	1342
588 (2)	591 (2)	610	606 (2)	1477 (2)	1482 (2)	1460	1364 (2)
598	599	595	665	1575	1575	1550	1481
641 (2)	653 (2)		666 (2)	1606 (2)	1613 (2)	1585	1470 (2)
688	688		706	2993 (2)	2993 (2)	2980	2954 (2)
698 (2)	698 (2)	740	758 (2)	2993	2995		2961
800 (2)	878 (2)	794	912 (2)	3051 (2)	3059 (2)		3066 (2)
803	812	750	833	3054	3088	3080	3068

[a] Units are cm^{-1}. The normal mode frequencies were obtained using analytical second derivatives of the potential.
[b] Surface with ring torsional barriers of 0.36 kcal/mol.
[c] Surface with ring torsional barriers of 10.69 kcal/mol.
[d] Iqbal *et al.*, Ref. 173.
[e] Coffin *et al.*, Ref. 174. The *ab initio* frequencies have been scaled by 10%.

Table VII. Experimental[a] Normal Mode Assignments and Computed[b] Frequencies for CH_3ONO

Mode Number[a]	13	12	11	10	9	8
				cis		
Composition[a]	δ(ONO) +δ(NOC)	ν(NO)- ν(N=O)- δ(NOC)	δ(ONO)- ν(NO)- ν(CO)	ν(CO)+ ... $\gamma_{\parallel}(CH_3)$- $\delta'(CH_3)$+ δ(ONO)	$\gamma_{\parallel}(CH_3)$	$\gamma_{\parallel}(CH_3)$- $\delta'(CH_3)$+δ(NOC)
Frequency: Normal Mode Analysis[b]	301.9	640.1	836.3	987.1	1003.5	1232.0
Frequency: Power Spectra[c]	295	620	770	865	950	1130
				trans		
Composition[a]	δ(NOC)- δ(ONO)	ν(NO)+ ν(CO)	ν(CO)- ν(NO)+ δ(ONO)	$\gamma_{\perp}(CH_3)$	ν(CO)+ $\gamma_{\parallel}(CH_3)$- δ(ONO)	$\gamma_{\parallel}(CH_3)$
Frequency: Normal Mode Analysis[b]	369.5	540.8	829.6	1028.3	1052.7	1207.7
Frequency: Power Spectra[c]	390	510	745	950	~970[d]	~1140[d]

[a] Ghosh and Günthard, Ref. 161.

[b] Present calculations. The normal mode frequencies were obtained using analytical second derivatives of the potential and confirmed with a low energy power spectrum. Units are in cm^{-1}.

[c] Frequencies obtained from the power spectra in Figs. 8-12. Total energy of the trajectories is 80.4 kcal/mol. Units are in cm^{-1}.

[d] Values are difficult to determine for the spectra shown in Fig. 8-12 as they are very close in frequency to *cis* bands. Approximate values were obtained from spectra with large *trans* well sampling.

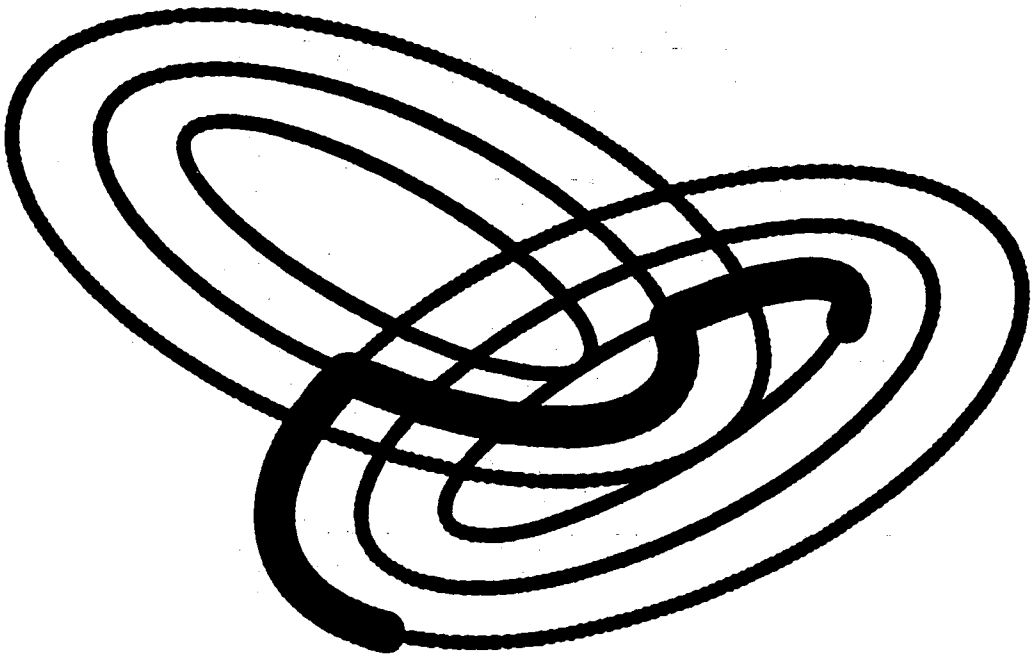

Figure 6. An illustration of why sampling of phase space is increased when more than one well is sampled. The trajectory (in bold) starts in one conformation, crosses to the other, and then returns to the original well. Upon returning to the original conformation, the trajectory is in a different region of phase space.

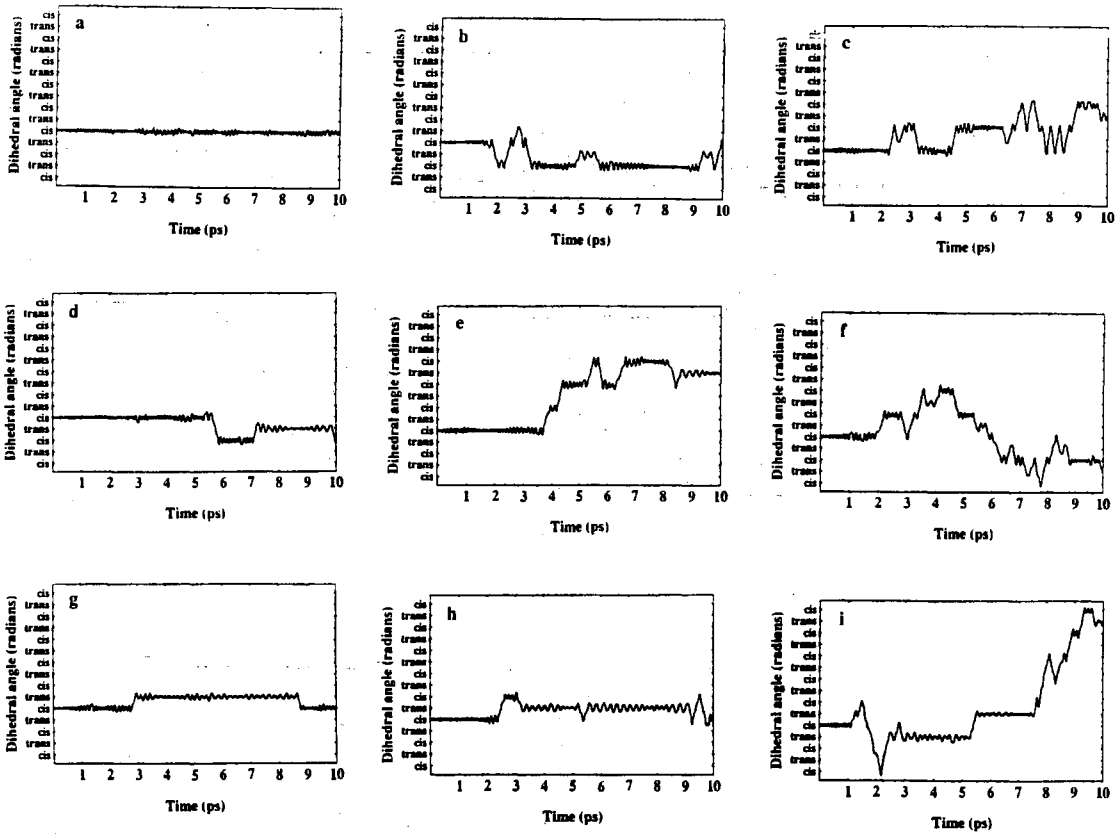

Figure 7. Plots of time histories of the isomerization coordinate, the ONOC dihedral angle, of CH_3ONO. We have selected individual trajectories and arranged them so as to represent different behaviors which lead to various changes in power spectral features. Column 1, panels a, d, and g: the trajectories cross the isomerization barrier infrequently in the 10 ps calculation time. Column 3, panels c, f, and i, trajectories cross the barrier frequently. Column 2 trajectories, panels b, e, and h, isomerize more often than Column 1 but less often than Column 3 trajectories. The rows vary in amounts of time spent in the *trans* well; Row 1 (panels a-c) trajectories spend the least amount of time in the *trans* well, Row 3 (panels g-i) trajectories spend the most time in the *trans* well, and Row 2 (panels d-f) trajectories spend an intermediate amount of time in the *trans* well. The effects these changes have on the power spectra are discussed in the text.

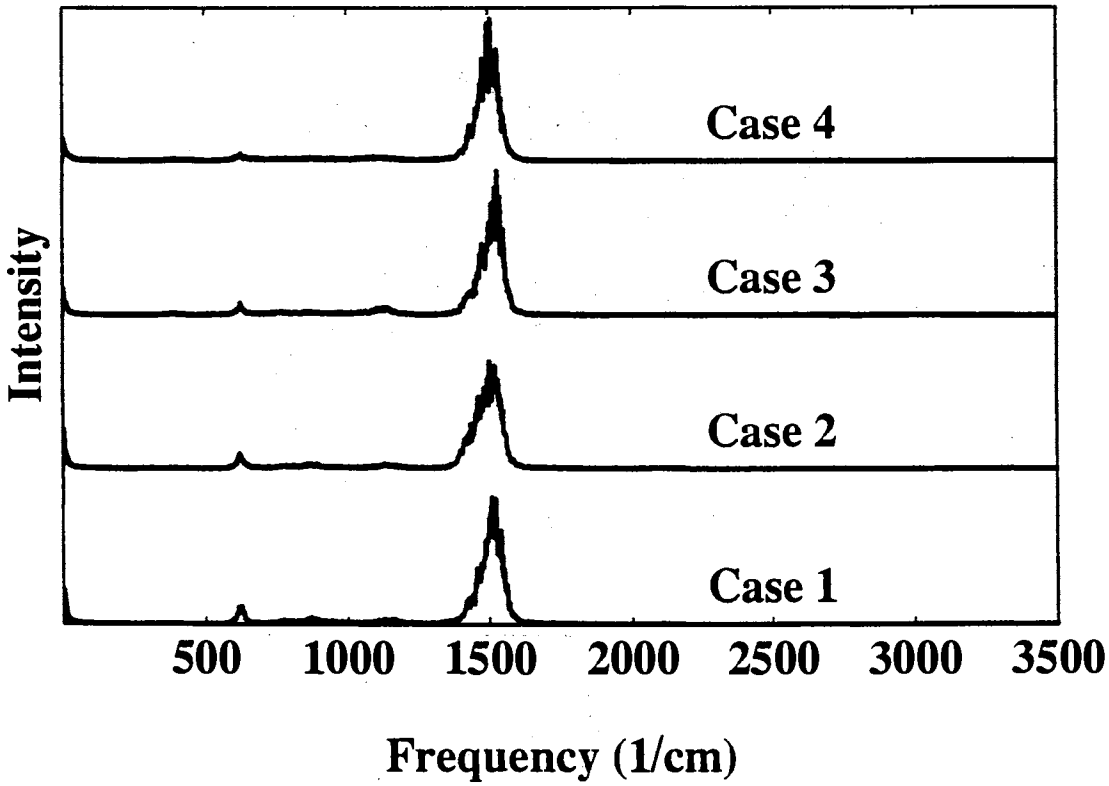

Figure 8. Power spectra of the N=O bonds for methyl nitrite for all four cases studied (see Fig. 2). All four cases are shown in a single panel for easier comparison, and are shifted for clarity.

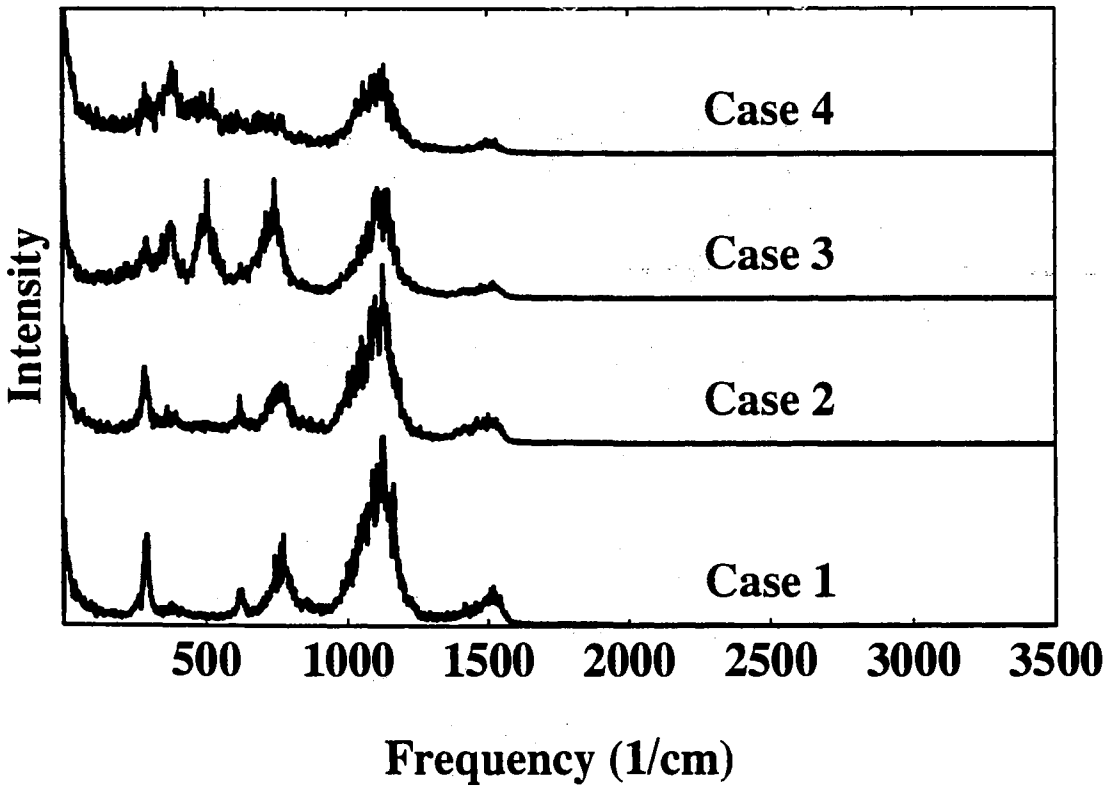

Figure 9. Power spectra of the O-N bonds for methyl nitrite for all four cases studied (see Fig. 2). All four cases are shown in a single panel for easier comparison, and are shifted for clarity.

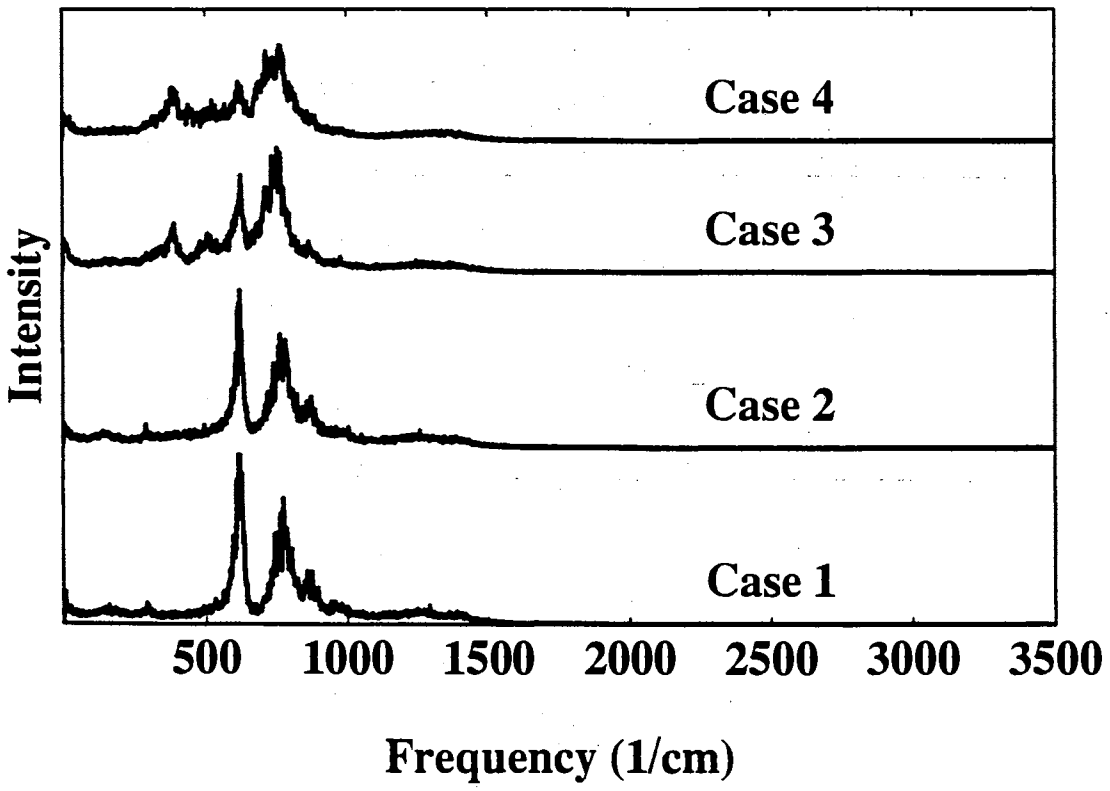

Figure 10. Power spectra of the O-C bonds for methyl nitrite for all four cases studied (see Fig. 2). All four cases are shown in a single panel for easier comparison, and are shifted for clarity.

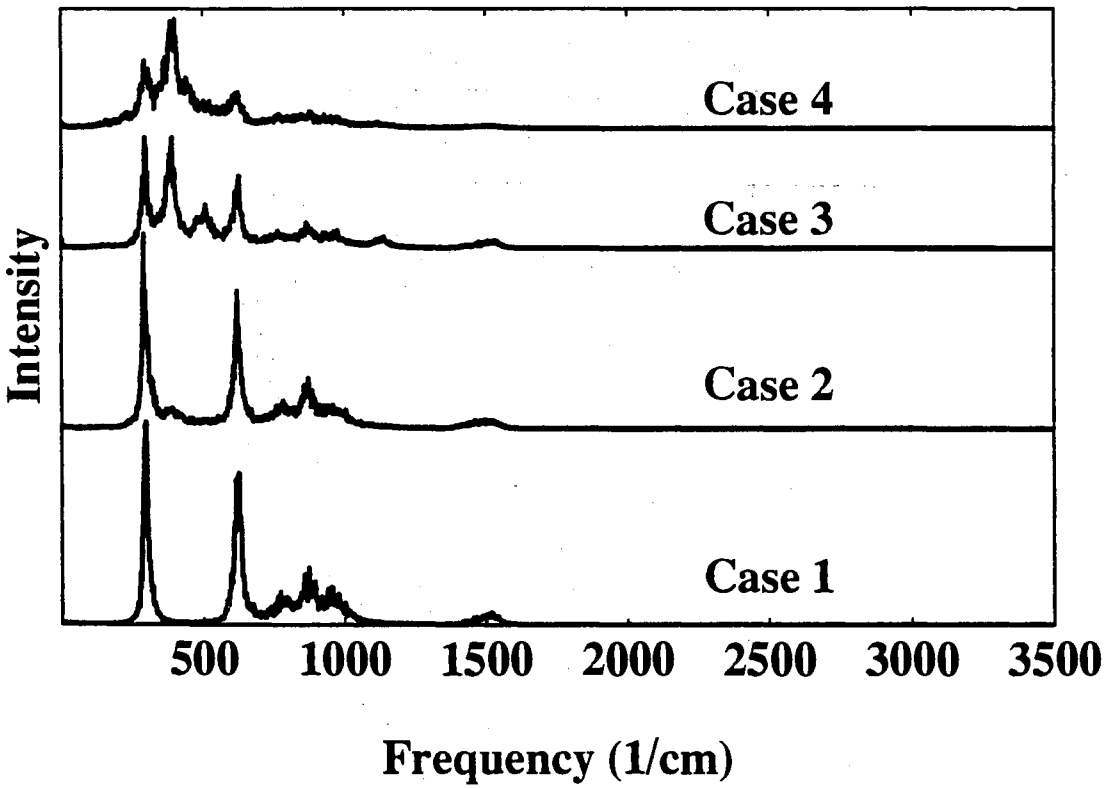

Figure 11. Power spectra of the NOC angles for methyl nitrite for all four cases studied (see Fig. 2). All four cases are shown in a single panel for easier comparison, and are shifted for clarity.

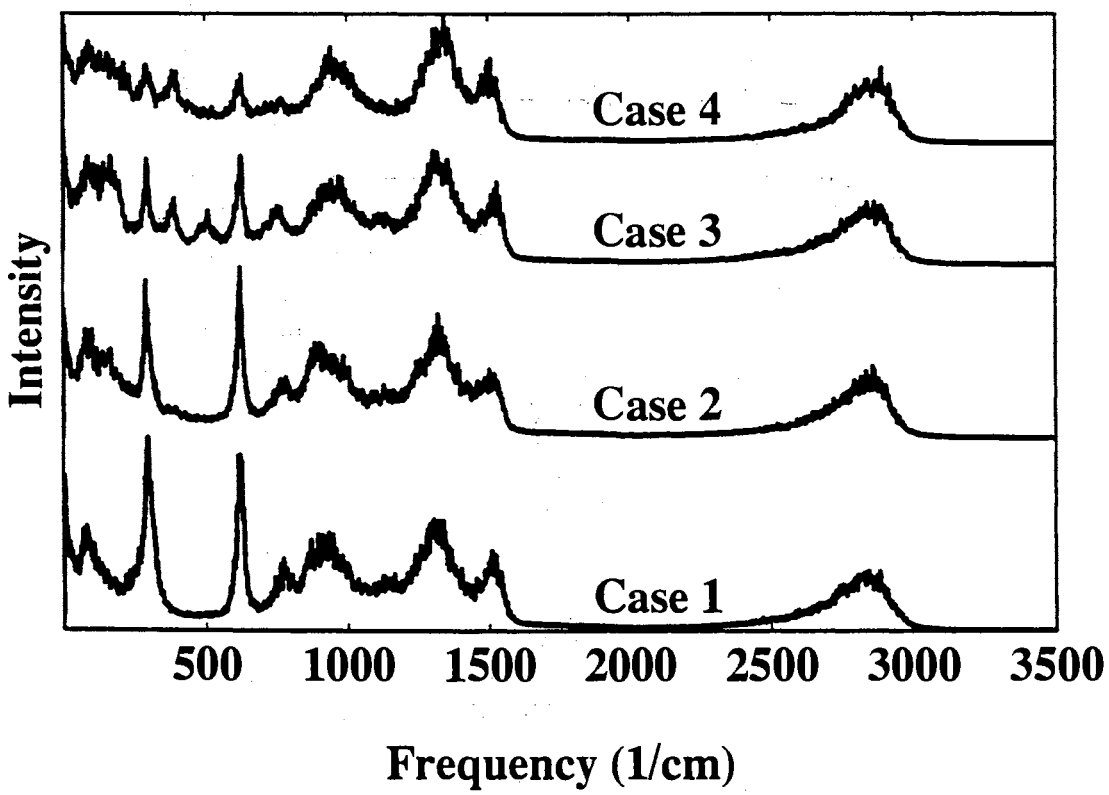

Figure 12. Composite power spectra of methyl nitrite for all four cases studied (see Fig. 2). All four cases are shown in a single panel for easier comparison, and are shifted for clarity.

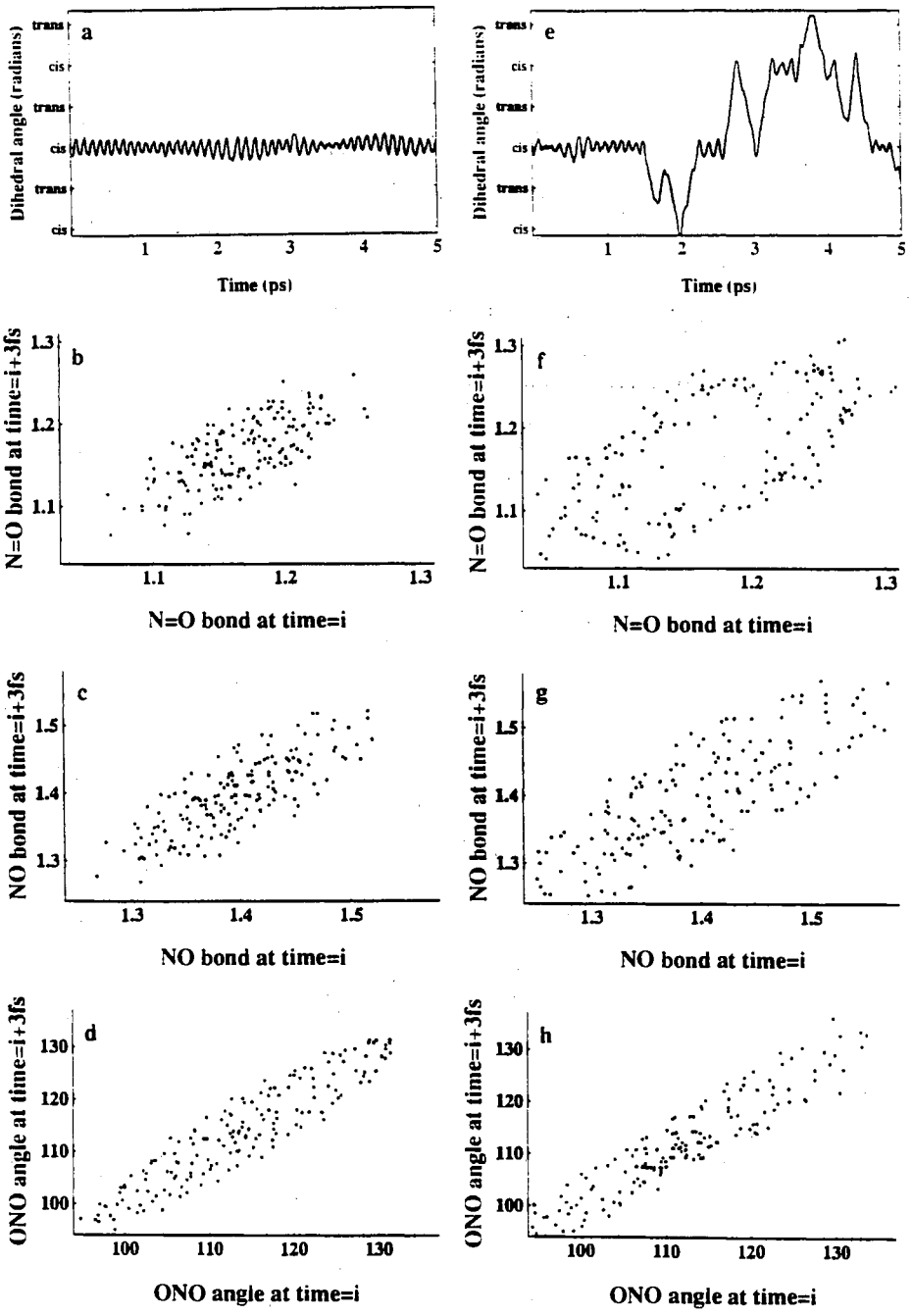

Figure 13. Panels a and e contain time histories of the methyl nitrite ONOC dihedral angle. Below each of these are time-delay mappings generated from the time ranges 3.94-4.14, 4.346-4.446, and 4.56-4.76 ps, while each trajectory resides in the *cis* conformation. Panels a and f, c and g, and d and h contain mappings of the N=O and ON bonds and the ONO angles, respectively. The mappings of the bonds are in Angstroms and the angles in degrees.

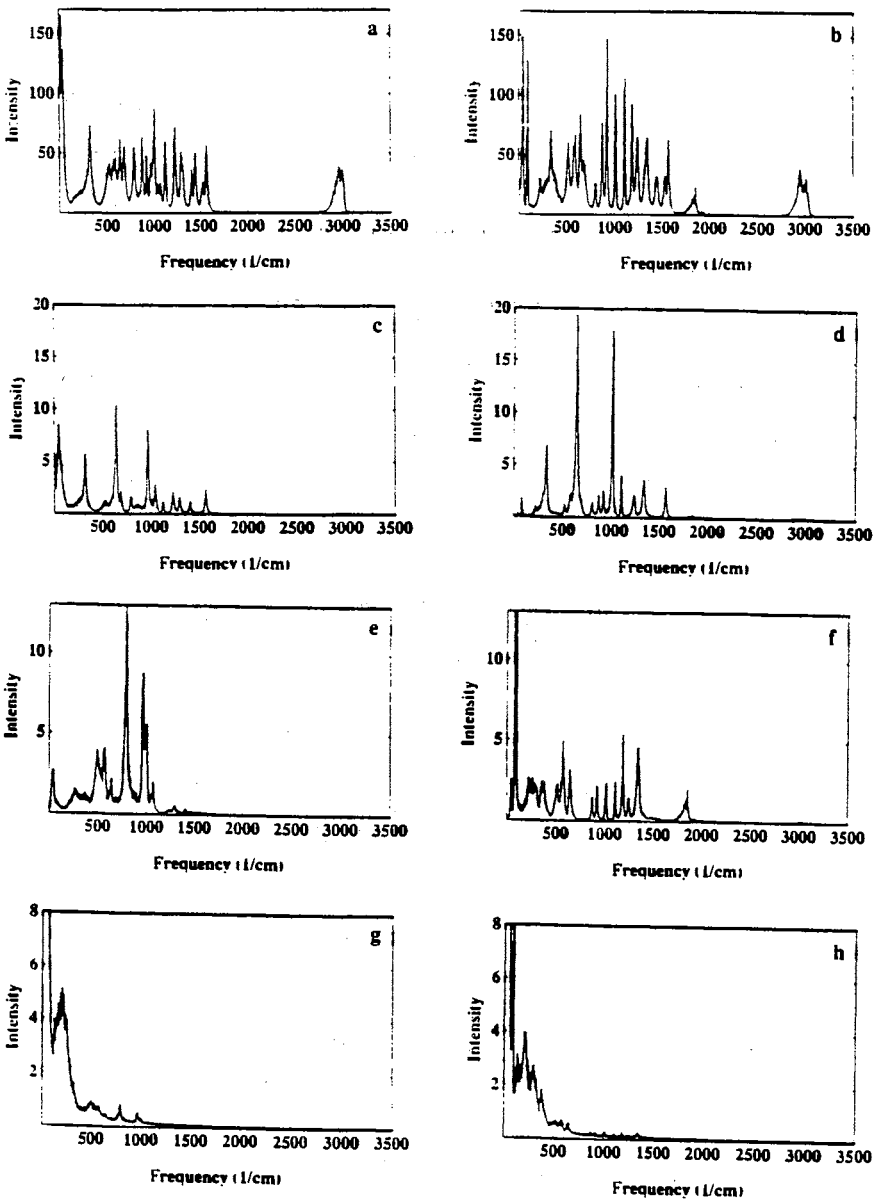

Figure 14. Composite and selected internal coordinate power spectra for RDX. The panels on the left contain spectra generated from the surface with low ring torsional barriers, and the panels on the right contain spectra from the surface with (aphysically) high ring-torsion barriers. Composite power spectra are shown in panels a and b. Panels c and d, e and f, and g and h contain spectra of the NCN bond, NCN-N wag, and CNNO dihedral angles, respectively. The composite spectra were computed by Fourier transforming all defined internal coordinates.

CHAPTER VI

RATES OF ISOMERIZATION FROM *CIS*, *TRANS*, AND FREE ROTOR TRAJECTORY SEGMENTS AND POWER SPECTRAL PEAKS: CH_3ONO

Introduction

The vibrational contributions to IR linewidths have been studied.[178-180] In Chapters IV and V we have presented results of our investigations of the vibrational contributions to the power spectral linewidths.[26,27] Among the contributors to broadening of spectral peaks is an increased rate of IVR.[6,36,37] When the system is an isomerizing species, it can also be related to the isomerization rate.[89-95] These two factors make the analysis of spectra complicated. Not only do spectral peaks broaden due to mode mixing in the molecule, but isomerization can lead to an increase in the broadening. We pose a question. Can the rate of reaction be extracted from power spectra? This is a complicated problem, as there are many factors which affect the peak shapes in the spectra of a seven atom molecule at energies above twice its zero-point energy. We have extract rates from spectral peaks of methyl nitrite generated using a harmonic potential-energy surface. We chose to use a harmonic PES for the study to decrease the amount of spectral broadening due to anharmonicity. While this makes the model less realistic, it makes the interpretation of the results simpler. Comparison of these rates of reaction to those from lifetime plots calculated using a time gap method shows they do not agree quantitatively, but follow the same

trends. Li *et al.*[181] have computed spectral linewidths (using quantum mechanical calculations) and found that they overestimate the experimentally obtained values by factors of 2 or 3.

We have chosen to study an isomerizing system, CH_3ONO, which does not undergo dissociation at the energies used in this study. This allows for the focus of the study to be on the rates of isomerization, since dissociation is not allowed. We found three different rates, one for the *cis* well, one for the *trans* well, and a third, much faster rate for when the molecule is in a free rotor state.

Potential-Energy Surface

A global potential-energy surface was constructed for CH_3ONO. The bonds and angles were represented by harmonic oscillators and the torsions by six-term cosine series. The analytical potential-energy surface has the form

$$V = \Sigma_{\text{bonds}} (k/2) (R - R_o)^2 + \Sigma_{\text{angles}} (k/2) (\theta - \theta_o)^2 + \Sigma_{\text{torsions}} [a_i \cos (i\tau)]. \quad (27)$$

Similar to our fit of the anharmonic surface (see Chapter IV), we fit both wells based on the equilibrium geometries[160] and frequencies[161] (see Chapter V for tables containing the geometries and calculated and experimental values of the frequencies). The force constants for the bonds were calculated from the parameters α and D_e using Eq. 3 and are given in Table VIII. The force constants are attenuated as the system undergoes the *cis-trans* isomerization based on the switching function given in Eq. 20.

The dihedral angle, ONOC, is represented by a six-term cosine series (Eq. 6).

A plot of this function as a function of the torsion is given in the top panel of Fig. 15. The switching functions (Eq. 20) depend on the ONOC dihedral angle. They smoothly attenuate the force constants of the bonds and angles which differ by more than 7% in the two wells as the molecule isomerizes. An example of a force constant changing as the ONOC dihedral angle goes from 0° to 180° to 360° (or 0°), corresponding to *cis*→*trans*→*cis* isomerization, is shown in the bottom panel of Fig. 15. The force constant for the OC bond is 544.419 and 363.381 kcal/molÅ^2 in the *cis* and *trans* conformations, respectively (see Table VIII). The bottom panel of Fig. 15 shows how the OC bond force constant changes as the molecule isomerizes.

(Note that the switching function introduces anharmonicity to the surface. Therefore, even though harmonic oscillator functions are used to represent the bonds and angles, the potential-energy surface is not harmonic.)

Calculations

The integration step size used for the calculations was 0.15 fs, and each trajectory was initiated in the *cis* conformation. Each ensemble consisted of 60 trajectories which were calculated for 20.0 ps. An equal amount of energy was initially placed into each mode using the method described by Bintz *et al.*,[11a,120] for a total energies of 65.5, 85.5, and 105.5 kcal/mol.

Power spectra were calculated by Fourier transforming[127,128] ensemble-averaged autocorrelation functions of the internal coordinates. The spectral resolutions is 1.67 cm^{-1}. The composite spectra were generated by summing the individual internal

coordinate spectra. Rates from spectral peaks were calculated using

$$k=2\pi\Delta\nu\ c \tag{28}$$

where $\Delta\nu$ is the half-width at half-height.

Lifetime plots were made by plotting the natural logarithm of N/N_o verses time. Usually, when determining rates from reactive trajectories, the trajectory is calculated until reaction at which point the trajectory is terminated; N_o is then the total number of trajectories, and N is the number of trajectories which have not isomerized (at all) by time t. In our calculations, we did not stop calculation of trajectories after isomerization. Rather, we counted each visit to a well as a "trajectory," or trajectory segment.

The lifetime plots are not linear. When these plots are not linear, the process is not first order. The different rates involved can be obtained by fitting each portion of the lifetime plots to a linear function. We fit two portions of the lifetime plots for all three energies. The rate constants obtained by the 0-0.333 ps range are denoted by k_{fast}, and those for 1.0 ps and up by k_{slow}.

The total number of trajectory segments for all trajectories in the ensemble then is N_o. Or, another way of wording it, is that N_o is the total number of times that either the *cis* or *trans* wells are visited. In our plots, the lifetimes are the times that a trajectory spends in a well (i.e., the times in which the trajectories do not undergo isomerization). The number of trajectory segments which have not undergone isomerization by time t, is represented by N. The lifetime plots from these ensembles were not linear. An additional 118 trajectories (at 65.5 kcal/mol)

were calculated for 20.0 ps. The resulting trajectory segments were separated into three categories: trajectory segments in the *cis* conformer, trajectory segments in the *trans* conformer, and trajectory segments which undergo free rotor motion. Note that the last of these includes both *cis* and *trans* conformers, but the trajectory segments in the free rotor category experience a different type of motion than that described by the other two categories.

Results and Discussion

Figure 16 contains the decay curves of the isomerization rate of methyl nitrite at three different energies: 65.5, 85.5, and 105.5 kcal/mol in panels a, b, and c, respectively. The plots are not linear and this will be discussed later. The initial region of rapid decay is due to periods of free rotation. The fast rates of reaction, k_{fast}, obtained by a linear fit of the curves in the 0-0.333 ps portion of plots are: 4.58144, 5.37688, and 6.49775 ps^{-1} for energies of 65.5, 85.5, and 105.5 kcal/mol, respectively. The slower rates of reaction, k_{slow}, obtained by a linear fit of the curves from 1.0 ps are: 0.33727, 0.45408, and 0.97700 ps^{-1} for energies of 65.5, 85.5, and 105.5 kcal/mol, respectively.

Composite power spectra calculated from the same three ensembles are shown in Fig. 17. The rates (calculated from the half-width at half-height) of two of the peaks in Fig. 17 are shown in Table IX along with the rates calculated from the lifetime plots. Note that while the rates calculated from the spectral peaks are not identical to those calculated from the lifetime plots of the trajectory segments, they

do follow the same trends.

It is obvious that the rates calculated from different spectral peaks will be different. This is because there are factors other than isomerization which enhance spectral broadening and both k_{fast} and k_{slow} contribute to the rate which is calculated from the spectral peak width. As can be seen from the spectra in Fig. 17 and the rates calculated from the peaks centered at approximately 295 and 2970 cm^{-1} listed in Table IX, the rate calculated from Eq. 28 will depend on the peak from which it is calculated.

Since we are comparing rates calculated from spectral peaks to rates calculated from lifetime plots, the most appropriate peak for the rate calculations should be that related to the torsional mode. The peak with the most torsional contribution (as determined by the power spectrum of the ONOC dihedral angle) is that centered at 295 cm^{-1}, although it should be noted that this peak is not purely a torsional mode. In other words, the ONOC motion is not separable from the other modes, as usually is the case for torsional modes.[101] Additionally, another band overlaps in this region (it comprises the δ(ONO) and δ(NOC) motions,[161] see Table VII, Chapter V). Yet it is still the most appropriate peak for comparison to the rates from the lifetime plots since it is the peak most strongly related to the reaction coordinate.

Figure 16a contains the lifetime plot calculated from the trajectory segments with 65.5 kcal/mol. Note that the plot is not linear. Thus, we sorted the trajectory segments into different groups: *cis, trans*, and free rotor trajectory segments. *Cis* and

trans segments are those which undergo a turning point in the *cis* or *trans* well. The free rotor segments, obviously, also "experience" the two conformers geometrically, but they are segments which did not have an isomerization turning point. Lifetime plots calculated by dividing the segments in this manner are shown in Fig. 18. (As discussed in the Calculations section, the ensemble used for the sorted (*cis*,*trans*, and free rotor) lifetime plots was much larger than that used for the lifetime plot shown in Fig. 16a.)

The rates calculated from the lifetime plots shown in Fig. 18 are 0.354, 0.348, and 8.63 ps^{-1} for the *cis*, *trans,* and free rotor trajectory segments, respectively. The relative rates of the *cis* and *trans* wells are consistent with what has been previously shown.[14] It is not unexpected that the free rotor has a much faster rate than the *cis* or *trans* well plots since the free rotor segments are those trajectory segments which are torsionally "activated" in the first place. This gives a reasonable explanation for the non-linear behavior of the lifetime plots shown Fig. 16.

A power spectrum does not yield data easily comparable to multiple rates. A single, time averaged rate is extracted from a spectral peak. A power spectrum does not allow for the delineation of the variety of behaviors a molecule experiences. The spectral peaks are broadened based on the combined rates of the *cis*, *trans*, and free rotor lifetime rates. Even then the peak half-width at half-height does not correspond solely to the rate of reaction since other factors contribute to spectral broadening.

As a supplement to this study, we would like to note a set of spectra which

we think warrants further study. The spectra were calculated using the anharmonic PES (and initial conditions, step size, etc.) and case sorting described for methyl nitrite in Chapters IV and V.

Figure 19 contains composite power spectra of methyl nitrite for the four cases studied (see Fig. 2 and Table I) for the frequency range 1250-1650 cm^{-1}. This range of the spectra at this energy (84. kcal/mol) contains many unresolved peaks from both the *cis* and *trans* conformers. Since they are not resolvable, statements cannot be made concerning any single peak (or pair of peaks). What is interesting about Fig. 19 is the position of the peaks. It has been suggested[81] that vibrational spectra of isomerizing molecules might show the coalescence of peaks as the rate of isomerization is increased. The Case 4 peaks in Fig. 19 have shifted towards each other compared to the peak centers of the other three cases. This is interesting because Case 4 *by design* contains trajectories which isomerize more often than trajectories in the other ensembles.

Conclusions

Rates of isomerization of methyl nitrite were studied using classical trajectories. The rate of isomerization is determined by two methods. Lifetime plots based on the time histories of the ONOC dihedral angle from ensembles with 65.5, 85.5, and 105.5 kcal/mol were used to calculate isomerization rates. Power spectra were calculated from these same trajectories and rates were calculated from the half-width at half-height of the appropriate peaks. Comparisons were made between the

two methods: while they do not agree quantitatively, the rates calculated from both methods show the same trends.

Additionally, the rate plots were subdivided into three categories of trajectory segments: *cis*, *trans* and free rotor. This division creates first order rate plots and clearly shows the combination of processes (*cis*→*trans*, *trans*→*cis*, and free rotor motion) which are all included in the broadening of a spectral peak, and yet cannot be divided out neatly in power spectra as they can in lifetime plots.

Table VIII. Harmonic Potential Parameters For CH_3ONO

Harmonic force constants:

k [kcal/(mol Å ^{2}) or kcal/(mol rad^2)]

coordinate	*cis*	*trans*
$r_{N=O}$	1470.61	1470.6
r_{ON}	951.919	458.346
r_{OC}	544.419	363.381
r_{CHi}	710.602	710.602
r_{CHo}	699.736	699.736
θ_{ONO}	184.270	486.711
θ_{NOC}	253.425	176.097
θ_{OCHi}	79.1443	101.942
θ_{OCHo}	85.7261	99.6123
θ_{HiCHo}	76.7735	73.4300
θ_{HoCHo}	71.6185	72.3286

Cosine Series Coefficients [kcal/mol]:

	a_0	a_1	a_2	a_3	a_4	a_5
ONOC	5.099403	-0.045548	-4.43329	-0.431542	-0.169819	-0.052026
$NOCH_i$	0.4397	0.0	0.0	0.4403	0.0	0.0

Table IX. Rates from Spectral Peaks and Lifetime Plots

Energy	Peak		Lifetime Plot	
(kcal/mol)	295 cm^{-1}	2970 cm^{-1}	k_{fast}	k_{slow}
65.5	1.16 ps^{-1}	2.99 ps^{-1}	4.58 ps^{-1}	0.337 ps^{-1}
85.5	1.90 ps^{-1}	3.50 ps^{-1}	5.38 ps^{-1}	0.454 ps^{-1}
105.5	2.04 ps^{-1}	3.88 ps^{-1}	6.50 ps^{-1}	0.977 ps^{-1}

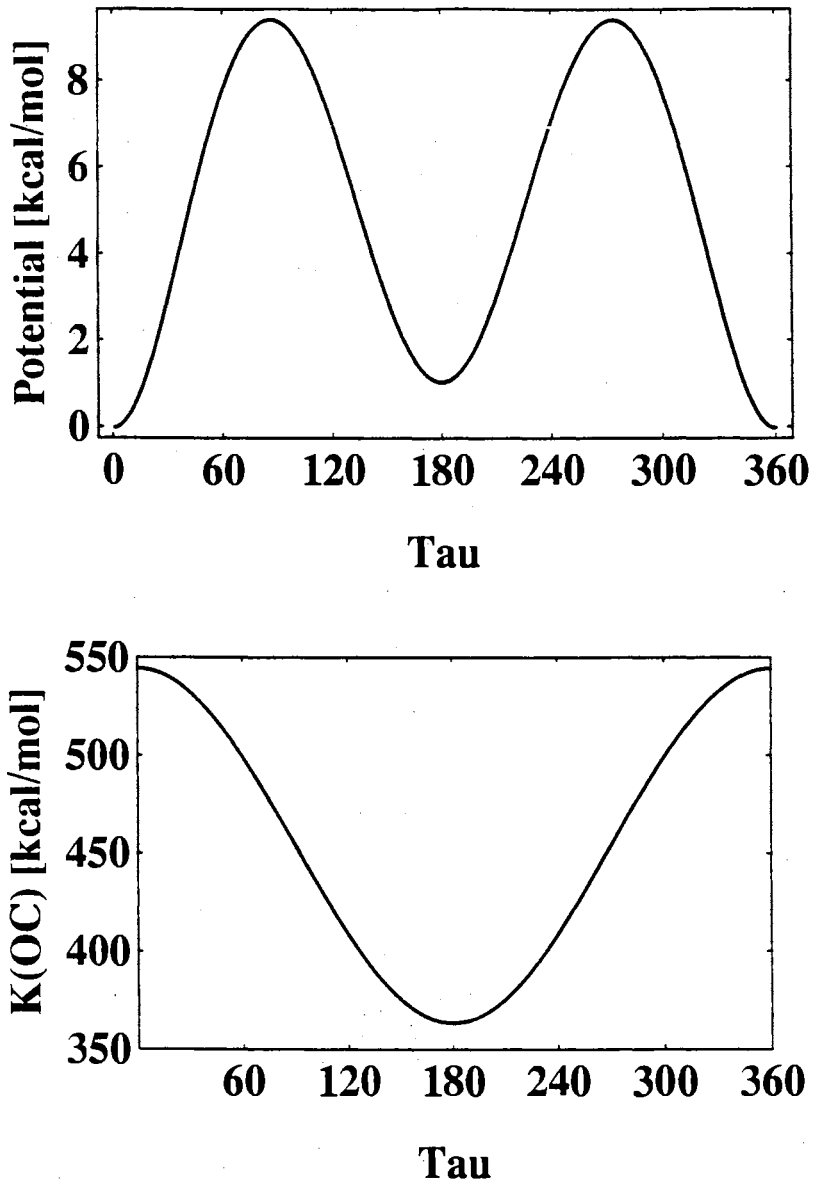

Figure 15. The top panel shows the potential energy function used to represent the ONOC dihedral angle as a function of the torsion. The bottom panel shows an example of a force constant attenuating as methyl nitrite isomerizes: *cis*→*trans*→*cis*. The force constant shown here is the OC bond force constant. In the equilibrium *cis* conformation, the value of K(OC) is 544.419 kcal/mol Å^2, in the equilibrium *trans* conformation, the value is 363.381 kcal/mol Å^2.

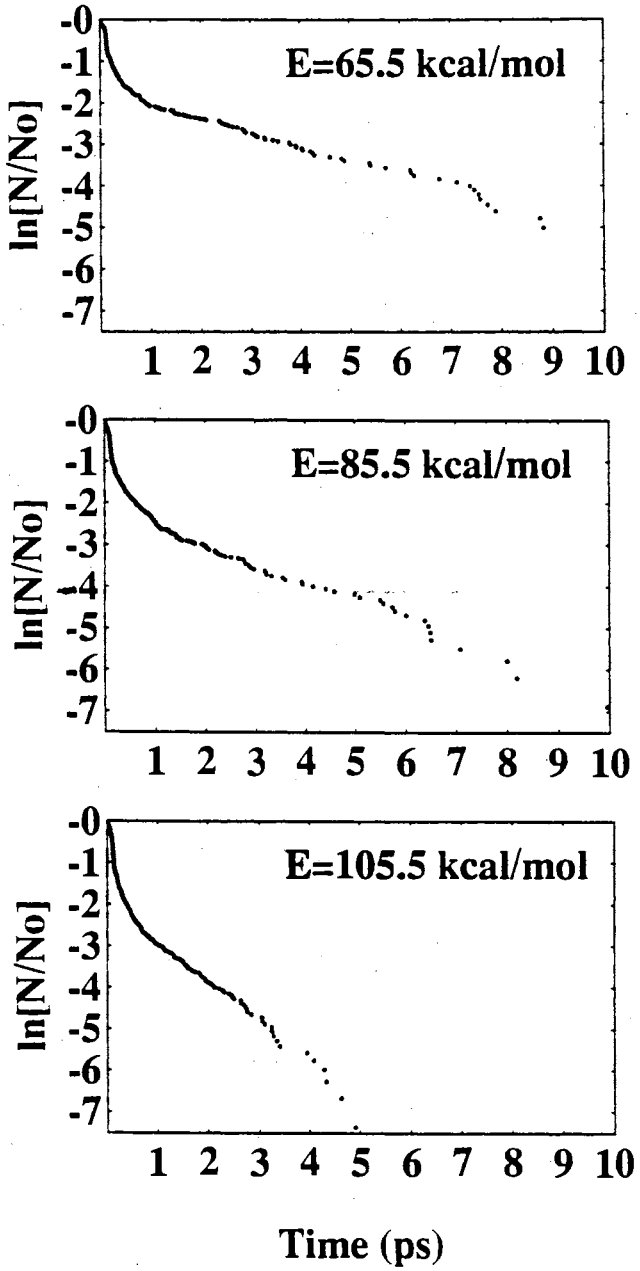

Figure 16. Lifetime plots calculated from trajectory segments of methyl nitrite from ensembles at three different energies: 65.5, 85.5, and 105.5 kcal/mol, panels a, b, and c, respectively. Power spectra calculated from Fourier transformed autocorrelation functions of the internal coordinates of the trajectories from these same ensembles are shown in Fig. 17.

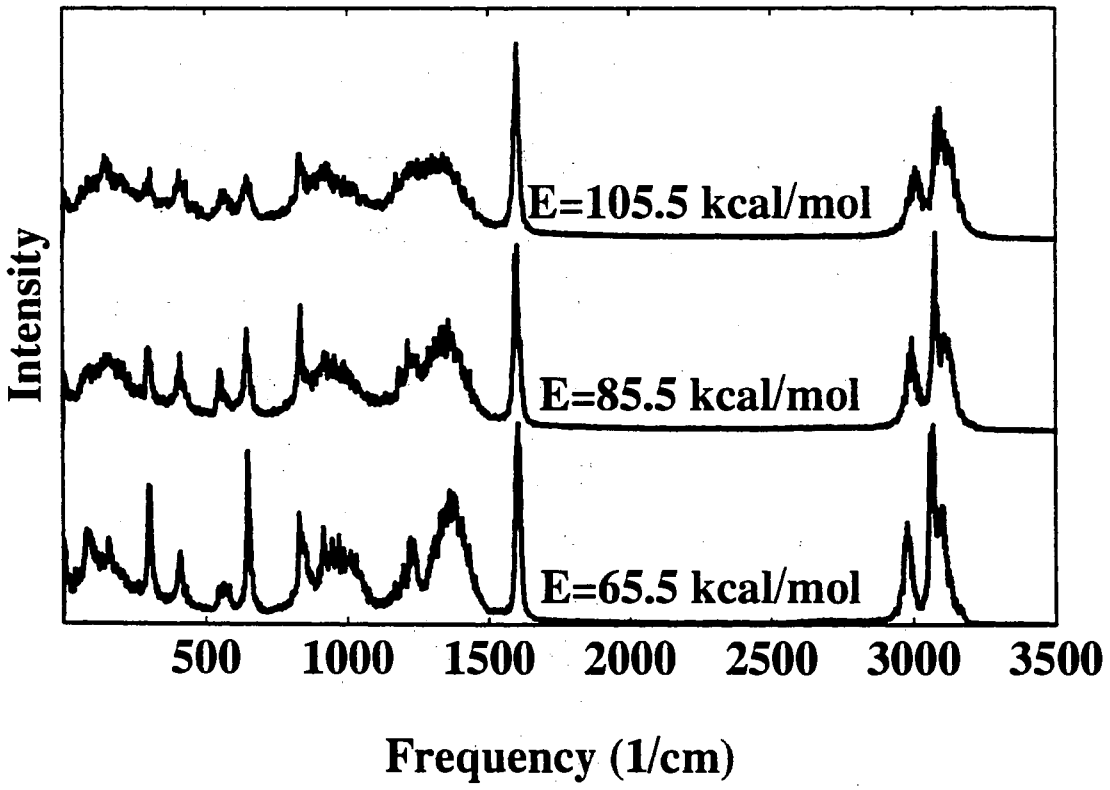

Figure 17. Power spectra from a harmonic potential-energy surface of methyl nitrite calculated at 65.5, 85.5, and 105.5 kcal/mol. Lifetime plots calculated from trajectory segments from the same ensembles used to generate the spectra shown in Fig. 17 are shown in Fig. 16.

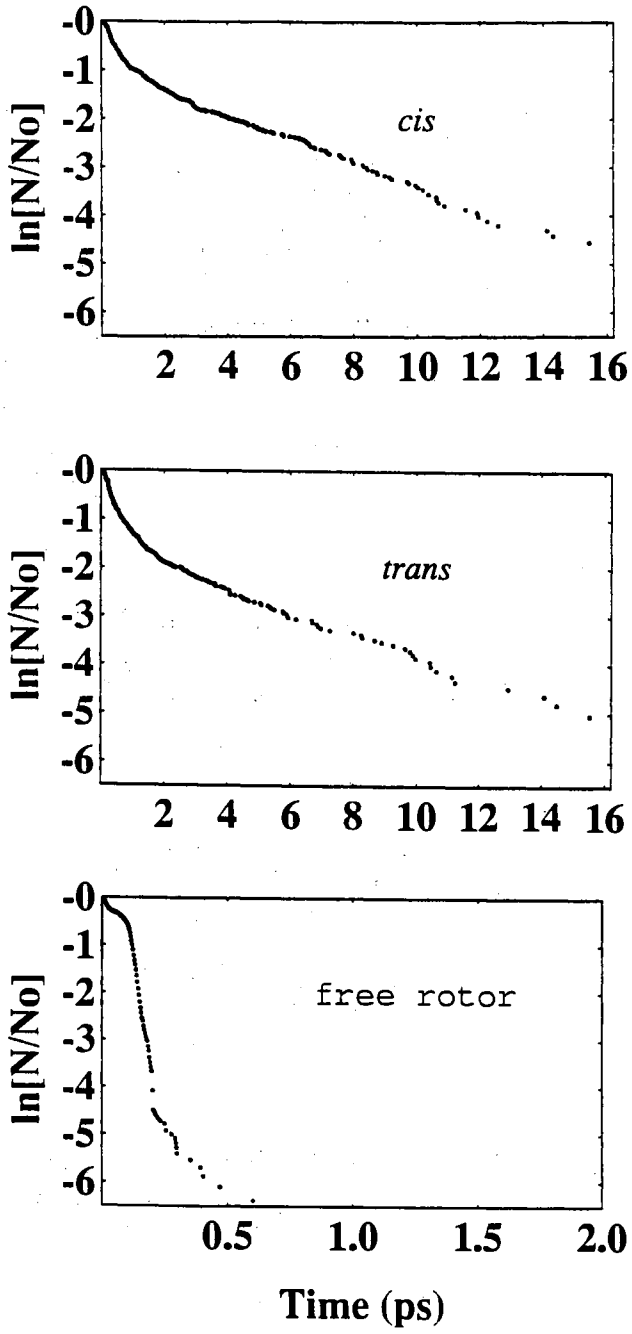

Figure 18. Lifetime plots generated from an ensemble of 178 trajectories of methyl nitrite at 65.5 kcal/mol. Panel a was calculated from those trajectory segments which had at least one turning point in this *cis* well. Panel b was calculated from those trajectory segments which had at least one turning point in this *trans* well. Panel c was calculated from those trajectory segments which did not have a turning point in either well.

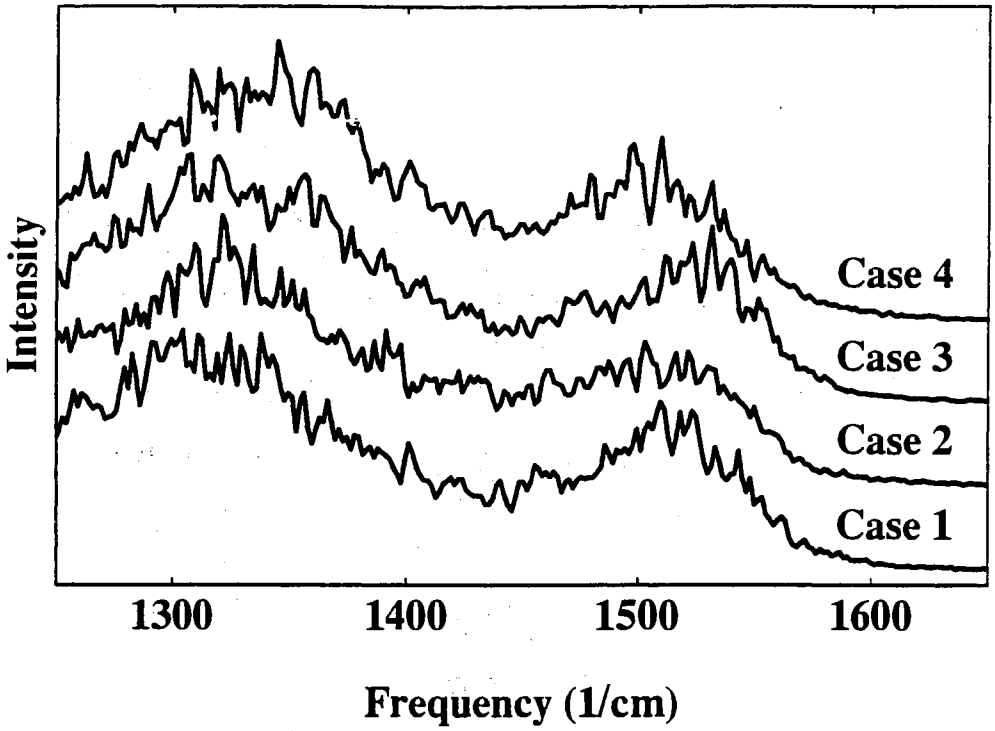

Figure 19. Composite power spectra of methyl nitrite calculated as described in Chapters IV and V and case sorting as defined in Fig. 2 and Table I. Note that the Case 4 peaks have shifted towards each other as compared to the spectral peaks from the other cases. This merging of spectral bands is indicative of an increased rate of isomerization.

CHAPTER VII

CLASSICAL POWER SPECTRAL STUDIES OF RDX

Introduction

There are certain threads common to most formulations of potential-energy surfaces (PES) for reactive polyatomic systems. Since medium-sized polyatomic molecules are, in general, capable of several distinct unimolecular reactions, it is often a difficult undertaking to formulate an analytical PES which explicitly models the global dynamics in a realistic way. From a practical standpoint, one is usually forced to make various simplifying assumptions in order to render the problem tractable. A typical example of this is to isolate from the full set of conceivable processes some subset which is thought to encompass the most interesting aspects of the overall dynamics, and to focus on accurately representing the features of the PES most germane to those processes.

Having settled on what features will be explicitly incorporated into the PES, one usually begins by writing down and parameterizing functional forms for the PES of the relevant reactants and products, with particular emphasis on reproducing measured or calculated geometries, vibrational frequencies, vibrational eigenvectors (if available), and thermochemical properties of the important species. Once this has been done, these "asymptotic regions" are combined to form a global PES by using switching functions to smoothly change the values of the parameters from those of

the reactant to those of the products as the system progresses along the reaction path connecting them. There are several ways of doing this. In some cases, quantum chemical calculations can be used to tailor the shapes of the switching functions.[182] More often than not, however, such information is not available and the switching functions must then be determined empirically using reasonable forms coupled with chemical intuition.

When forms for the switching functions are chosen arbitrarily, the principal requirements are that they be continuous with continuous first derivatives and that they provide sufficient flexibility to reproduce the known PES features. Functions of tanh, trigonometric, or Gaussian form are most commonly employed,[182a,183] although other possibilities have been explored.[182f] Regardless of the form(s) chosen, the switching functions necessarily introduce potential coupling into the Hamiltonian and will affect the anharmonicity of the system. Thus, the extent of mode mixing and consequently intramolecular vibrational energy redistribution (IVR) can be expected to depend, sensitively in some cases, on the details of the switching functions.

We recently reported a power spectral study of the classical dynamics of RDX (hexahydro-1,3,5-trinitro-1,3,5-triazine).[26] RDX undergoes unimolecular decay via competing reaction path, namely, concerted molecular elimination and simple bond rupture yielding radicals. These kinds of competing reactions are common in large molecules.[114,119,184] The energy required for N-N bond rupture (R1) is 47.8 kcal/mol.[184] The barrier to concerted ring fission (R2) has not been measured, but quantum chemical calculations by Habibollahzadeh *et al.*[175] yield values in the range

72-75 kcal/mol. In our original study,[26] which predated the work of Habibollahzadeh *et al.*,[175] we used a PES with a barrier of 38.3 kcal/mol to the ring-fission reaction. It employs a somewhat cumbersome array of switching functions used to span regions of configuration space that are poorly characterized. The results of the power spectral study[26] revealed that, even at the zero-point energy, there is significant broadening of the spectral peaks. Such broadening is a qualitative indicator of intramolecular vibrational energy redistribution (IVR).[6,36,37] The calculated broadening in RDX[26] was substantially greater than that obtained in analogous studies of smaller molecules (e.g., SiF_4, C_2H_4, and CH_3ONO) at their respective zero-point energies.[25] We argued that the exaggerated broadening in the spectra for RDX might arise as a consequence of the relatively low barriers to the two principal primary reaction channels (R1 and R2) and the fact that significant deviation of the potential-energy surface from that corresponding to the "zeroth-order reactant" sets in with relatively small excursions from the equilibrium geometry. Both of these suspected factors are crucially dependent on the choice of switching functions since they essentially define the height, shape, and position of the barrier. As a test of that seemingly plausible hypothesis, we removed the reaction channels, i.e., the switching functions, and found that the power spectra were significantly sharper than those obtained using the full potential-energy surface.[26]

The purpose here is to further investigate the ramifications of various choices of switching functions, barrier heights, and barrier positions for the vibrational dynamics of RDX, as manifested in power spectra. The functional form of the

potential-energy surface used in the present work is an improvement of the one used earlier[26] (and is described in greater detail in Chapter VIII). The height, shape, and position of the barrier to ring fission on this potential-energy surface are specified through the parameterization of the switching functions used; the asymptotic thermodynamics is unaffected by modification of switching function parameters. Since the value of the barrier to ring fission is not known, we have varied it in the present study to determine the sensitivity of the results (for nonreactive trajectories) to its magnitude and to the shapes of the switching functions used to obtain it. Specifically, switching function parameterizations leading to ring-fission barriers of 37, 67, and 71 kcal/mol have been considered (PES I, II, and III, respectively). A less-realistic potential which precludes (by excluding all switching functions) the possibility of ring fission except at very high energies has been included as well (PES IV).

Computational Methods

The computational approach taken in the current work is similar to that employed in several previous studies by Thompson and coworkers.[9-23] Briefly, ensembles of classical trajectories are propagated from well-defined initial conditions. The time histories of selected internal coordinates of the molecule are stored for each trajectory in a given ensemble. These time series are used to calculate normalized autocorrelation functions of the internal coordinates. An ensemble-averaged autocorrelation function for each internal coordinate is then

obtained as the arithmetic mean of the single-trajectory autocorrelation functions. Next, a power spectrum for each internal coordinate is obtained as the Fourier transform of the ensemble-averaged autocorrelation function. Finally, composite power spectra are obtained as the direct superposition of the power spectra for the individual internal coordinates.

Classical trajectories were computed using the trajectory code GenDyn.[124] Initial conditions were obtained using either the Efficient Microcanonical Sampling (EMS) Metropolis algorithm[125,126] or quasiclassical projection techniques.[120] The first approach leads to a microcanonical distribution of points in phase space while the latter allows for the generation of phase-averaged, mode-selective excitations of the equilibrium vibrational normal modes. Both methods are included as standard options in GenDyn. All initial conditions considered in the present study correspond to zero total angular momentum.

The trajectories were propagated by solving Hamilton's equations of motion in lab-fixed Cartesian coordinates using a fourth-order Runge-Kutta-Gill algorithm with a fixed stepsize of 1.0×10^{-16} s. Ensembles of 40 trajectories were computed for a given choice of potential-energy surface and initial conditions. Individual trajectories were followed for 10 ps. The values of the internal coordinates were written to disk at trajectory-time intervals of 4 fs.

The resolution of a power spectrum is determined by the duration of the time series from which it is derived.[128] Exploiting the fact that the autocorrelation functions are even functions of time lag, we obtain a spectral resolution of 1.7 cm^{-1}.

The Nyquist cutoff frequency for the spectrum is determined by the time density of the stored internal coordinate histories;[128] our sampling interval leads to a cutoff frequency of 4169 cm^{-1}, which is well beyond the spectral domain in which we are interested.

Potential-energy surface

A. Analytical form

Complete details of the potential-energy surfaces used in this work will be described in Chapter VIII. The analytical form is based on a valence force field and comprises a sum of 21 Morse stretches for the valence bonds, harmonic oscillator terms for each of 36 three-atom bends and three wag angles, and twelve six-term cosine series expansions for the dihedral angles describing the torsional motion of the molecule is the form given in Eq. 8.

This differs from the form of the PES used in our previous study[26] in that the cross-ring and ring/exocyclic Lennard-Jones nonbonded interactions are replaced with cosine series to represent the potentials for ring and ring-exocyclic dihedral angles. (Torsional motion of the products of ring fission was not restricted in the original potential-energy surface.[113] Also, some of the reactant and product vibrational modes were absent in the previous work (due to incomplete treatment of the torsional motion). All vibrational normal modes are present in the new potential.) In addition to these changes in the functional form of the potential, some of the reactant and product parameter values have been modified to more accurately

reproduce what is now known[174,175,185,186] about the equilibrium force fields of the RDX molecule and the reaction products.

B. Switching Functions

The switching functions used are of the same forms as in Ref. 113 and are given in Eqs. 22 and 23. The rate at which a parameter such as a Morse well depth, force constant, equilibrium bond length or equilibrium angle is attenuated depends upon the shape of the switching functions.

The PES used in this study employs 198 switching functions. By modifying the parameters of Eqs. 22 and 23, we were able to obtain potentials having barriers to ring fission of 37, 67, and 71 kcal/mol (PES I, II, and III, respectively) without having any effect on the overall reaction exothermicities. Table X contains the parameters used to define the switching functions for these three cases. The minimum-energy path for N-N scission is endothermic by 47.8 kcal/mol with no barrier to back reaction.

As mentioned earlier, some of the values of the force-field parameters in Eq. 8 are different from those of Ref. 113 and the treatment of the torsional motion is more complete in the present PES. Consequently, while the switching-function parameters used in PES I are the same as those used previously,[113] the underlying equilibrium RDX and CH_2NNO_2 potential models are different, resulting in different PES.

We now illustrate with a few typical examples how selected force-field

parameters are attenuated in the current PES as chemical reactions occur. (We restrict ourselves to a consideration of PES I and III, since the values of the switching function parameters appearing in PES II are quite similar to those of PES I, see Table X.)

The six CNN angles in RDX are defined in terms of adjacent CN and NN bonds. As either the CN or NN bond defining a given CNN angle undergoes dissociation, the associated angle-bending force constant must approach zero. Both cases are presented in Fig. 20. (The arrangement of the figure is such that the left- and right-hand columns correspond to PES I and PES III, respectively.) Diminution of the CNN force constant for the case of NN scission on the two potentials is depicted in panels a and b of Fig. 20; that resulting from CN rupture is shown in panels c and d. Panels e and f are similar to the other pairs except that they present the variations in the equilibrium value of the NCH angle as the adjacent CN bond breaks.

Panels a, b, c, and d in Fig. 20 show switching functions of the form given by Eq. 22. The value of β appearing as a coefficient to the argument of the exponential in Eq. 22 is unity for the cases in panels a and b; the exponent of the argument, n, is 2 for panel a and 4 for panel b. Thus, the distance over which the function in panel a varies is large relative to that in panel b. The attenuation of the associated force constant is slow and gradual in panel a, requiring over 2 Å to diminish to zero; in panel b, the onset of attenuation is slow initially, but then occurs abruptly over a distance of about 1 Å . In panels c and d, n=4, but β differs. The value of β is 1.2

times larger in panel c than in d (see Table X). However, since β is only a multiplicative factor to (rather than a exponent of) the variable argument of Eq. 22, the effect of modest variations in its magnitude are smaller than for n. The behaviors of the tanh switching functions shown in panels e and f can be interpreted in a similar fashion. The smaller value of the exponent of the argument of the switching function used in PES I (panel e) leads to a more gradual variation of the function between its asymptotic limits than for the case of PES III (panel f). The effect of the coefficient to the argument of the switching function is once again relatively unimportant.

One important point to note is that using n=2 in Eq. 22 leads to a discontinuity in the second derivative of that function when the argument vanishes; the ordinate changes from zero (left side of the discontinuity) to -2β (right side of the discontinuity). There is no such discontinuity for n=4. (Analogous remarks apply to the case of Eq. 23.) As has been noted before,[26] discontinuities in the second derivatives can affect trajectory integration accuracy. Moreover, given that the discontinuity frequently occurs at the equilibrium geometry of the molecule, one cannot obtain a meaningful normal-mode analysis in the usual way since the second derivatives are not well behaved. The calculation of power spectra from a very low-energy trajectory does of course allow one to obtain the effective normal-mode frequencies.

C. Minimum-Energy Profiles

Figure 21 consists of plots of the minimum-energy profiles (MEP) for concerted ring fission using the three different sets of switching function parameters listed in Table X. The method used to calculate the MEP is described in Ref. 113. Briefly, alternating C-N bonds are incrementally extended while allowing the remaining C-N bonds and the fifteen exocyclic atoms to relax to their equilibrium values. By using the same values of the switching function parameters as in the previous RDX studies[26,113] but a different analytical form for the equilibrium force fields of the reactant and products, we obtain a low-barrier PES (PES I; panel a) which has a somewhat different shape than that in Ref. 113 (see Fig. 4 of Ref. 113) for small excursions from equilibrium.

Minimum-energy profiles for PES II and III are shown in Figs. 21b and 21c, respectively. Potential-energy surface II (panel b) differs from PES I only in the value of the coefficient of the argument of the tanh switching function, Eq. 23, (PES I is 1.4 times that of PES II). Still, this difference is sufficient to raise the barrier to ring fission on PES II by 30 kcal/mol relative to that of PES I, yielding a value of 67 kcal/mol. However, the positions of the barriers on PES I and II are quite similar.

By contrast, none of the three basic switching functions in PES I is the same as in PES III (see Table X); each varies in the specification of at least one of the constituent parameters. The barrier for PES III (71 kcal/mol) is nearly twice that for PES I (37 kcal/mol) and the maximum occurs at a significantly smaller value of the reaction coordinate, which we crudely model as the extension of the three equivalent

CN bonds being cleaved during ring fission.

In summary, one can see from Fig. 21 that we have one pair of potentials with quite similar barrier positions but significantly differing barrier heights (PES I and II, panels a and b, respectively) and another pair with similar barrier heights but significantly differing barrier positions (PES II and III, panels b and c respectively). It is of interest to examine the effects of these differing features of the potentials on the nonreactive dynamics of the molecule.

Results and Discussion

We suggested in our previous power spectral study of IVR in RDX[26] that the significant broadening of the power spectra (i.e., the efficient mode mixing) resulted from extensive potential coupling introduced by our choice of switching functions, the low barrier to reaction (ring fission), and the large disparity in the bond energies of the reactant and products. Here, we test that proposition by comparing the power spectra obtained from PES I and PES II, which have similar switching-function parameters and barrier positions, but barrier heights for ring fission which differ by 30 kcal/mol. The shapes of the corresponding switching functions in these two potentials are quite similar due to the near equality of the parameters used in them. In order to further facilitate the comparison, we use PES III, which has a barrier height close to that of PES II, but values of switching function parameters which are significantly different from those of PES I and PES II. The shape of the switching functions of PES III differ significantly from those of PES I and PES II. Taken

together, these comparisons should allow us to reach some conclusions about whether it is simply the magnitude of the barrier height or the nature of the switching functions which is the dominant factor in determining the extent of IVR in RDX.

Composite power spectra are presented in Fig. 22. Figure 22a corresponds to very low-energy trajectories (0.02 kcal/mol above the minimum). Results for each of the four PES are shown. The spectra differ. The reason for the difference is that PES I and II have discontinuities in the second derivatives of the switching functions whereas PES III and IV do not. Thus, the normal-mode structures are not equivalent. While this is certainly a hindrance to our analysis, since we cannot simply perform a one-to-one comparison of the spectral features, we think that we can learn something by comparing the average peak widths and the extent to which isolated peaks in the normal-mode-limit spectra retain their identity in the spectra computed at higher energies.

Ensemble-averaged spectra computed from trajectories at the zero-point energy for all four surfaces are presented in Fig. 22b. The total energy, 81 kcal/mol, was partitioned in accordance with the quasiclassical prescription, using normal modes obtained from the unattenuated potential defined by Eq. 8. The spectra in Fig. 22b can be readily traced back to those in Fig. 22a; for example, the neatly split peaks for PES III and IV in the region beginning at roughly 1500 cm^{-1} are still clearly evident, as is the quartet of bands starting at 500 cm^{-1}. It is difficult to make a clear distinction between the spectrum for PES III (barrier of 71 kcal/mol) and that for PES IV (very high barrier); the implication is that the presence of the switching

functions is having little effect on the zero-point energy dynamics of PES III. By contrast, the spectra for PES I (barrier of 37 kcal/mol) and PES II (67 kcal/mol), while similar to each other, do exhibit some noteworthy differences. First, the broad peak centered around 350 cm^{-1} for PES I is red shifted relative to the corresponding peak for PES II. Also, the next peak towards the "blue" is noticeably smeared out in the PES I spectrum.

On the whole, the peaks associated with PES I and II are less sharp than those for PES III and IV. Some of this is probably due to the distribution of normal modes, but this cannot be the explanation over the entire spectral range, as low-energy multiplets in the spectra for PES III and IV are better resolved than comparably dense groups in PES I and II. Thus, although the differences in the underlying normal-mode structure of the composite spectra prevent us from drawing an unequivocal conclusion, we tend to ascribe the qualitative difference in the sharpness to disparate extents of IVR in the two cases. Given that the barriers for PES II and III are so similar, it seems logical to argue that the difference in sharpness arises principally due to the difference in the shapes of the switching functions and only secondarily to the differing barrier heights. Consequently, our previous speculation[26] that the origin of the extensive power spectral broadening in RDX is associated with the (assumed) low barrier to ring fission is not supported by the current results.

Somewhat more convincing evidence is obtained when the spectra for selected internal coordinates are considered. Power spectra computed at the zero-point

energy for the CN bonds and CNN angles are presented in Fig. 23, for the same conditions leading to Fig. 22b. The top and bottom panels contain CN bond and CNN angle spectra, respectively. The differences are far more striking for these single-coordinate spectra than for the composite cases. While the effects of normal-mode structure remain obvious in the overall "envelope" of the various spectra, the differences arising due to the parameterizations of the switching functions are now clearly observable. The spectra for PES III and IV are virtually indistinguishable, consisting of very sharp peaks. On the other hand, the spectra for PES I and II comprise a sequence of broadened, relatively ill-defined peaks.

The peaks for PES I are significantly less distinct than those for PES II, especially for the CN bond spectra shown in the top panel, for which the PES I result is highly broadened. This is not surprising since this bond is directly involved in the reaction coordinate, and large differences in the barrier heights are ultimately expected to exert some influence on the extent of mode mixing, irrespective of the shapes of the switching functions. This is especially true for the CN bonds since the triazine ring is modelled as a kind of "competitive feedback loop" wherein the motions of alternate CN bonds (say, *i*, *k*, *m*) affect the parameters of the remaining CN bonds (*j*, *l*, and *n*). However, on the whole, the differences in the broadness of the spectral peaks of PES I and II are less than the differences in the broadness of those of PES II and III. Thus, the potentials which have barrier heights differing by 30 cal/mol (but which are based on very similar choices of switching functions) give rise to more similar spectra, in terms of sharpness, than do those having barrier

heights differing by only 4 kcal/mol (but which are obtained from potential-energy surfaces having quite different switching function parameters).

We carried out a few calculations designed to search for mode-specific effects in the spectra of RDX at experimentally interesting energies. Zhao *et al.*[114] have studied the infra-red multiphoton dissociation of RDX in a molecular beam. They estimated that about 80 kcal/mol of excitation energy is deposited into the molecule, giving a net energy (zero-point energy plus excitation) of approximately 160 kcal/mol. We focussed our attention on PES III (barrier of 71 kcal/mol) since it gives rise to minimal broadening, and since our normal-mode analysis is "correct" for that potential (no discontinuities in the second derivatives). Whether it is a more reasonable model for RDX than PES II is an open question.

Figure 24 contains a series of spectra for the three NCN and three wag angles (panels a and b, respectively). The top spectrum in each panel (Random) corresponds to trajectories initiated using a classical microcanonical sampling procedure[125,126] in which the total energy is randomly distributed over the molecule using a Markov chain. The middle spectrum in each panel (QCT) corresponds to a mode-specific, quasiclassical excitation[120] in which zero-point energy is first assigned to the vibrational normal modes, after which 80 kcal/mol of excitation energy is added to a single ring mode. The bottom spectrum in each panel (ZPE) corresponds to a quasiclassical partitioning of the zero-point energy and simply serve as reference spectra.

The results shown in Fig. 24 indicate that mode specificity persists for at least

10 ps. The top and middle spectra differ considerably in the distribution of intensity. For the case of the NCN angle (top panel), the spectrum corresponding to mode-specific excitation (QCT) has sharper peaks than the one obtained for random excitation (Random), suggesting relatively restricted energy flow in the former case. The peak centered around 1000 cm^{-1} is most affected, but the effect can also be seen in the other peaks. For the case of the exocyclic wagging motion (bottom panel), the main effect is an "exchange" of intensity between the very low- and high-frequency peaks.

While the lifetime for RDX at this energy is presumably orders of magnitude longer than what is being considered here, it is still interesting that one can see a non-negligible signature of non-global IVR in the spectra at such high energies (twice the zero-point level).

Conclusions

We have qualitatively explored the sensitivity of power spectra (and thus IVR) in a large, polyatomic molecule (RDX) to details of how the potential-energy surface is constructed and to the initial distribution of excitation energy. The main thrust has been to vary the barrier height and position by way of adjustment of the parameters appearing in the switching functions used to incorporate the complex reaction channels which are present in the molecule, and to probe the extent of IVR on the different surface parameterizations using power spectra as our diagnostic tool.

Markedly different degrees of energy transfer were implied by the power

spectra obtained for two potentials having barrier heights which differ by only 6 per cent (67 and 71 kcal/mol). By contrast, spectra obtained from two potential-energy surfaces having barrier heights differing by nearly a factor of two (37 and 67 kcal/mol) were more reminiscent of one another, in terms of average peak widths, than were those differing by 6 per cent. These results emphasize the important role of the shapes of the switching functions, i.e., the characteristics of the modes orthogonal to the reaction coordinate, in determining the vibrational dynamics.

One of the potentials was probed in greater detail in an effort to determine whether mode specificity was present over the time scales considered in this work. The results indicate that this is the case. Different methods of partitioning the energy led to non-negligible differences in the resulting power spectra obtained from 10 ps trajectories. Whether this restricted IVR persists to higher energies is not obvious, but is an area of continuing interest.

Our results underscore the fact that simply adjusting the barrier height in a many degree-of-freedom system to reproduce an experimentally measured or theoretically calculated value for the barrier is a risky approach to take when constructing potential-energy surfaces. The state of the art for generation of potential-energy surfaces for large polyatomic molecules has probably evolved to a level where it is almost indefensible to not incorporate *ab initio* information into the development of a new PES. While it is not practical (nor particularly desirable) to map the entirety of a polyatomic potential-energy surface using quantum chemical techniques, useful information about the behavior of crucial parameters along the

minimum-energy path can be obtained even for molecules containing dozens of atoms, and should be used as a guide in the development of potentials for studies of large molecules.

Table X. Switching Function Parameters

	Surface I[a]	Surface II[b]	Surface III[c]	Surface IV[d]
S^e(NN) n	2	2	4	-
β	1.0	1.0	1.0	0.0
S^e(CN) n	4	4	4	-
β	5.5	5.5	4.5	0.0
S^f(CN) n	2	2	4	-
β	3.5	2.5	8.5	0.0

[a] Concerted ring dissociation barrier height of 37 kcal/mol.
[b] Concerted ring dissociation barrier height of 67 kcal/mol.
[c] Concerted ring dissociation barrier height of 71 kcal/mol.
[d] No potential-energy surface attenuation.
[e] Equation (22).
[f] Equation (23).

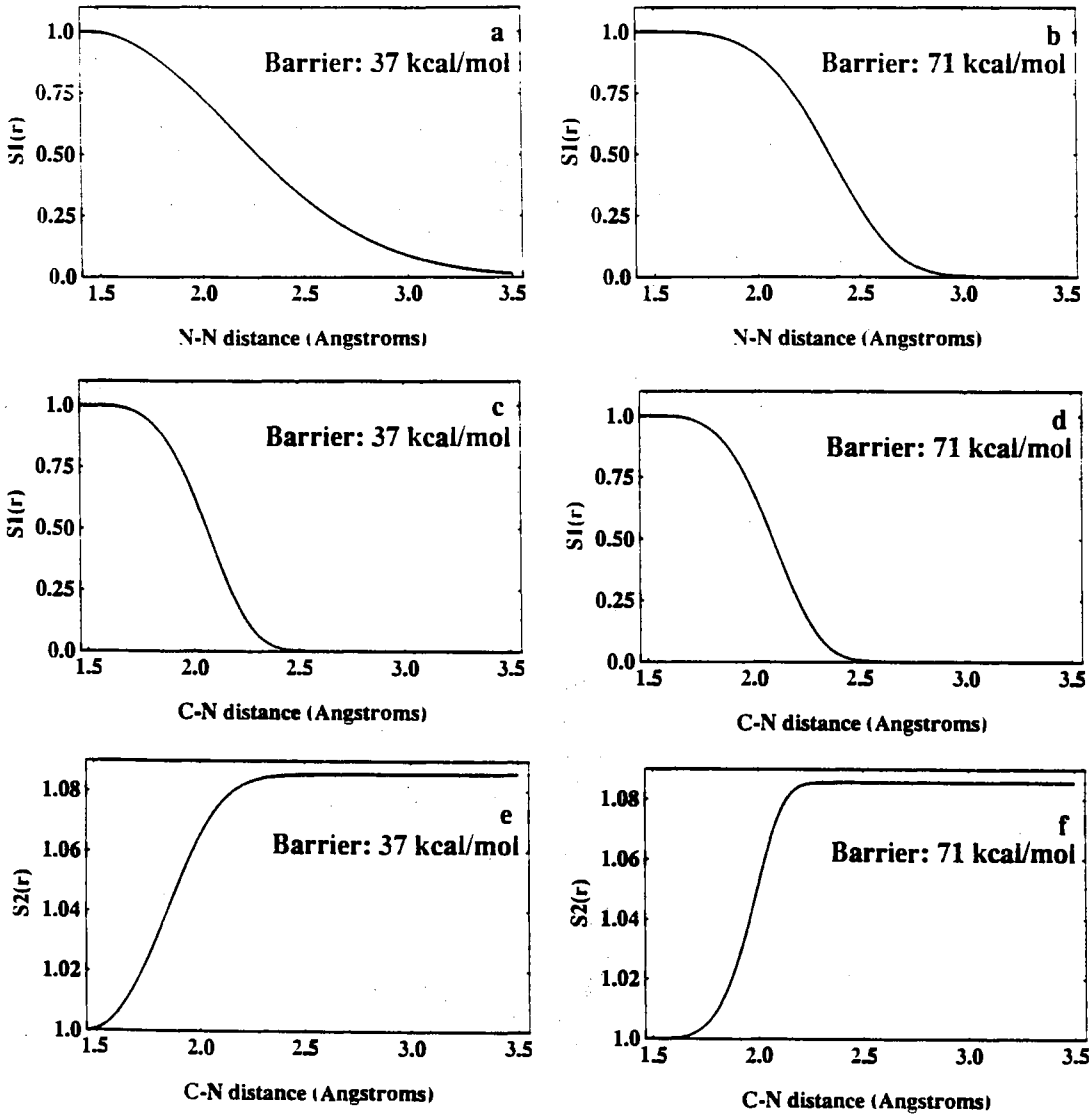

Figure 20. Representative switching functions are shown for RDX PES I (left-hand column) and RDX PES III (right-hand column). Panels a and b (top row) depict the switching functions used to attenuate the angle-bending force constant for a CNN angle as the N-N bond dissociates. Panels c and d (middle row) are similar to a and b except that they correspond to fission of the involved C-N bond. Panels e and f (bottom row) consist of the switching functions used to modify the equilibrium NCH angle as the adjacent CN' bond dissociates.

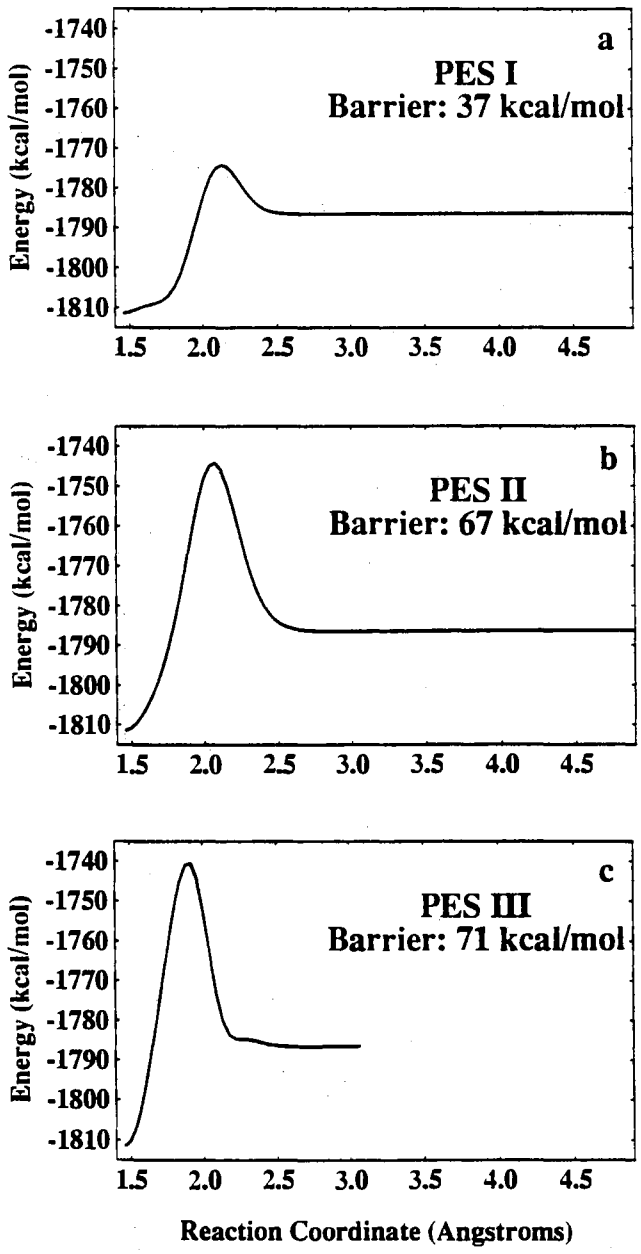

Figure 21. Minimum-energy profiles for symmetric ring fission of RDX on PES I, II, and III are presented. Panel a: PES I; panel b: PES II; panel c: PES III. The barrier heights are 37, 67, and 71 kcal/mol, respectively. The abscissa corresponds to the extension of the three C-N bonds being cleaved in the ring-fission process.

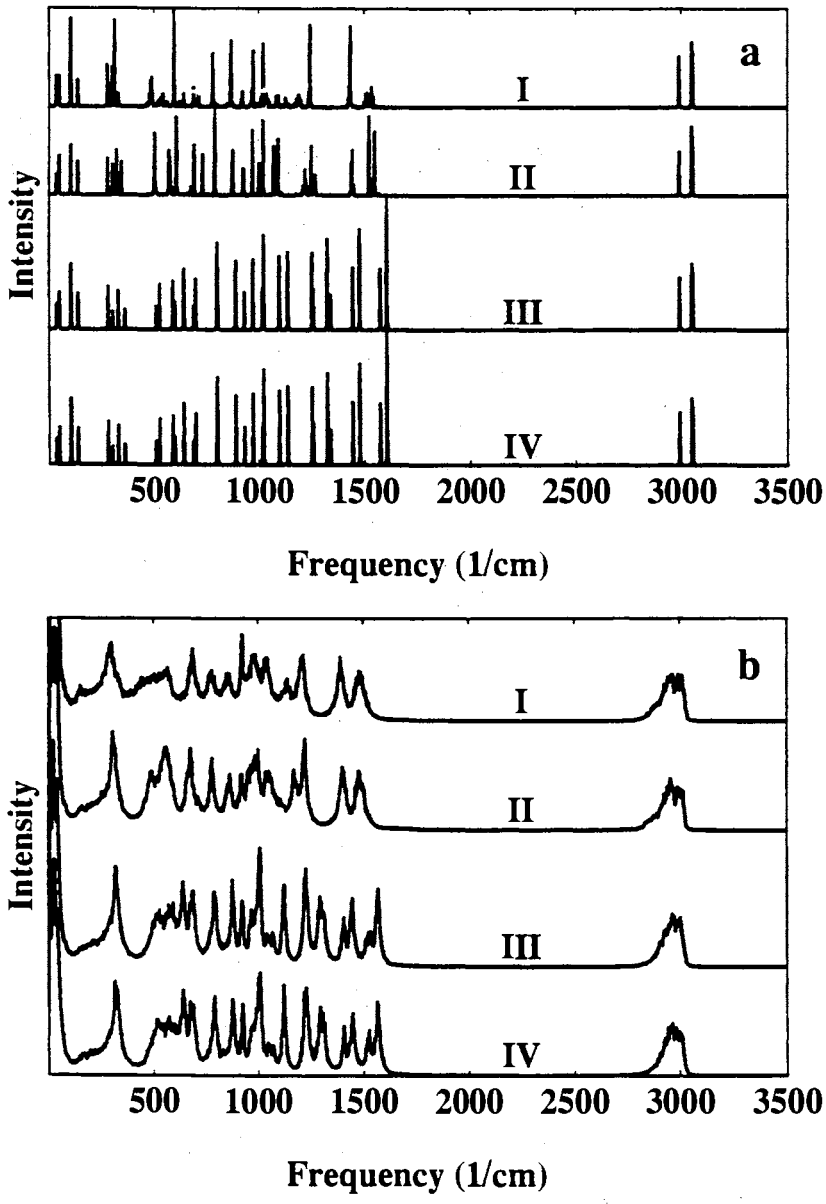

Figure 22. Composite power spectra of RDX for trajectories computed at very low total energy (panel a) and zero-point energy (panel b). The spectra are shifted for clarity. The labels accompanying each trace correspond to the PES designations defined in the text. The origin of the differences in the spectra shown in panel a (and persisting in panel b) is the presence (PES I and II) or absence (PES III and IV) of discontinuities in the second derivatives of the switching functions used.

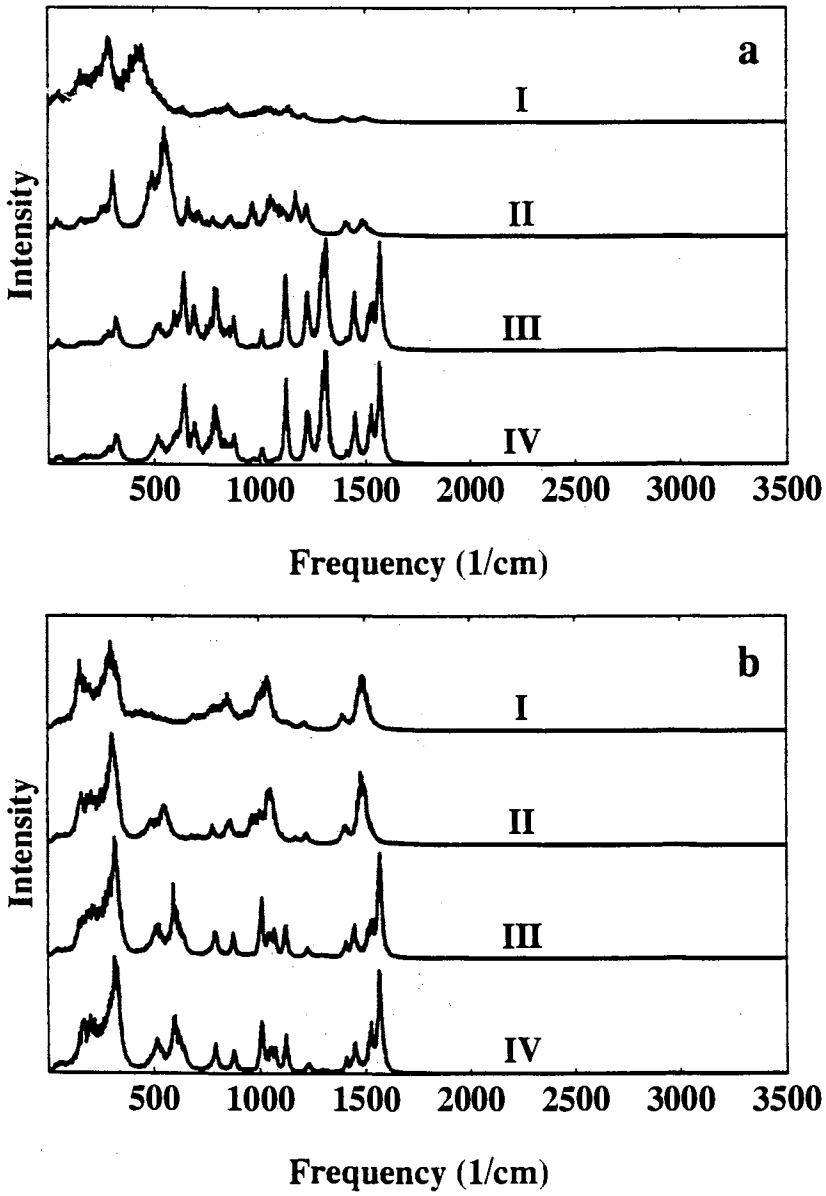

Figure 23. Ensemble-averaged, zero-point energy power spectra of the CN bonds and CNN angles in RDX are shown. Initial conditions were obtained using quasiclassical projection methods. Results for the CN bonds are shown in the left-hand column (panel a); those for the CNN angles are in the right-hand column (panel b). Individual traces are labelled in accordance with the PES designations defined in the text.

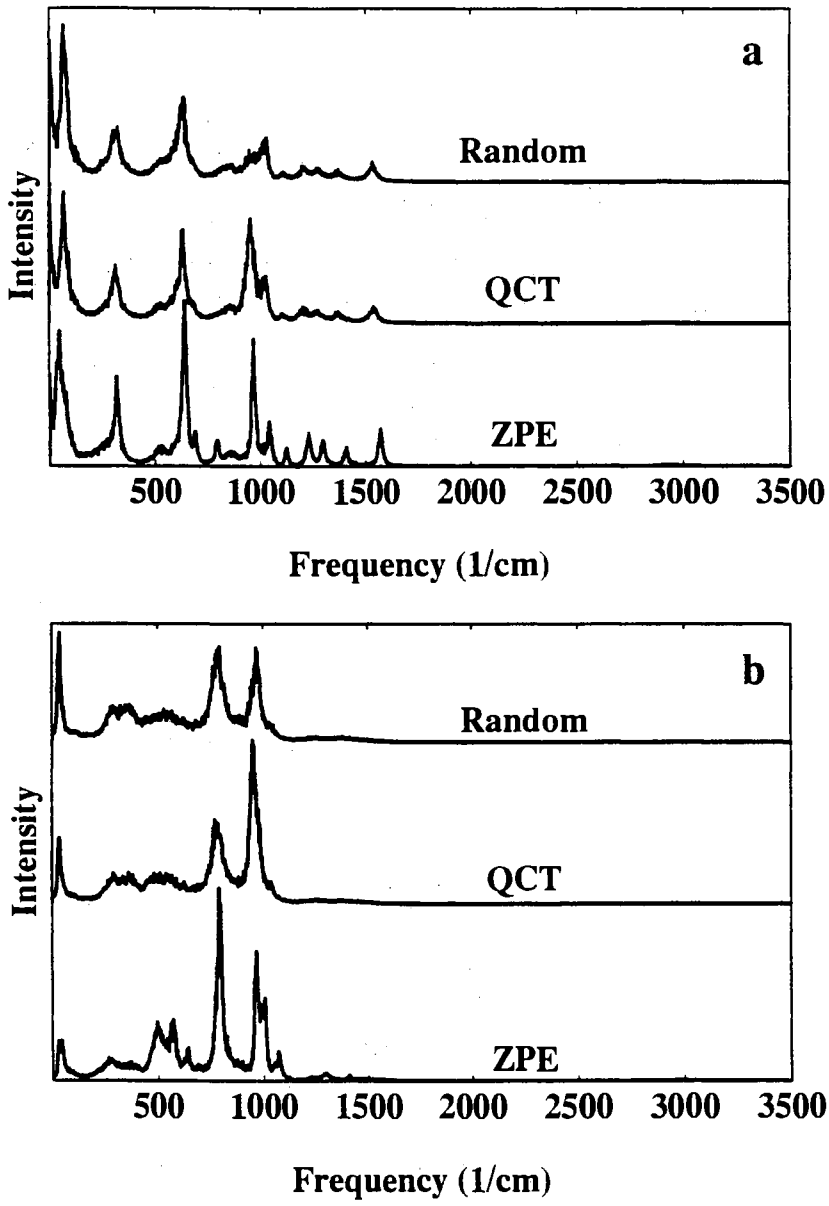

Figure 24. Ensemble-averaged power spectra of RDX indicating the presence of mode specificity in the classical dynamics of PES III are shown. Top and bottom panels correspond to spectra for the NCN bending and NO_2 wagging angles, respectively. The spectra labeled random correspond to a microcanonical distribution of 160.0 kcal/mol of energy over the vibrational degrees of freedom. The spectra labeled QCT correspond to quasiclassical partitioning of the zero-point energy (81 kcal/mol) followed by selective excitation of a single "ring mode" to yield the same total energy as in the random ensembles. The spectra labeled ZPE correspond to zero-point energy spectra for the two internal coordinates and are intended to serve as a reference.

CHAPTER VIII

FURTHER STUDIES OF THE CLASSICAL DYNAMICS OF THE UNIMOLECULAR DISSOCIATION OF RDX

Introduction

Recently several studies have been reported on the classical dynamics of RDX (hexahydro-1,3,5-trinitro-1,3,5-triazine).[26,113,172,177] These studies have focused on the unimolecular reaction dynamics,[113] conformational changes,[172,182] and the basic behavior of the vibrational dynamics.[26] The challenge in modeling the chemical dynamics of RDX is the formulation of an accurate potential-energy surface (PES). *Ab initio* methods are of limited use in determining the global potential that includes the reaction channels because of the size of the molecule. Thus, we have developed a PES that is based mainly on experimental data. Some *ab initio* results for the equilibrium reactant and product molecules are available in the literature and were used in adjusting the PES parameters.

In an earlier study[113] of the unimolecular reaction dynamics of RDX, Sewell and Thompson computed the rates for the ring fission reaction that gives 3 H_2CNNO_2 molecules and the simple N-N bond rupture reaction giving the radicals NO_2 and $C_2H_4N_4O_4$, and the product energy distributions, over the energy range 250-350 kcal/mol. These reaction channels were proposed by Zhao, Hintsa and Lee.[114] They used infrared multiphoton dissociation (IRMPD) to study RDX in a molecular beam. Their results indicate that the ratio of the rate of the molecular elimination

reaction to that of the N-N bond rupture reaction is about 2 at a total energy estimated to be in the range 150-170 kcal/mol. That is, they found that the two channels are competitive.

Sewell and Thompson[113] used potential-energy surfaces for which the barrier to N-N fission is 47.8 kcal/mol (the reaction endothermicity) and barrier heights of 35.7, 38.3, and 41.0 kcal/mol for the ring fission reaction (most of the calculations were done for the 38.3 kcal/mol barrier). They calculated branching ratios in the range 1.0-2.4. These results and the computed product energy distributions are in qualitative agreement with the molecular beam results of Zhao *et al.*[114] The calculations are for energies well in excess of those in the experiments and thus it is necessary to extrapolate the computed values to lower energies for the comparison. Because of the statistical error in the calculated values of the branching ratio, it is not clear how quantitative the agreement is. Nevertheless, the comparison with experiment suggests that the PES is qualitatively correct. However, some *ab initio* calculations have given values on the order of 70 to 80 kcal/mol for the ring fission reaction.[115] This seems high in light of the Zhao *et al.*[114] conclusion that this channel is competitive with the N-N bond fission reaction, which has an energy requirement of about 46-50 kcal/mol.

In the present study we have carried out extensive classical trajectory calculations on similar but new PESs. The main reason for further study of the classical reaction dynamics of RDX is to help resolve the question of the barrier height for the ring fission reaction. That is, can a reasonable PES with a ring fission

energy barrier on the order of 70 kcal/mol (as predicted by *ab initio* calculations) yield a branching ratio of 2:1 for ring fission to N-N bond fission (which has a barrier of less than 50 kcal/mol)? Most of the calculations reported here were done for surfaces with ring fission barrier heights of 37, 56, and 71 kcal/mol (which we will denote as PES I, II, and III). The energy required for N-N bond rupture is 47.8 kcal/mol for all three PES. Trajectories were calculated over the energy range 200-450 kcal/mol.

We also address problems in reconciling reported estimates of the RDX bond energies with the thermodynamics of the reaction to give the secondary products and the bond energies of the secondary product molecules. Also, we have preformed a small number of calculations to investigate changes in the reaction rates if the RDX well depths are adjusted to be in reasonable agreement with the thermodynamics of observing the secondary reaction products (as reported by Zhao *et al.*[114]).

RDX has been the subject of considerable interest and some controversy lately. For a brief summary, see Chapter I. In short, there is now enough experimental data with which to make comparisons and thus provide guidance for the development of models for realistic simulations of RDX.

Computational Methods

We have constructed three anharmonic potential-energy surfaces that include the two reaction pathways, NN bond rupture and concerted ring fission. The surfaces were constructed by using available experimental[173,186] and theoretical[174,175,185,187] data.

The three surfaces have barrier heights of 37, 56, and 71 kcal/mol for the ring fission reaction and 47.8 kcal/mol for the N-N bond fission reaction.

Trajectories were calculated on all three surfaces over the energy range 200-450 kcal/mol. Unimolecular dissociation rate coefficients were calculated for the two reactions. The branching ratio of ring fission to NN bond rupture was calculated as a function of energy over the range 200-450 kcal/mol.

Our general classical trajectory code GenDyn[124] was used to calculate the trajectories. Hamilton's equations of motion were integrated by using a fourth-order Runge-Kutta-Gill routine in a space-fixed Cartesian coordinate system. The integration step size was 1.0×10^{-16}s, and the trajectories were calculated for 50 ps, or until the molecule dissociated. Initial conditions for the trajectories were selected by Monte Carlo quasiclassical and classical microcanonical methods; in the former, the energy is projected onto the normal modes[120] and in the latter classical initial conditions were generated by using a metropolis procedure developed by Nordholm and coworkers.[125,126] The total angular momentum is zero in all of the calculations.

The first-order rate coefficients, k, for the overall decay of RDX were computed by fitting the lifetimes to

$$\ln(N_t/N_o) = -kt, \qquad (29)$$

where N_t is the number of unreacted molecules at time t and N_o is the number of trajectories in the ensemble. Since the molecule decays by two competing reactions:

$$3\ H_2C{=}N\text{-}NO_2 \qquad k\ (ring) \qquad (R1)$$

$$RDX \nearrow \searrow$$

$$C_3H_6N_3O_4 + NO_2 \qquad k\ (NN) \qquad (R2)$$

the rate coefficients for the two channels are obtained from

$$k = k\ (ring) + k\ (NN) \qquad (30)$$

and

$$k\ (NN) = k / (1 + N\ (ring) / N\ (NN)); \qquad (31)$$

where k (ring) and k (NN) are the rates of reactions R1 and R2, respectively, N (ring) and N (NN) are the numbers of trajectories which led to reactions R1 and R2, respectively. The branching ratio of concerted ring fission to N-N bond rupture is

$$Branching\ Ratio = k\ (ring) / k\ (NN) \qquad (32)$$

Potential-Energy Surface

A. Thermodynamics of Reactants, Primary and Secondary Products

The dissociation of RDX into its final products is believed to involve several reaction pathways. Zhao *et al.*[114] have shown that the primary pathways are simple NN bond rupture and concerted ring fission in the gas-phase. The products of the initial reactions further decompose. One of the products of the decomposition of CH_2NNO_2 is HCN + HONO.[185,188] Determination of the values of the bond energies in RDX based upon primary products leads to dramatically different well depths[113]

than does a similar determination based upon the secondary products.[14,16,185,189,190] In this study, most of our calculations were done using PESs in which the well depths for the reactants and the primary products are based on the observed thermochemistry of the primary products. A few calculations were performed using much weaker bond strengths derived from the known thermochemistry of the secondary products.[185,189] The calculated branching ratios are approximately the same for the two different "parameterizations" of the PES.

Sewell and Thompson[113] reviewed the thermochemistry of the reactant and products. The sum of the RDX bond energies calculated using the Sewell-Thompson PES is 1811.4 kcal/mol, and the sum of the bond energies of the secondary products is 483.249 kcal/mol.[14,16,190] The secondary product bond energies, multiplied by three (three [HCN + HONO] can be produced from one RDX molecule) gives product bond energies of 1449.747 kcal/mol. This leaves a resulting reaction endothermicity from reactants to *secondary* products of 361.653 kcal/mol.

The exothermicity of the reaction $CH_2NNO_2 \rightarrow HCN + HONO$ has been reported by Beyer and Morgon[189] to be 10.3 kcal/mol and by Mowrey *et al.*[185] to be 23.8 kcal/mol. These values, multiplied by three, give exothermicities of 30.9 and 71.4 kcal/mol, respectively. These reported bond energies of RDX and the secondary products are not reconcilable with the reported thermochemical values.

Figure 25, contains an illustration of the ranges of values of thermochemical quantities for the decomposition of RDX via the concerted ring fission pathway to primary and secondary products that are obtained using the various values given in

the literature. We take the classical ground-state of RDX to be the zero of energy. The products $3CH_2NNO_2$ have been estimated to be as low as 24.4.[113] Since it has been suggested that the barrier height for concerted ring fission may be as high as 72-75 kcal/mol,[175] supposing that there is no back barrier to reaction, we might assume an uppermost limit of 75 kcal/mol. Then, the secondary products are 30.9 to 71.4 kcal/mol (three times the values reported by Beyer and Morgon[189] and Mowrey *et al.*[185]) lower in energy than the primary products. The maximum endothermicity of the reaction from the reactant (RDX) to the products (HCN+HONO) is only 44.1 kcal/mol and the maximum exothermicity is 47.0 kcal/mol; this is a broad range. The asterisk in Fig. 24 marks the suggested endothermicity of Zhao *et al.*[114] of 32 kcal/mol ("endothermicity of Eq VII," Ref. 114). If the range of exothermicities of the reaction of primary products to secondary products is correct, the value quoted by Zhao *et al.*[114] for the entire reaction endothermicity is not possible unless the endothermicity of the primary reaction is at least 62.9 kcal/mol.

In order to reconcile these differences, we adjusted the reactant and product (CH_2NNO_2) bond strengths so as be consistent with available experimental and theoretical data, but not necessarily consistent with the available information on the bond strengths of the reactant.[184] Calculations of the branching ratio gave values that are similar to those for the PES for which the bond strengths were derived from only thermochemical data for RDX and primary products as well as values suggested elsewhere in the literature.[113,184] There are two points which should be noted. This

comparison is for calculations preformed on PESs with a barrier to concerted ring fission of 71 kcal/mol. The other is that while at this point we cannot conclusively say which set of bond strengths for RDX and CH_2NNO_2 is correct, we have elected to use those suggested in the literature. We note that they may not be correct. However, the branching ratios calculated on the two surfaces are comparable, indicating that using the other values of the well depths would yield similar results. In other words, the branching ratio does not appear to be very sensitive to these parameters.

B. Analytical form of the Potential-Energy Surface

We have used potential-energy surfaces based on anharmonic stretches (Morse functions), harmonic bends, and truncated cosine series for torsions. Not only does this simplify the dynamics for the analysis, but as has been previously shown with a series of studies[9-23] that such simple forms of potentials suffice to realistically describe important aspects of IVR. The analytical form, based on a valence force field, is that of Eq. 8. It is the sum of Morse functions for the 21 bonds, harmonic oscillators for the 36 angles and 3 wags, and six-term cosine series for 12 torsional angles.

We constructed three reactive surfaces by modeling the reactant molecule and the products based on information available in the literature. Geometries and frequencies of the products are available for only one set of the products, those due to concerted ring fission. Such information was not available for the fragment $C_3H_6N_5O_4$, which results from simple NN bond rupture, thus we attenuated the values

of the adjacent NNO, CNN, and C_2N-N angle force constants to zero as the NN bond distance became large; the other potential parameters (e.g. bond parameters) of the fragment were not attenuated. Information is available to construct a CH_2NNO_2 force field.[185,187] The reactant and product force fields were then used to construct a global potential by using switching functions (given in Table XI). The equilibrium geometries of the reactants[186] and products[185] are shown in Table XII. All of the surfaces used in this study have the same values of these geometric parameters.

The bond strengths in RDX and CH_2NNO_2 are the same on all but one of the surfaces. (As discussed above, we calculated a single ensemble with bond strengths different from those used in the remainder of the study and found essentially the same results.) The bond energies used here (for PESs I, II, and III) are those that have been suggested elsewhere for RDX[10b,113,184] and CH_2NNO_2[113,184] and are given in Table XIII along with the force constants.

The frequencies which were obtained from a normal mode analysis (Eq. 8) and those obtained from experiment[173] and *ab initio* calculations[174] for RDX are given in Table XIV. The eigenvalues listed in Table XIV are not assigned to particular experimental frequencies, since the experimental normal mode assignments were not available. Yet, an attempt was made to fit the eigenvectors (and eigenvalues) to assignments suggested by the *ab initio* calculations.[174] Table XV compares the normal mode frequencies calculated from the normal mode analysis for CH_2NNO_2 and the values from an *ab initio* calculation.[185]

The forms of the switching functions used to connect the reactant and product wells are the same for all the surfaces studied. The parameters of the switching functions were adjusted so as to give the desired barrier height to concerted ring fission. The switching functions used are those given in Eqs. 22 and 23; they are used when $r>r^R$, when $r<r^R$ S1(r) and S2(r) are unity. (See Ref. 113 for a discussion of the calculation of the coefficients $a(r,q^R,q^P)$.) Table XVI contains the values of the parameters used to define the switching functions for the various surfaces. The switching functions are designed to force a "competitive feed-back loop" similar to that used in the Sewell-Thompson[113] potential-energy surface. Since Zhao *et al.*[114] have suggested that the two main reaction channels are simple NN bond rupture and concerted ring fission (not single or double CN bond breakage) the switching functions used attenuate the PES such that as a single CN bond stretches, the nearest neighbor CN bonds attenuate to product values (CH_2NNO_2) and the "second" neighbor CN bonds begin to attenuate to breakage (zero well-depth). See Table XI for the details of the attenuation of each potential parameter.

The rate at which a parameter such as a well depth, force constant, equilibrium bond length, or equilibrium angle changes during reaction is controlled by the shape of the switching functions that smoothly connects reactant and product parameters. We used 198 switching functions to incorporate the reaction channels in RDX. Different sets of values of the switching function parameters were used give barriers of 37, 56, and 71 kcal/mol (PES I, II, and III, respectively) for the ring fission reaction (see Table XVI).

C. Barriers to Reaction

Figure 26 shows plots of the minimum-energy paths (MEP) for concerted ring fission using the three different sets of values of the switching function parameters (see Table XVI). We calculated the MEP as described in Ref. 113. The endothermicity of the reaction, 24.4 kcal/mol, is the same on all three surfaces. The MEP were calculated by extending the alternating CN bonds by 0.01 angstroms and then allowing the remaining coordinates to relax to the local minima corresponding to the particular extension of the breaking CN bonds. Starting with the equilibrium geometry of RDX, the alternating CN bonds 1, 3, and 5 (if the ring bonds are numbered 1 through 6) are expanded while bonds 2, 4, and 6 are allowed to relax to their equilibrium values. The MEP is obtained by plotting the minimum energy as bonds 1, 3, and 5 are extended.

There are several features of the MEP that should be noted. When the switching function parameters were varied to obtain the desired barrier heights, other features of the MEP changed as well. The initial regions of the MEP differ. The MEP with a height of 37 kcal/mol (PES I) remains at low energy for longer reaction coordinate distances than does the MEP with a height of 71 kcal/mol (PES III). The shape of the MEP with a height of 56 kcal/mol (PES II) is intermediate between these two. Another distinguishing feature is the position of the barrier. The MEP with heights of 37 and 56 kcal/mol have barriers which occur at greater reaction coordinate distances than the barrier of the surface with a barrier height of 71 kcal/mol. Data is currently not available to fit these other features.

Note that with the same switching function parameters as used in the previous study,[113] but with a different analytical form of the PES, the profile of the low barrier, 37 kcal/mol, (see Fig. 26) has a different shape at low values of the reaction coordinate from the previous surface (see Ref. 113, Fig. 4).

D. Comparison to the Sewell-Thompson Potential-Energy Surface

In the previous study of the unimolecular dissociation of RDX[113] a similar PES was used, although there are a number of important differences from those used here. The new PESs presented here were constructed with data which were not available when the previous surface was constructed. There are differences from the Sewell-Thompson surface[113] in the reactants, products, and regions between the reactants and products (due to fact that the attenuation of the PESs differ from that used in Ref. 113). Additionally, the new PESs include more of the internal motions, thus they are more realistic.

The analytical form of the Sewell-Thompson[113] PES is also based on a valence force field, however, non-bonded interactions were used instead of cosine series. The PES is given by,

$$V=\Sigma_{\text{stretches}}\,[\,D_e\{1-\exp[-\alpha(R-R_e)]\}^2-D_e] + \Sigma_{\text{bends}}\,(1/2)\,k\,(\theta-\theta_e)^2 + \Sigma_{\text{wags}}\,(1/2)\,k\,(\gamma-\gamma_e)^2 + \Sigma_{LJ}\,4\epsilon[(\sigma/r)^{12}-(\sigma/r)^6], \quad (33)$$

a sum of Morse functions for the 21 bonds, harmonic oscillators for the 36 angles and 3 wags, and 9 Lennard-Jones potentials for the non-bonded interactions. The non-bonded interactions, not included in the present PESs (see Eq. 8), are interactions

between the C and N atoms across the ring, C and the N atoms of the $-NO_2$ groups across the ring, and the N atoms of the $-NO_2$ groups interacting with the N atoms of the other $-NO_2$ groups (there are three of each of the listed non-bonded interactions included in the Sewell-Thompson PES). The new PES, on the other hand, includes 12 terms to represent the torsional forces in the ring (τ_{CNCN} and τ_{NCNC}) and the forces for the $-NO_2$ group twisting motions (τ_{CNNO}), terms which were not used in the Sewell-Thompson surface.[113]

Different equilibrium geometries for RDX and CH_2NNO_2 were used for the new PESs. The Sewell-Thompson PES[113] was based on the crystal-phase structure reported by Choi and Prince.[191] A tetrahedral ring geometry was assumed as well as C_2N-N wag angles of 0° with $-NO_2$ groups which were neither equatorial nor axial. The new PESs are based on the gas-phase geometry determined by electron diffraction by Shishkov *et al.*[186] Two of the most significant differences are that the nitro groups are in axial positions and that the C_2N-N wag angle is 19.9° for the new PESs. This difference in the positioning and orientation of the nitro groups probably affects the dynamics.[192]

The only vibrational frequencies available at the time of the construction of the Sewell-Thompson surface[113] were those from the experimental work by Iqbal *et al.*[173] There were thirteen normal mode frequencies[113] for which experimental values are still not available. For the PESs, we fit the eigenvalues to the frequencies reported by Iqbal *et al.*[173] and to the *ab initio* frequencies (which we scaled by 90%) reported by Coffin *et al.*[174] Additionally, we attempted to fit the eigenvectors using

the reported contributions of internal coordinates to the normal modes from the *ab initio* calculations.[174] Comparisons of the eigenvectors for the new PESs with those calculated from the Sewell-Thompson PES reveal that they are quite different except for the high frequency CH stretch modes.

The attenuation of the potential parameters as the system goes from reactants to products is similar for the two surfaces. The forms of the switching functions (see Eqs. 22 and 23) are identical. For PES I, which has the lowest barrier (37 kcal/mol) to concerted ring fission, even the switching function parameters are the same. The only difference is that four parameters (α_{NO}, k_{ONO}, k_{HCH}, and $\gamma_{CNC\text{-}N}$) are attenuated on PES I which are not attenuated on the Sewell-Thompson PES.[113]

Finally, there are some differences in the CH_2NNO_2 product molecule portions of the surfaces as well. The differences are similar to those described for the reactant portion of the surfaces. Well depths for the bonds are the same in all PESs. The geometry used for them were calculated by Mowrey *et al.*,[185] but different calculations of the geometry and frequencies were used for the three PESs used in this study. The Sewell-Thompson PES[113] used CH_2NNO_2 geometries and frequencies from the calculations at the stationary points for NN bond rupture (Table III, Ref. 185). Whereas the current PES uses CH_2NNO_2 geometries and frequencies from the calculations at the stationary points for concerted dissociation (Table I, Ref. 185). Again, these variations in the construction of the PESs lead to different values of the force constants.

Results and Discussion

The rate coefficients and branching ratios were calculated over the energy ranges 200-450 (PES I), 250-400 (PES II) and 250-450 kcal/mol (PES III). The results are summarized in Table XVII. We did not observed the ring fission reaction at 250 kcal/mol for ensembles of 50 trajectories integrated for 50 ps on PESs II and III, therefore, we did not calculate trajectories at lower energies on these PESs. We calculated an ensemble of 29 trajectories at 160 kcal/mol (the estimated energy in the Zhao *et al.*[114] experiments) on PES I, but found no reaction in either channel in the 50 ps trajectory calculation time. Based on extrapolation of the higher energy results to this energy this is not surprising, since the decay time of the concerted ring fission would be on the order of 2-3 x 10^3 ps.

Figures 27 and 28 contains RRK plots for the two reaction channels, NN bond rupture (Fig. 27) and concerted ring fission (Fig. 28). The data were fit to

$$\ln[k(E)]=\ln[A]+(s-1)\ln[1-(E_o/E)] \quad (34)$$

where E_o was taken to be 47.8 kcal/mol for all three surfaces for the NN bond fission reaction and E_o was set equal to 37, 56, and 71 kcal/mol for the concerted ring reaction channel for PES I, II, and III, respectively. From fits of the data to Eq. 34, we obtained frequency factors (A) of 2220, 27.9, and 27.6 ps^{-1} from the NN reaction RRK plots from surfaces I, II, and III, respectively. Frequency factors of 373, 62.4, and 2760 ps^{-1} were calculated from fits to the rates of the concerted ring fission reaction as a function of energy for surfaces I, II, and III, respectively. The calculated effective degrees of freedom, s, are 36, 17, and 13 for the NN reaction

channels and 40, 30, and 44 for the concerted ring fission channels for surfaces I, II, and III, respectively.

Figure 29 contains plots of the branching ratios as a function of energy for the three surfaces studied, (the experimentally determined[114] branching ratio at approximately 160 kcal/mol is shown as a solid triangle). One can see that PESs II and III, with barriers to concerted ring fission of 56 and 71 kcal/mol, give values of the branching ratio that are quite small and, for the range of energies studied, are essentially independent of the energy. It does not appear, based on these results, that they will lead to a branching ratio of 2:1 at 160 kcal/mol. In our calculations, we did not observe the ring reaction at 250 kcal/mol on either surface.

The computed branching ratios for PES I are shown as solid circles in Fig. 29. At energies above 300 kcal/mol the ratio is essentially independent of energy. As the energy decreases from 300 to 250 kcal/mol the ratio increases (the statistical behavior causes some nonmonotonic behavior) such that a reasonable extrapolation to 160 kcal/mol would give a value in accord with the experimental value (~2), shown as a solid triangle in Fig. 29.

We performed some calculations on this surface at 160 kcal/mol, but found no reaction in the 50 ps calculation times. Based on the RRK fit, we would expect the rate of ring reaction at 160 kcal/mol (on surface I) to be 3.74×10^{-4} ps^{-1}. Thus, it is not surprising that we did not observe reaction.

The mode-specific excitations yielded rates quite different from the random excitations. The rates and branching ratios resulting from calculations on PES I with

a ring mode initially excited are given in the last column of Table XVII. The branching ratios as a function of energy for both the mode-specific and random initial condition ensembles are shown in Fig. 30. At higher energies, initial excitation of the ring mode enhances the k_{ring}:k_{NN} branching ratio. This is a rather dramatic effect, especially in a molecule of this size. However, at lower energy (250 kcal/mol) the initial conditions do not appear to affect the branching ratio, although the rates are still affected.

Conclusions

Classical trajectories have been used to study the rates of dissociation of hexahydro-1,3,5-trinitro-1,3,5-triazine (RDX) in the gas-phase. Realistic models of RDX and the products of the ring fission, CH_2NNO_2, are used in conjunction with three barrier heights for concerted ring fission, 37, 56, and 71 kcal/mol, to study the branching ratios from the two reaction channels at energies from 200-450 kcal/mol. An attempt is made to reconcile the suggested[114] branching ratio of 2:1 (k_{ring}:k_{NN}) at approximately 160 kcal/mol and the suggested[175] barrier height of approximately 72-75 kcal/mol for concerted ring fission. We find that the lowest of the barriers used in our study (37 kcal/mol) yields branching ratios most reconcilable with experiment.

Finally, it has been shown that we can selectively excite a ring mode so as to enhance the branching ratio at high energy.

Table XI. Attenuation on the RDX PES

Coordinate	Parameter Based on Switching Function
CN bond	$D_{e,CN}^{\,i} = D_{e,CN}^{\,R}\, S^3(r_{CN}^{\,i-1})\, S^3(r_{CN}^{\,i+1})\, S^1(r_{CN}^{\,i-2})\, S^1(r_{CN}^{\,i+2})$ $\alpha_{CN}^{\,i} = \alpha_{CN}^{\,R}\, S^3(r_{CN}^{\,i-1})\, S^3(r_{CN}^{\,i+1})$ $r^{o}_{CN}{}^{i} = r_{CN}^{\,R}\, S^3(r_{CN}^{\,i-1})\, S^3(r_{CN}^{\,i+1})$
NN bond	$D_{e,NN} = D_{e,NN}^{\,R}\, S^2(r_{CN}^{\,i})\, S^2(r_{CN}^{\,i+1})$ $\alpha_{NN} = \alpha_{NN}^{\,R}\, S^2(r_{CN}^{\,i})\, S^2(r_{CN}^{\,i+1})$ $r^{o}_{NN} = r_{NN}^{\,R}\, S^2(r_{CN}^{\,i})\, S^2(r_{CN}^{\,i+1})$
NO bond	$\alpha_{NO} = \alpha_{NO}^{\,R}\, S^2(r_{CN}^{\,i})\, S^2(r_{CN}^{\,i+1})$
CH bond	$D_{e,CH} = D_{e,CH}^{\,R}\, S^2(r_{CN}^{\,i})\, S^2(r_{CN}^{\,i+1})$ $\alpha_{CH} = \alpha_{CH}^{\,R}\, S^2(r_{CN}^{\,i})\, S^2(r_{CN}^{\,i+1})$
intra ring angles	$k_{\theta}^{\,i} = k_{\theta}^{\,R}\, S^1(r_{CN}^{\,i})\, S^1(r_{CN}^{\,i+1})$
CNN angle	$k_{\theta,CNN}^{\,i} = k_{\theta,CNN}^{\,R}\, S^1(r_{CN}^{\,i})\, S^1(r_{NN})$ $\theta^{o}_{CNN}{}^{i} = \theta^{o}_{CNN}{}^{R}\, S^2(r_{CN}^{\,i+1})$
NNO angle	$k_{\theta,NNO}^{\,i} = k_{\theta,NNO}^{\,R}\, S^1(r_{NN})$
ONO angle	$k_{\theta,ONO} = k_{\theta,ONO}^{\,R}\, S^2(r_{CN}^{\,i})\, S^2(r_{CN}^{\,i+1})$
NCH angle	$k_{\theta,NCH}^{\,i} = k_{\theta,NCH}^{\,R}\, S^1(r_{CN}^{\,i})$ $\theta^{o}_{NCH}{}^{i} = \theta^{o}_{NCH}{}^{R}\, S^2(r_{CN}^{\,i+1})$ $k_{\theta,NCH}^{\,j} = k_{\theta,NCH}^{\,R}\, S^1(r_{CN}^{\,i})$ $\theta^{o}_{NCH}{}^{j} = \theta^{o}_{NCH}{}^{R}\, S^2(r_{CN}^{\,i+1})$
HCH angle	$k_{\theta,HCH} = k_{\theta,HCH}^{\,R}\, S^2(r_{CN}^{\,i})\, S^2(r_{CN}^{\,i+1})$ $\theta^{o}_{HCH}{}^{i} = \theta^{o}_{HCH}{}^{R}\, S^2(r_{CN}^{\,i})\, S^2(r_{CN}^{\,i+1})$
C_2N-N wag	$k_{\gamma} = k_{\gamma}^{\,R}\, S^1(r_{CN}^{\,i})\, S^1(r_{CN}^{\,i+1})\, S^1(r_{NN})$ $\gamma^{o}_{CNC\text{-}N}{}^{i} = \gamma^{o}_{CNC\text{-}N}{}^{R}\, S^1(r_{CN}^{\,i})\, S^1(r_{CN}^{\,i+1})\, S^1(r_{NN})$

Table XII. Equilibrium Geometries of RDX and CH_2NNO_2

	RDX[a]	CH_2NNO_2	
bonds (Å)		this study	*ab initio*[b]
CN	1.464	1.271	1.271
NN	1.413	1.441	1.441
NO	1.213	1.213	1.240, 1.303[c]
CH	1.089	1.089	1.073, 1.071[c]
angles (deg)			
CNC	123.7	***	***
NCN	109.4	***	***
CNN	116.3	115.7	115.7
NNO	117.25	117.25	114.5, 121.1[c]
ONO	125.5	125.5	124.4
NCH	110.571577	120.05	124.1, 116.0[c]
HCH	105.1	120.0	120.0
NCN-N	20.091558	***	***
CNCN, NCNC	36.34012	***	***
CNNO	19.1	***	***

[a] I.F. Shishkov *et al.* Ref 186.
[b] R.C. Mowrey *et al.* Ref. 185.
[c] Two bonds or angles reflect differences between similar coordinates.

Table XIII. Potential Parameters for RDX and CH_2NNO_2

Morse Parameters:

bond	RDX D_e (kcal/mol)	RDX α ($Å^{-1}$)	$CH_2N_2O_2$ D_e (kcal/mol)	$CH_2N_2O_2$ α ($Å^{-1}$)
r_{CN}	85.0[a]	1.954422	153.07[c]	1.734451
r_{NN}	47.8[a]	2.651632	30.60[a]	2.675695
r_{NO}	98.0[b]	1.951689	98.0	2.576902
r_{CH}	95.0[a]	1.941979	108.0	1.861508

Harmonic Force Constants:

angle	k_θ, (kcal/mol rad^2) RDX	$CH_2N_2O_2$
θ_{CNC}	189.593228	* * *
θ_{NCN}	145.334935	* * *
θ_{CNN}	231.652616	357.118978
θ_{NNO}	241.113503	319.754009
θ_{ONO}	205.484711	245.08904
θ_{NCH}	58.274924	63.025996
θ_{HCH}	56.180756	52.472672
γ_{CNC-N}	95.001720	0.0

Cosine Series Coefficients [kcal/(mol rad^2)]:

dihedral angle	a_0	a_1	a_2	a_3	a_4	a_5
τ_{CNCN}	0.425221	0.0	-0.430135	0.0	0.361213	0.0
τ_{CNNO}	1.17345	0.0	-1.65016	0.0	0.524958	0.0

[a] C.F. Melius and J.S. Binkley, Ref. 184.
[b] B.G. Sumpter and D.L. Thompson, Ref. 10b.
[c] T.D. Sewell and D.L. Thompson, Ref. 113.

Table XIV. RDX Normal Mode Frequencies[a]

Calc.	Expt.[b]	*Ab Initio*[c]	Calc.	Expt.[b]	*Ab Initio*[c]
36 (2)		22 (2)	889 (2)	910	995 (2)
39		52	931	885	912
46		64	972	935	1053
49 (2)		87 (2)	1023 (2)	1015	1070 (2)
104 (2)		198 (2)	1018	1045	1117
138		291	1098		1215
280 (2)		346 (2)	1137 (2)		1121 (2)
302		415	1257	1230	1238
328 (2)		380 (2)	1251 (2)	1270	1309 (2)
360		426	1323 (2)	1320	1348 (2)
508		535	1339	1392	1274
525 (2)		537 (2)	1444	1435	1342
588 (2)	610	606 (2)	1477 (2)	1460	1364 (2)
598	595	665	1575	1550	1481
641 (2)		666 (2)	1606 (2)	1585	1470 (2)
688		706	2993 (2)	2980	2954 (2)
698 (2)	740	758 (2)	2993		2961
800 (2)	794	912 (2)	3051 (2)		3066 (2)
803	750	833	3054	3080	3068

[a] Units are cm^{-1}. The normal mode frequencies were obtained by using second derivatives of the potential.

[b] Z. Iqbal *et al.* Ref. 173.

[c] J.M. Coffin *et al.* Ref. 174. The *ab initio* frequencies have been scaled by 90%.

Table XV. CH_2NNO_2 Normal Mode Frequencies

Calculated[a] (cm^{-1})	*Ab initio*[b] (cm^{-1})
c	90.0
370.1	351.9
c	504.5
553.0	558.7
589.7	598.6
779.7	784.7
780.5	806.1
928.3	1098.4
1038.7	1135.1
1140.5	1179.5
1371.4	1422.0
1479.9	1450.7
1618.2	1655.1
3022.3	3024.5
3144.8	3134.3

[a] The normal mode frequencies were obtained by using second derivatives of the potential.

[b] R.C. Mowrey *et al.* Ref. 185. The *ab initio* frequencies have been scaled by 90%.

Table XVI. Switching Function Parameters

		Surface I[a]	Surface II[b]	Surface III[c]
S^d(NN)	n	2	2	4
	β	1.0	1.0	1.0
S^d(CN)	n	4	4	4
	β	5.5	5.5	4.5
S^e(CN)	n	2	2	4
	β	3.5	2.8	8.5

[a] Concerted ring dissociation barrier height of 37 kcal/mol.
[b] Concerted ring dissociation barrier height of 56 kcal/mol.
[c] Concerted ring dissociation barrier height of 71 kcal/mol.
[d] Equation (22).
[e] Equation (23).

Table XVII. Reaction Rates and Branching Ratios[a]

Energy (kcal/mol)		I[b]	II[c]	III[d]	I'[e]
200	k(ring)	0.0029			
	k(NN)	0.0031			
branching ratio		0.93 (366)			
225	k(ring)	0.0086			
	k(NN)	0.018			
branching ratio		0.47 (431)			
250	k(ring)	0.035	0.0	0.0	0.021
	k(NN)	0.051	0.055	0.24	0.032
branching ratio		0.69 (247)	0.0 (19)	0.0 (121)	0.66 (275)
300	k(ring)	0.082	0.0052	0.00069	0.060
	k(NN)	0.23	0.19	0.11	0.039
branching ratio		0.36 (473)	0.028 (311)	0.0063(323)	1.5 (620)
350	k(ring)	0.11	0.011	0.0072	0.16
	k(NN)	0.47	0.33	0.31	0.072
branching ratio		0.25 (205)	0.033 (186)	0.023 (310)	2.3 (299)
400	k(ring)	0.21	0.022	0.023	
	k(NN)	0.67	0.56	0.65	
branching ratio		0.31 (312)	0.039 (539)	0.035 (468)	
450	k(ring)	0.40		0.044	
	k(NN)	0.91		0.78	
branching ratio		0.44 (538)		0.056 (631)	

[a] Rates are in ps^{-1} and branching ratios are k(ring):k(NN). Numbers in parentheses are ensemble sizes.
[b] Surface with a barrier to concerted ring fission of 37 kcal/mol.
[c] Surface with a barrier to concerted ring fission of 56 kcal/mol.
[d] Surface with a barrier to concerted ring fission of 71 kcal/mol.
[e] Same as surface I, only with different initial conditions, a ring mode was initially excited.

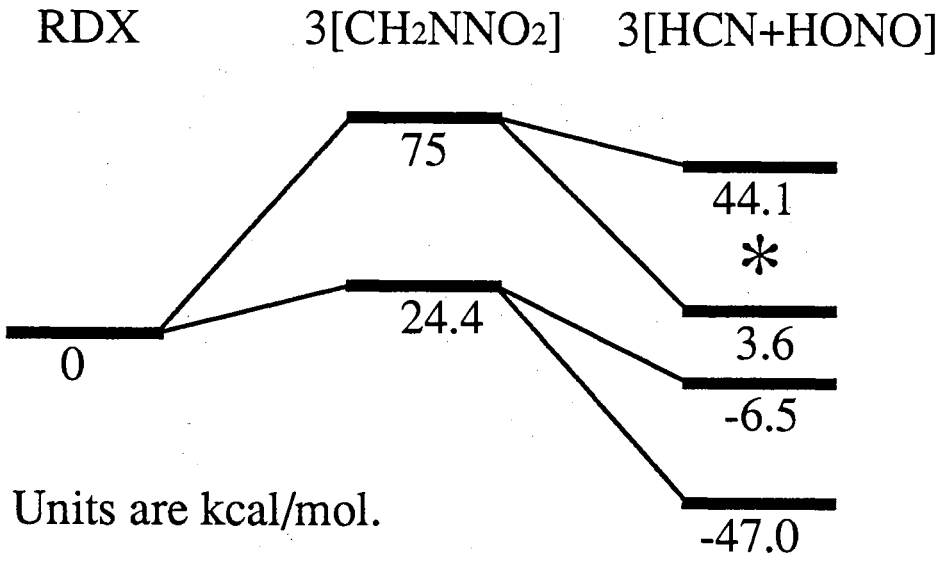

Figure 25. This is an illustration of the range of possible thermochemistry (available in the literature) of the RDX molecule and one of its primary decomposition pathways (concerted ring fission) followed by further decomposition to secondary products. Maximum and minimum possible values for the endothermicity are obtained from different combinations of published values of the heat of formation of solid RDX, the heat of sublimation of RDX, the heat of formation of gaseous RDX, and the heat of formation of CH_2NNO_2. The maximum and minimum exothermicities of the secondary reaction shown are available in the literature as well. The asterisk marks the endothermicity suggested by Zhao *et al.*[114]

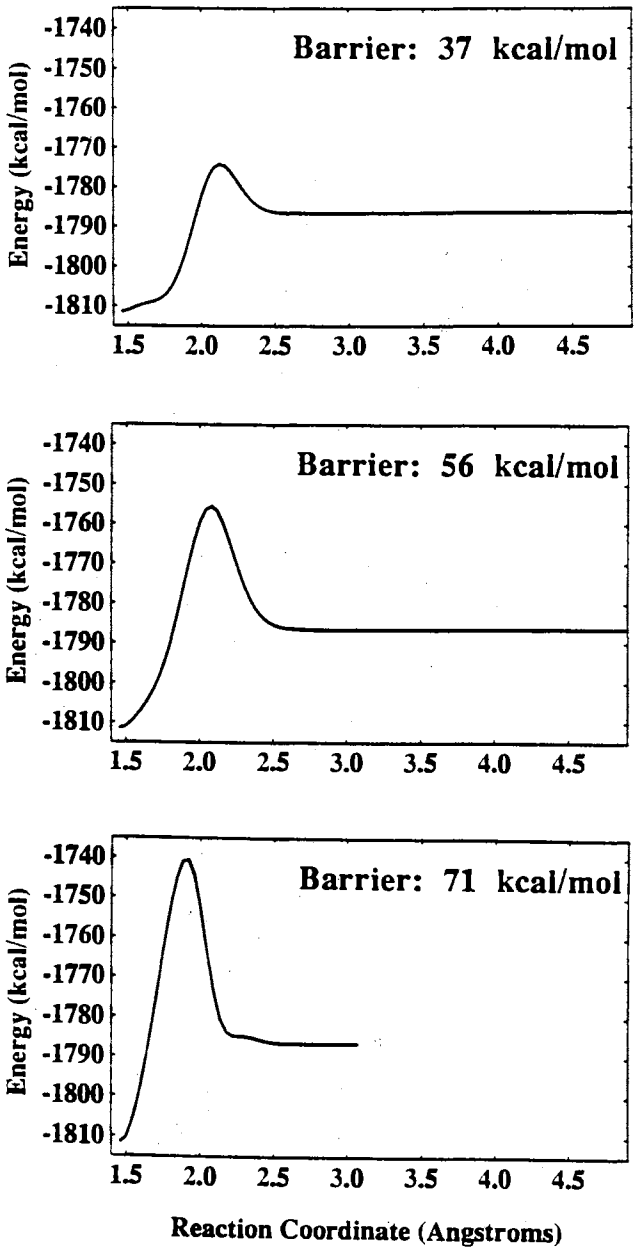

Figure 26. Plots of energy profiles along the minimum energy paths (MEPs) for ring fission in RDX for PES I, II, and III. The endothermicity of the reaction, 24.4 kcal/mol, is the same on all three surfaces. The MEPs were calculated by extending the alternating CN bonds by 0.01 angstroms and then allowing the remaining coordinates to relax to the local minimum corresponding to the particular extension of the breaking CN bonds. Starting with the equilibrium geometry of RDX we extend alternate bonds 1, 3, and 5 (where we number the ring bonds 1 through 6) while allowing bonds 2, 4, and 6 to relax. The MEP is obtained by plotting the minimized energy as bonds 1, 3, and 5 are extended.

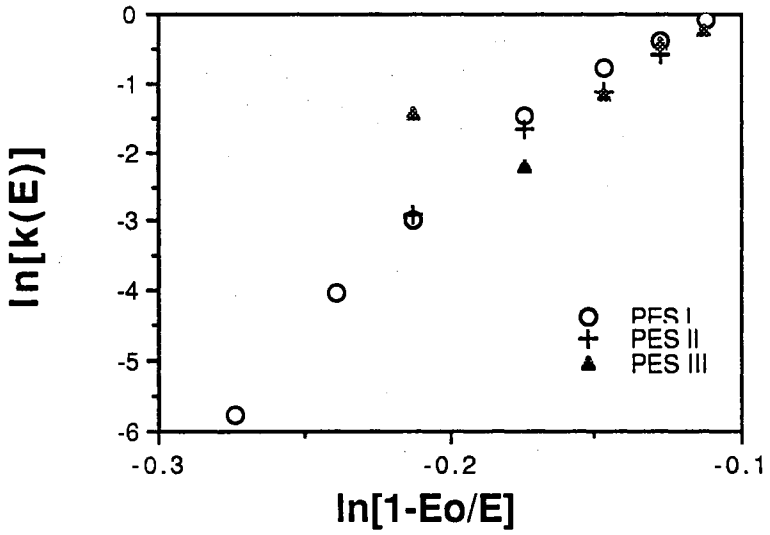

Figure 27. RRK plots for the NN reaction channel in RDX for all three surfaces.

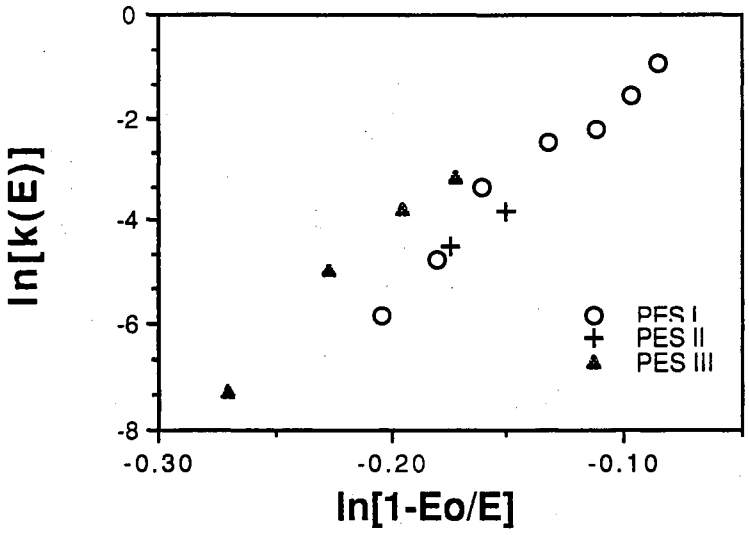

Figure 28. RRK plots for the concerted ring reaction in RDX for all three surfaces.

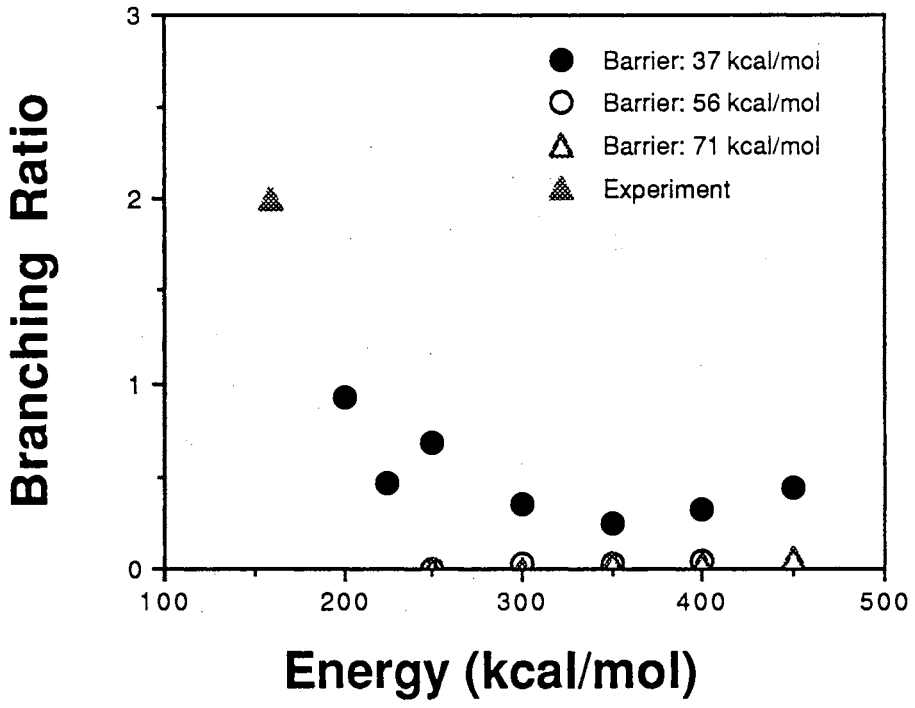

Figure 29. These are the branching ratios (k_{ring}:k_{NN}) as a function of energy on the three RDX potential-energy surfaces studied. Note that the ring reaction on the two surfaces with the higher barriers is quenched at 250 kcal/mol. These results, along with the k_{ring} and k_{NN} rates, are listed in Table XVII.

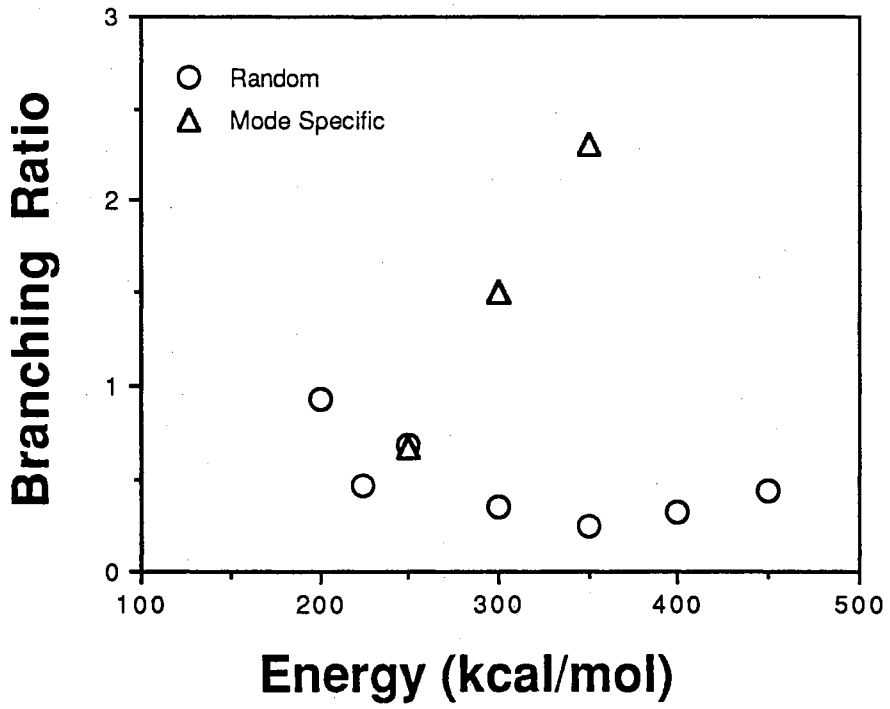

Figure 30. These are branching ratios as a function of energy on the RDX potential-energy surface with a barrier to concerted ring fission of 37 kcal/mol. Classical microcanonical methods (circles) and Monte Carlo quasiclassical methods (triangles) were used for initial condition selection of the trajectories. In the case of the Monte Carlo quasiclassical methods, we selected a ring mode on which to project the energy.

CHAPTER IX

CLASSICAL TRAJECTORY STUDIES ON A TWENTY-EIGHT ATOM POTENTIAL-ENERGY SURFACE: HMX

Introduction

We present results of a study that is an extension of the study described in the previous chapter. We have constructed a PES for octahydro-1,3,5,7-tetranitro-1,3,5,7-tetrazocine (HMX) based on the RDX PES. The studies of RDX have focused on the unimolecular reaction dynamics,[113] conformational changes,[172,177] and the basic behavior of the vibrational dynamics.[26] The challenge in modeling the chemical dynamics of RDX and HMX is the formulation of an accurate potential-energy surface (PES). *Ab initio* methods cannot be used to determine a global potential that includes the reaction channels because of the size of the molecule. Thus, we formulate a surface by making use of available experimental data for the equilibrium reactant and product molecules and by using *ab initio* results when experimental data are not available.

In our study of the unimolecular reaction dynamics of RDX (see Chapter VIII), we computed the rates for the ring fission reaction that gives 3 H_2CNNO_2 molecules and the simple N-N bond rupture reaction giving the radicals NO_2 and $C_2H_4N_4O_4$, and the product energy distributions, over the energy range 200-450 kcal/mol. These reaction channels were proposed by Zhao, Hintsa and Lee.[114] They used infrared multiphoton dissociation (IRMPD) in a molecular beam to study RDX.

Their results indicate that the ratio of the rate of the molecular elimination reaction to that of the N-N bond rupture reaction is about 2 at a total energy estimated to be in the range 150-170 kcal/mol. That is, they found that the two channels are competitive.

In our study of reactions of RDX, we used potential-energy surfaces for which the barrier to N-N fission is 47.8 kcal/mol (the reaction endothermicity) and barrier heights of 37, 56, and 71 kcal/mol for the ring fission reaction (most of the calculations were done for the 71 and 37 kcal/mol barriers). The calculated branching ratios are in qualitative agreement with the molecular beam results of Zhao *et al.*[114] The calculations are for energies in excess of those in the experiments and thus it is necessary to extrapolate the computed values to lower energies for the comparison. Comparison with experiment suggests that the PES are qualitatively correct.

In the present study we have extended what we have learned about cyclic nitramines, by constructing a potential-energy surface for HMX based on some of the parameters used for RDX. We find that using experimental values for the geometry of HMX and well depths and force constants used for RDX, vibrational frequencies are close to experimental values.

Brill and coworkers[117,193] have studied the surface region of energetic materials (RDX and HMX) heated by a T-jump method. They analyzed the product gases as functions of time by FTIR.

Adams and Shaw[119,194] have recently reviewed this subject. Although there

currently is not as much data for gas-phase HMX as there is for RDX, there is now enough experimental data with which to make comparisons and thus provide guidance for the development of models for realistic simulations of HMX.

Potential-Energy Surface

The dissociation of HMX into its final products is believed to involve several reaction pathways. The primary pathways being simple NN bond rupture and concerted ring fission. Following the initial dissociation, the products further decompose.

We have constructed an anharmonic PES that includes the two reaction pathways, NN bond rupture and concerted ring fission. The surface was constructed by using available experimental[195,196] and theoretical[185,187] data (when no information was available, RDX values were utilized). The surface has a barrier of 47.8 kcal/mol for the N-N bond fission reaction.

The PES is based on anharmonic stretches (Morse functions), harmonic bends, and truncated cosine series for torsions. Not only does this simplify the dynamics for the analysis, but it has been shown with a series of studies[9-23] that this simple form of potentials suffices to realistically describe important aspects of IVR. The analytical form, based on a valence force field, is that of Eq. 8. It is the sum of Morse functions for the 28 bonds, harmonic oscillators for the 48 angles and 4 wags, and six-term cosine series for 16 torsional angles.

The geometry of the reactant, α-HMX, was that obtained by Cady *et al.*,[195] and

is given in Table XVIII along with the geometry of CH_2NNO_2.[185] The bond energies used in this study have been suggested elsewhere.[10b,113,184] For both the reactants[10b,113,184] and products[113,184] (CH_2NNO_2) we used the same well depths and force constants as we did in the RDX PES (see Table XIX).

This somewhat crudely constructed PES (simply using the identical parameters used in the RDX PES) produces vibrational frequencies in reasonable agreement with experimental values[196] (see Table XX). Since *ab initio* assignments of the normal modes were not available for HMX, as they were for RDX, the eigenvectors were not considered in the potential-energy surface fitting. Although, for the most part, HMX eigenvectors are very similar to RDX eigenvectors when comparing the correspond eigenvalues in the same frequency range.

The forms of the switching functions used to connect the reactant and product wells are the same as those used in the RDX PES (Eqs. 22 and 23). The parameters used are those which were used for the RDX PES with a barrier of 37 kcal/mol to concerted ring fission. The attenuation of the parameters (bonds, angles, force constants, and well depths) is the same as that listed in Table XI for RDX.

Power spectra were calculated by Fourier transforming[127,128] ensemble-averaged autocorrelation functions of internal coordinates. Composite spectra were calculated by summing the individual internal coordinate spectra.

Calculations

Our general classical trajectory code GenDyn[124] was used to calculate the

trajectories. Hamilton's equations of motion were integrated by using a fourth-order Runge-Kutta-Gill routine in a space-fixed Cartesian coordinate system. The integration step size used was 1.0×10^{-16}s and the trajectories were calculated for 50 ps (40 trajectories of 10 ps lengths were calculated for the power spectral calculations). Initial conditions for the trajectories were selected by Monte Carlo quasiclassical and classical microcanonical methods; in the former, the energy is projected onto the normal modes[120] and in the latter, classical initial conditions were generated by using a metropolis procedure developed by Nordholm and coworkers.[125,126] The total angular momentum is zero in all of the calculations.

Trajectories were calculated on all three surfaces over the energy range 350-500 kcal/mol. Unimolecular dissociation rate coefficients were calculated for the two reactions. The branching ratio of ring fission to NN bond rupture was calculated as a function of energy.

The first order rate coefficients, k, for the overall decay of HMX were computed by fitting the lifetimes to Eq. 29, where N_t is the number of unreacted molecules at time t and N_o is the number of trajectories in the ensemble. Since the molecule decays by two competing reactions,

$$\text{HMX} \begin{cases} \nearrow\ 4\ H_2C{=}N{-}NO_2 & k\ (\text{ring}) \quad (R3) \\ \searrow\ C_3H_6N_3O_4 + NO_2 & k\ (\text{NN}) \quad (R4) \end{cases}$$

The rate coefficients for the two channels are obtained from Eqs. 30 and 31, where k (ring) and k (NN) are the rates of reactions R3 and R4, repectively, N (ring) and N (NN) are the numbers of trajectories which led to reactions R3 and R4, respectively. The branching ratio of concerted ring fission to N-N bond rupture is given by Eq. 32.

Results and Discussion

The rate coefficients and branching ratios were calculated over the energy range 350-500 kcal/mol. These results are summarized in Table XXI. We can estimate values for the frequency factor, A, and the effective degrees of freedom, s, based on the RDX study with identical potential parameters (scaling E, based on the energies per mode in the two molecules) and obtain an estimate for E_o. Multiplying the frequency factors and effective degrees of freedom by 4/3 (since RDX consists of $3CH_2NNO_2$ and HMX consists of $4CH_2NNO_2$) gives approximations for these parameters. For the NN reaction channel, R4, (for which we know the value of E_o) we obtain approximations of 2964.0 ps^{-1} and 48.0 for the frequency factor and the effective degrees of freedom, respectively. For the concerted ring fission, reaction channel R3, (for which the value of E_o is not known) the frequency factor and effective degrees of freedom are approximately 497.3 ps^{-1} and 53.3, respectively. Table XXII contains values of E_o calculated using Eq. 34 for both reaction channels at all energies studied.

The value of the NN dissociation energy is known to be 47.8 kcal/mol; the

estimated values of E_o (Table XXII) are in good agreement. In fact, the largest deviation is only 3.3 kcal/mol. It seems reasonable, then, that the values E_o for the concerted ring fission channel provide a good approximation for the barrier to concerted ring fission for this potential-energy surface. The values obtained for E_o for the NN reaction channel show that the parameters A and s from Eq. 34 can be estimated for the cyclic nitramines based on similar potential-energy surfaces.

Figure 31 contains a power spectrum of HMX at its zero-point energy (for a PES with the switching functions removed). Note that it, not surprisingly, is very similar with respect to the lineshapes to a spectrum of RDX at its zero-point energy.

Conclusion

Classical trajectories have been used to study the rates of dissociation of octahydro-1,3,5,7-tetranitro-1,3,5,7-tetrazocine (HMX) in the gas-phase. Realistic models of HMX and the products of the ring fission, CH_2NNO_2, are used to study reaction of the two primary dissociation pathways. We used parameters from the RDX PES with a barrier to concerted ring fission of 71 kcal/mol and find reasonable agreement with experimental frequencies.[196] Additionally, a power spectrum of HMX at its zero-point energy has been presented; its spectral lineshapes are similar to a RDX spectrum calculated at its zero-point energy.

Since branching ratio data are not available for HMX, we can only present the branching ratios, but no statement can be made concerning their accuracy. However, approximating the frequency factors and effective degrees of freedom based on the

RDX potential-energy surface with the same potential parameters (and switching function parameters) allows for an estimation of the NN bond strength and the barrier to concerted ring fission. The values obtained for the barrier to simple NN bond rupture are in very close agreement with the well depth used for the NN bonds. If the analogous calculation for the concerted ring fission is as accurate as the NN bond strength calculation, then the barrier (to concerted ring fission) is 50.4 kcal/mol.

Table XVIII. Equilibrium Geometries of HMX and CH_2NNO_2

	HMX[a]	CH_2NNO_2	
bonds (Å)		this study	*ab initio*[b]
CN	1.463	1.271	1.271
NN	1.364	1.441	1.441
NO	1.217	1.213	1.240, 1.303[c]
CH	1.100	1.089	1.073, 1.071[c]
angles (deg)			
CNC	123.1	***	***
NCN	111.9	***	***
CNN	118.45	115.7	115.7
NNO	116.9	117.25	114.5, 121.1[c]
ONO	126.2	125.5	124.4
NCH	109.2	120.05	124.1, 116.0[c]
HCH	107.9	120.0	120.0
NCN-N	0.0	***	***
CNCN	85.4	***	***
CNNO	0.0	***	***

[a] Cady *et al.*, Ref. 195.
[b] R.C. Mowrey *et al.*, Ref. 185.
[c] Two bonds or angles reflect differences between similar coordinates.

Table XIX. Potential Parameters of HMX and CH_2NNO_2

Morse Parameters:

	HMX		$CH_2N_2O_2$	
bond	D_e (kcal/mol)	α (Å^{-1})	D_e (kcal/mol)	α (Å^{-1})
r_{CN}	85.0[a]	1.954422	153.07[c]	1.734451
r_{NN}	47.8[a]	2.651632	30.60[a]	2.675695
r_{NO}	98.0[b]	1.951689	98.0	2.576902
r_{CH}	95.0[a]	1.941979	108.0	1.861508

Harmonic Force Constants:

	k_θ, (kcal/mol rad^2)	
angle	HMX	$CH_2N_2O_2$
θ_{CNC}	189.593228	* * *
θ_{NCN}	145.334935	* * *
θ_{CNN}	231.652616	357.118978
θ_{NNO}	241.113503	319.754009
θ_{ONO}	205.484711	245.08904
θ_{NCH}	58.274924	63.025996
θ_{HCH}	56.180756	52.472672
γ_{CNC-N}	95.001720	0.0

Cosine Series Coefficients [kcal/(mol rad ^{2})]:

dihedral angle	a_0	a_1	a_2	a_3	a_4	a_5
τ_{CNCN}[d]	0.515363	-0.289059	0.241886	0.039059	-0.257249	0.0
τ_{CNNO}	1.3125	-0.1875	-1.5	0.09375	0.1875	0.09375

[a] C.F. Melius and J.S. Binkley, Ref. 187.

[b] B.G. Sumpter and D.L. Thompson, Ref. 10b.

[c] T.D. Sewell and D.L. Thompson, Ref. 113.

[d] Coefficients for the τ_{NCNC} six-term cosine series potential are the same as those used to represent the τ_{CNCN} potential.

Table XX. HMX Normal Mode Frequencies[a]

Calc.	Expt.[b]	Calc.	Expt.[b]	Calc.	Expt.[b]
16		563		1144	1258
32		578		1231(2)	1280
52		589	594	1247	1318
56(2)		653	620	1265	1368
61		664	646	1269	1385
63		693(2)		1334(2)	1391
64(2)		703	712	1347	1412
130		704	740	1456(2)	1422
149(2)		711	750	1459	1448
173		744(2)	758	1470	1502
224	200	848(2)	846	1608	1524
239	233	875	878	1625(2)	1539
260(2)		920	893	1628	1561
271		921(2)	928	2985	2967
352		998	945	2986(2)	2975
378(2)	375	1006	995	2987	
402	400	1019		3056	3047
445	450	1038(2)	1030	3059(2)	
495(2)		1091(2)	1085	3063	3053
551(2)		1124	1215		

[a] Units are cm^{-1}. The normal mode frequencies were obtained by diagonalization of the Cartesian force constant matrix.

[b] F. Goetz and T.B. Brill, Ref. 196.

Table XXI. Reaction Rates and Branching Ratios for HMX

Energy (kcal/mol)	k_{ring}	k_{NN}	Branching Ratio
350	0.00336	0.09244	0.036
400	0.01319	0.21365	0.062
450	0.04445	0.34270	0.130
500	0.04809	0.55940	0.086

Table XXII. Estimated E_o for NN Bond Rupture and Concerted Ring Fission

Energy (kcal/mol)	E_o [kcal/mol] (NN)	E_o [kcal/mol] (concerted ring fission)
350	47.6	51.9
400	48.2	50.3
450	50.2	47.4
500	51.1	51.9

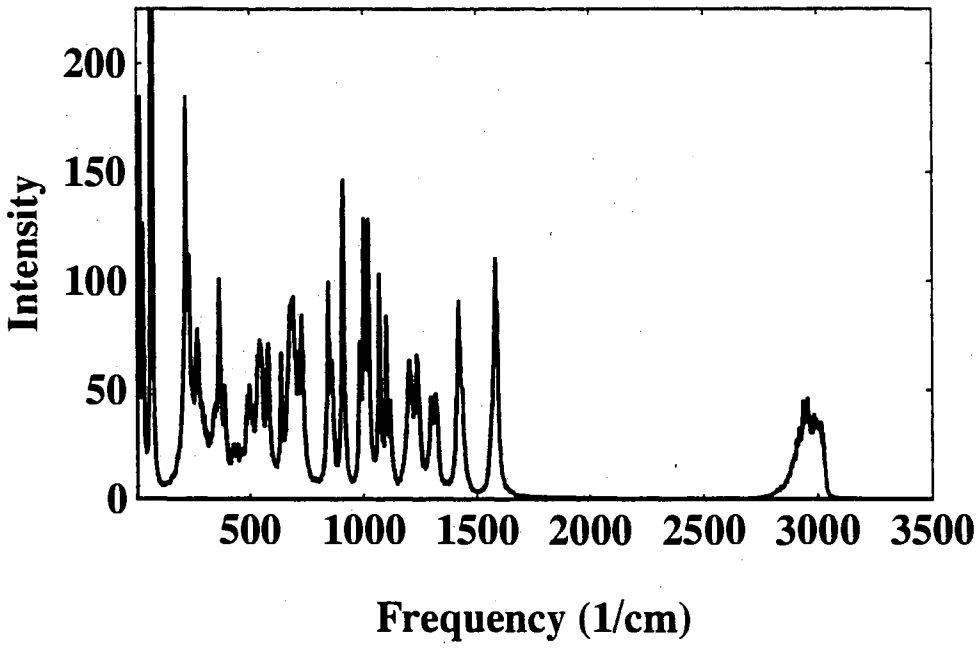

Figure 31. Composite power spectrum of HMX calculated at its zero-point energy.

CHAPTER X

CONCLUSIONS AND PROJECTIONS

Enhancement of Mode Mixing due to Barrier Crossings

We have investigated the effects of repeated crossings of a potential energy barrier on power spectra of classical trajectories. We examined the causes to broadening and shifting of peaks in the power spectra of HONO, CH_3ONO, and RDX. Time-delay maps were also used to study the extent of phase space exploration in methyl nitrite.

The results show that broadening of power spectral bandshapes increases with an increase in the number of passages through the transition state, thus, an enhancement of vibrational mode mixing. We have illustrated this effect in two systems which undergo *cis-trans* conversion and one which undergoes chair-boat conversion. An analogous system in which it would be of interest to confirm this effect is a system which undergoes molecular inversion.

The results presented in these studies show that there is a relationship between power spectral line widths and the number of times a molecule passes through a transition state between two conformations. Although, it should be noted that these results do not definitively illustrate that the sampling of multiple sets of normal modes *leads* to an enhanced rate of IVR. Other dynamical factors related to isomerization (although we have precluded a number of factors, such as time spent in the barrier region, there may be others factors which our study has not precluded)

may lead to the broadening of the power spectral lines as well. This point certainly warrants further study.

The various causes of changes in power spectra has been investigated by the careful construction of special ensembles which illustrate various types of dynamical behavior. This method could be extended to other studies. Many dynamics calculations consist of studying a molecule by more than one method (for instance, different set of initial conditions), comparing the results of the studies, and then formulating an explanation (or further studies) for the difference in the results based on, say different initial conditions. The construction of "special ensembles" or "sub-ensembles" from a large ensemble of trajectories which were initiated in the same manner allows for a more definitive study.

Extraction of Rates of Reaction from Spectra

Classical trajectories have been used to study the rates of isomerization of methyl nitrite. Two different methods were used in the calculation of the rates (lifetime plots and power spectral broadening). The results showed qualitative agreement of the rates calculated by the two methods.

The biggest improvement on this study would be to be able to calculate IR spectra from an FFT of the dipole moments and to quantitatively relate broadening of these spectral peak widths to rates of isomerization from lifetime plots. Furthermore, it would be ideal if experimental data were available for comparison. A good model for such a study would be 1,2 dichloroethane. Cohen and Weiss[91]

have reported IR spectra of 1,2 dichloroethane and calculated rates of isomerization based on the spectral peak widths. Unfortunately, data on the dipole moments of 1,2 dichloroethane are not available at this time to allow for an accurate theoretical modeling of the IR spectrum.

Classical Simulations of Unimolecular Reactions in Cyclic Nitramines

We have studied the rates of dissociation of hexahydro-1,3,5-trinitro-1,3,5-triazine (RDX) and octahydro-1,3,5,7-tetranitro-1,3,5,7-tetrazocine (HMX) in the gas-phase using classical trajectories. The branching ratios produced from the RDX PES (with a barrier to concerted ring fission of 37 kcal/mol) are in reasonable agreement with experiment.[114] Other studies,[175] indicate that the barrier to concerted ring fission is twice that value. We have constructed a potential-energy surface with a barrier of 71 kcal/mol to concerted ring fission, and find that we cannot reconcile the resulting branching ratios with experiment.[114] These calculations indicate that the barrier to concerted ring fission cannot be as high as 70 kcal/mol and produce a branching ratio of 2:1 (k_{ring}:k_{NN}) with the energy inserted randomly.

The power spectral calculations, on the other hand, indicate that dramatically different dynamics can be produced by potential-energy surfaces which have similar barriers to concerted ring fission. If studies continue to support a higher barrier to concerted ring fission, perhaps switching functions which begin to attenuate at lower reactions coordinates would produce a surface with a barrier around 70 kcal/mol, and yet branching ratios similar to those of the lower barriers which have been presented

here and elsewhere.[113]

Beyond this, a further step which would enhance the understanding of RDX and its dissociation, would be the inclusion of the secondary reactions. The thermodynamics of RDX→$3CH_2NNO_2$→3[HONO+HCN] would first need to be reconciled, as discussed in Chapter VIII.

References

1. R.H. Abraham and C. D. Shaw, *Dynamics: The Geometry of Behavior* (Addison-Wesley, New York, 1992).
2. R.D. Levine and R.B. Bernstein, *Molecular Reaction Dynamics and Chemical Reactivity* (Oxford, New York, 1987).
3. J.C. Lorquet and V.B. Pavlov-Verevkin, J. Chem. Phys. **93**, 520 (1990).
4. K.D. Hänsel, J. Chem. Phys. **70**, 1830 (1979).
5. J.P. Pique, M. Joyeux, J. Manners, and G. Sitja, J. Chem. Phys. **95**, 8744 (1991).
6. K.D. Hänsel, Chem. Phys. **33**, 35 (1978).
7. S.C. Farantos and J.N. Murrell, Chem. Phys. **55**, 205 (1981).
8. J. Tennyson and S.C. Farantos, Chem. Phys. **93**, 237 (1985).
9. X. Chang, D.L. Thomspon, and L.M. Raff, Chem. Phys. Lett. **206**, 137 (1993).
10. (a) B.G. Sumpter and D.L. Thompson, J. Chem. Phys. **82**, 4557 (1985); (b) *Ibid.*, **86**, 3301 (1987); (c) *Ibid.*, **87**, 5809 (1987).
11. (a) K.L. Bintz, D.L. Thompson, and J.W. Brady, J. Chem. Phys. **85**, 1848 (1986); (b) *Ibid.*, 86, 4411 (1987); (c) *Ibid.,* Chem. Phys. Lett. **131**, 398 (1986).
12. K.L. Bintz and D.L. Thompson, J. Chem. Phys. **85**, 1848 (1986); Chem. Phys. Lett. **131**, 398 (1986); J. Chem. Phys. **86**, 4411 (1987).
13. K.L. Bintz and D.L. Thompson, Chem. Phys. Lett. **187**, 166 (1991).
14. Y. Guan, G.C. Lynch, and D.L. Thompson, J. Chem. Phys. **87**, 6957 (1987).
15. Y. Guan and D.L. Thompson, J. Chem. Phys. **88**, 2355 (1988); *Ibid.*, Chem.

Phys. **92**, 313 (1990).

16. Y. Guan and D.L. Thompson, Chem. Phys. **139**, 147 (1989).

17. T. Uzer, B.D. MacDonald, Y. Guan, and D.L. Thompson, Chem. Phys. Lett. **152**, 405 (1988).

18. T. Uzer, B.D. MacDonald, Y. Guan, and D.L. Thompson in *Advances in Molecular Vibrations and Collision Dynamics,* Vol. 1B, ed. J.M. Bowman and M. Ratner (JAI Press, Greenwich, Connecticut, 1991), p. 81.

19. H. Gai, D.L. Thompson, and G.A. Fisk, J. Chem. Phys. **90**, 7055 (1989).

20. H. Gai and D.L. Thompson, Chem. Phys. Lett. **168**, 119 (1990).

21. H.W. Schranz, L.M. Raff, and D.L. Thompson, J. Chem. Phys. **95**, 106 (1991).

22. Y. Qin and D.L. Thompson, **96**, 1992 (1992).

23. A. Preiskorn and D.L. Thompson, J. Chem. Phys. **91**, 2299 (1989).

24. T.D. Sewell, H.W. Schranz, L.M. Raff, and D.L. Thompson, J. Chem. Phys. **95**, 8089 (1991).

25. T.D. Sewell, D.L. Thompson, and R.D. Levine, J. Phys. Chem. **96**, 8006 (1992).

26. T.D. Sewell, C.C. Chambers, D.L. Thompson, and R.D. Levine, Chem. Phys. Lett. **208**, 125 (1993).

27. C.C. Chambers and D.L. Thompson, Chem. Phys. Lett. **218**, 166 (1994).

28. H.W. Schranz, L.M. Raff, and D.L. Thompson, J. Chem. Phys. **94**, 4219 (1991).

29. L.M. Raff, J. Chem. Phys. **95**, 8901 (1991).

30. L.M. Raff, J. Chem. Phys. **97**, 7459 (1992).

31. L.M. Raff, J. Chem. Phys. **93**, 3160 (1990).

32. L.M. Raff, J. Chem. Phys. **90**, 6313 (1989).

33. L.M. Raff, J. Chem. Phys. **89**, 5680 (1988).

34. M.B. Ford, A.D. Foxworthy, G.J. Mains, and L.M. Raff, J. Phys. Chem. **97**, 12134 (1993).

35. T. Uzer and W.H. Miller, Phys. Rep. **199**, 73 (1991).

36. M.A. Sepúlveda, R. Badii, and E. Pollak, Phys. Rev. Lett. **63**, 1226 (1989).

37. B. Eckhardt, J.M.G Llorente and E. Pollak, Chem. Phys. Lett. **174**, 325 (1990).

38. A. Stuchebruckhov, S. Ionov, and V. Letokhov, J. Phys. Chem. **93**, 5357 (1989).

39. E.L. Sibert III, W.P. Reinhardt, and J.T. Hynes, J. Chem. Phys. **81**, 1115 (1984).

40. E.L. Sibert III, W.P. Reinhardt, and J.T. Hynes, J. Chem. Phys. **81**, 1135 (1984).

41. R.J. Wolf and W.L. Hase **73**, 3779 (1980).

42. D.H. Lu and W.L. Hase, J. Chem. Phys. **89**, 6723 (1988).

43. D.H. Lu and W.L. Hase, J. Phys. Chem. **92**, 3217 (1988).

44. D.H. Lu and W.L. Hase, Chem. Phys. Lett. **142**, 187 (1987).

45. P.J. Nagy and W.L. Hase, Chem. Phys. Lett. **54**, 73 (1978).

46. V. Buch, R.B. Gerber, and M.A. Ratner, J. Chem. Phys. **81**, 3393 (1984).

47. S. Shi and W.H. Miller, Theo. Chim. Acta **68**, 1 (1985).

48. D.L. Clarke and M.A. Collins, J. Chem. Phys. **86**, 6871 (1987).

49. A. Garcia-Ayllon, J. Santamaria, and G. S. Ezra, J. Chem. Phys. **89**, 801 (1988).

50. K.V. Reddy, D.F. Heller, and M.J. Berry, J. Chem. Phys. **76**, 2814 (1982).

51. J.M.G. Llorente, O. Hahn, and H.S. Taylor, J. Chem. Phys. **92**, 2762 (1990).

52. I.W.M. Smith in *Molecular Energy Transfer*, edited by R.D. Levine and J. Jortner (Wiley, New York, 1976).

53. N. De Leon and B.J. Berne, J. Chem. Phys. **77**, 283 (1982).

54. H.O. Pritchard, J. Phys. Chem. **89**, 3970 (1985).

55. H.L. Kim, T.J. Kulp, and J.D. McDonald, J. Chem. Phys. **87**, 4376 (1987).

56. I. Hamilton, D. Carter, and P. Brumer, J. Phys. Chem. **86**, 1224 (1982).

57. R.A. Marcus in *Energy Storage and Redistribution in Molecules*, edited by J. Hinze (Plenum Press, New York, 1983).

58. D.W. Noid, M.L. Koszykowski, and R.A. Marcus, Ann. Rev. Phys. Chem. **32**, 267 (1981).

59. K.F. Freed and A. Nitzaan, J. Chem. Phys. **73**, 4765 (1980).

60. K.W. Sandusky, J.B. Page, and K.E. Schmidt, Phys. Rev. B **46**, 6161 (1992).

61. W.J. Bullock, D.K. Adams, and W.D. Lawrance, J. Chem. Phys. **93**, 3085 (1990).

62. E.R. Davidson, H.J. Elston, and C.S. Parmenter, Chem. Phys. Lett. **197**, 123 (1992).

63. R.S. Berry, J. Chem. Phys. **78**, 3976 (1983).

64. C.C. Martens and W.P. Reinhardt, J. Chem. Phys. **93**, 5621 (1990).

65. R.Naaman, D.M. Lubman, and R.N. Zare in *Spectroscopy in Chemistry and Physics: Modern Trends* edited by F.J. Comes, A. Müller, and W.J. Orville-Thomas (Elsevier, New York, 1980).

66. A.A. Kosterev, A.L. Malinovsky, and E.A. Ryabov, Chem. Phys. Lett. **199**, 349 (1992).

67. J. Manz and C.S. Parmenter, Chem. Phys. **139**, 1 (1987).

68. F. Remacle and R.D. Levine, J. Chem. Phys. **98**, 2144 (1993).

69. F. Remacle and R.D. Levine, J. Phys. Chem. **95**, 7124 (1991).

70. T.A. Holme and R.D. Levine, J. Phys. Chem. **89**, 3379 (1988).

71. T.A. Holme and R.D. Levine, Chem. Phys. **131**, 169 (1989).

72. J.C. Lorquet, Y.M. Engel, and R.D. Levine, Chem. Phys. Lett. **175**, 461 (1990).

73. W.P. Reinhardt, J. Phys. Chem. **86**, 2158 (1982).

74. P. Brumer and J.W. Duff, J. Phys. Chem. **65**, 3566 (1976).

75. J.W. Duff and P. Brumer, J. Phys. Chem. **67**, 4898 (1977).

76. J.S. Hutchinson and R.E. Wyatt, J. Chem. Phys. **70**, 3509 (1979).

77. C. Cerjan and W.P. Reinhardt, J. Chem. Phys. **71**, 1819 (1979).

78. R.B. Shirts and W.P. Reinhardt, J. Chem. Phys. **77**, 5204 (1982).

79. C. Jaffé and P. Brumer, J. Phys. Chem. **88**, 4829 (1984).

80. I. Hamilton, D. Carter, and P. Brumer, J. Phys. Chem. **86**, 42124 (1982).

81. K.S. Seshadri and R. Jones, Spectrochimica Acta **19** 1013 (1963).

82. M. Eigen, Angew, Chem. Int. Ed. Eng. **3**, 1 (1964).

83. M. Eigen, W. Kruse, G. Maassm and L. De Maeyer, Prog. React. Kinetics **2**, 285 (1964).

84. K.A. Wood and H.L. Strauss, J. Phys. Chem. **94**, 5677 (1990).

85. M.M. Kreevoy and C.A. Mead, J. Am. Chem. Soc. **84**, 4596 (1962).

86. M.M. Kreevoy and C.A. Mead, Discuss. Faraday Soc. **39**, 166 (1965).

87. J.M. Williams and M. Kreevoy, J. Am. Chem. Soc. **89**, 5499 (1967).

88. J. Husar and M.M. Kreevoy, J. Am. Chem. Soc. **94**, 2902 (1972).

89. B. Cohen and S. Weiss, J. Chem. Phys. **72**, 6804 (1980).

90. B. Cohen and S. Weiss, J. Chem. Phys. **74**, 3635 (1981).

91 B. Cohen and S. Weiss, J. Phys. Chem. **87**, 3606 (1983).

92. B. Cohen and S. Weiss, J. Phys. Chem. **88**, 3159 (1984).

93. B. Cohen and S. Weiss, J. Phys. Chem. **88**, 3974 (1984).

94. B. Cohen and S. Weiss, J. Phys. Chem. **90**, 6275 (1986).

95. S. Weiss, Mol. Phys. **76**, 669 (1992).

96. T.S. Jones, S. Holloway, and J.W. Gadzuk, Surf. Sci. **184**, L421 (1987).

97. R.B. Cundall, Prog. React. Kinetics **2**, 165 (1964).

98. S. Mizushima, Pure Appl. Chem. **7**, 1 (1963).

99. S. Mixushima, *Structure of Molecules and Internal Rotation* (Academic, New York, 1954).

100. C.E. Dykstra, Ann. Rev. Phys. Chem. **32**, 25 (1981).

101. W.J. Orville-Thomas, *Internal Rotation in Molecules* (Wiley, New York, 1974).

102. N. De Leon and B.J. Berne, J. Chem. Phys. **75**, 3495 (1981).

103. B.J. Berne, N. De Leon, and R.O. Rosenberg, J. Phys. Chem. **86**, 2166 (1982).

104. N. De Leon, M.A. Mehta, and R.Q. Topper, J. Chem. Phys. **94**, 8310 (1991).

105. N. De Leon, M.A. Mehta, and R.Q. Topper, J. Chem. Phys. **94**, 8329 (1991).

106. C.C. Marston and N. De Leon, J. Chem. Phys. **91**, 3392 (1989).

107. N. De Leon and C.C. Marston, J. Chem. Phys. **91**, 3405 (1989).

108. S.K. Gray and S.A. Rice, J. Chem. Phys. **86**, 2020 (1987).

109. M. Zhao and S.A. Rice, J. Chem. Phys. **97**, 943 (1992).

110. M.J. Davis and S.K. Gray, J. Chem. Phys. **84**, 5389 (1986).

111. E.B. Wilson, Jr., J.C. Decius, and P.C. Cross *Molecular Vibrations* (Dover, New York, 1955).

112. J.E. Anderson, in *Topics in Current Chemistry: Dynamic Chemistry*, edited by F. Boschke (Springer, New York, 1974).

113. T.D. Sewell and D.L. Thompson, J. Phys. Chem. **95**, 6228 (1991).

114. X. Zhao, E.J. Hintsa, and Y.T. Lee, J. Chem. Phys. **88**, 801 (1988).

115. C.A. Wight and T.R. Botcher, J. Am. Chem. Soc. **114**, 8303 (1992); *Ibid.*, J. Phys. Chem. **97**, 9149 (1993).

116. R. Behrens, Jr. and S. Bulusu, J. Phys. Chem. **96**, 8877 (1992); *ibid.* **96**, 8891 (1992).

117. Y. Oyumi, T.B. Brill, A.L. Rheingold, and T.M. Haller, J. Phys. Chem. **89**, 4317 (1985); D.V. Mesaros, Y. Oyumi, T.B. Brill, and C. Dybowski, J. Phys. Chem. **90**, 1970 (1986); Y. Oyumi and T.B. Brill, J. Phys. Chem. **91**, 3657

(1987).

118. A.P. Snyder, J.H. Kremer, S.A. Liebman, M.A. Schroeder, and R.A. Fifer, Org. Mass. Spectrom. **24**, 15 (1984); A.P. Snyder, S.A. Liebman, M.A. Schroeder, and R.A. Fifer, *ibid.* **25**, 15 (1990).

119. G.F. Adams and R.W. Shaw, Jr., Ann. Rev. Phys. Chem. **43**, 311 (1992).

120. L.M. Raff and D.L. Thompson in *Theory of Chemical Reaction Dynamics, Vol. 3* edited by M. Baer (CRC Press, Boca Raton, 1985).

121. R.N. Porter and L.M. Raff in *Dynamics of Molecular Collisions, Part B* edited by W.H. Miller (Plenum, New York, 1976).

122. J.I. Steinfeld, J.S. Francisco, and W.L. Hase, *Chemical Kinetics and Dynamics* (Prentice-Hall, New Jersey, 1989).

123. R.M. Benito and F.J. Aoiz in *Computational Chemistry: Structure, Interactions, and Reactivity* edited by S. Fraga (Elsevier Science, New York, 1992).

124. For a description of the original version of the GenDyn code, see: K.L. Bintz, M.S. Thesis, Oklahoma State University (1986).

125. H.W. Schranz, S. Nordholm, and G. Nyman, J. Chem. Phys. **94**, 1487 (1991).

126. G. Nyman, S. Nordholm, and H.W. Schranz, J. Chem. Phys. **93**, 6767 (1990).

127. R.G. Gordon, Adv. Magn. Reson. **3**, 1 (1968).

128. J.S. Bendat and A.G. Piersol, *Engineering Applications of Correlation and Spectral Analysis* (Wiley, New York, 1980).

129. P.H. Berens, J.P. Bergsma, and K.R. Wilson in *Time-Resolved Vibrational Spectroscopy* edited by G.H. Atkinson (Academic, New York, 1983).

130. D.W. Noid, M.L. Kozykowski, and R.A. Marcus in *Quantum Mechanics in Mathematics, Chemistry, and Physics* edited by K.E. Gustafson and W.P. Reinhardt (Plenum Publishing Corporation, 1981).

131. D.W. Noid, M.L. Kozykowski, and R.A. Marcus, J. Chem. Phys. **67**, 404 (1977).

132. R.S. Dumont and P. Brumer, J. Chem. Phys. **88**, 1481 (1988).

133. R.W. Field, O.B. d'Azy, M. Lavollée, R. Lopez-Delgado, and A. Tramer, J. Chem. Phys. **78**, 2838 (1983).

134. I. Schek, J. Jortner, and M. Sage, Chem. Phys. Lett. **64**, 209 (1979).

135. M. Eidelsberg, F. Rostas, J. Breton, and B. Thieblemont, J. Chem. Phys. **96**, 5585 (1992).

136. J.M. Watson, I. Noorbatcha, and R.R. Lucchese, J. Chem. Phys. **96**, 7771 (1992).

137. G.E. Powell and I.C. Percival, J. Phys. A **12**, 2053 (1979).

138. S.C. Farantos and J.N. Murrell, Chem. Phys. **55**, 205 (1981).

139. D. Carter and P. Brumer, J. Chem. Phys. **77**, 4208 (1982).

140. P.H. Berens and K.R. Wilson, J. Chem. Phys. **74**, 4872 (1981).

141. P.H. Berens, S.R. White, and K.R. Wilson, J. Chem. Phys. **75**, 515 (1981).

142. S.M. Llorente, J. Zakrzewski, H.S. Taylor, and K.C. Kulander, J. Chem. Phys. **90**, 1505 (1989).

143. R.S. Smith and R.B. Shirts, J. Chem. Phys. **89**, 2948 (1988).

144. R. Roy, B.G. Sumpter, G.A. Pfeffer, S.K. Gray, and D.W. Noid, Phys. Rep.

205, 109 (1991).

145. J. Crutchfield, R.J. Donnelly, D. Farmer, G. Jones, N. Packard, and R. Shaw, Phys. Lett. **76A**, 1 (1980).

146. J.C. Tully, Y.J. Chabal, K. Raghavachari, J.M. Bowman, and R.R. Lucchese, Phys. Rev. B, **31**, 1184 (1985).

147. X.Y. Chang, T.D. Sewell, L.M. Raff, and D.L. Thompson, J. Chem. Phys. **97**, 7354 (1992).

148. E.J. Heller, E.B. Stechel, and M.J. Daivs, J. Chem. Phys. **71**, 4759 (1979).

149. E.J. Heller, Physica D **7**, 356 (1983).

150. S.C. Farantos, J. Chem. Phys. **85**, 641 (1986).

151. S.C. Farantos, J.M.G. Llorente, O. Hahn, and H.S. Taylor, Int. J. Quant. Chem. **24**, 429 (1990).

152. N.H. Packard, J.P. Crutchfield, J.D. Farmer, and R.S. Shaw, Phys. Rev. Lett. **45**, 712 (1980).

153. J.A. Vastano and R.D. Moser, J. Fluid Mech. **233**, 83 (1991).

154. P. Cray and S.K. Scott, *Chemical Oscillations and Instabilities* (Clarendon, Oxford, 1990).

155. Y.S. Cho, P.R. Winter, H.H. Harris, E.E. Fleischmann, and J.E. Adams, J. Phys. Chem. **94**, 1847 (1990).

156. I. Ohime and H. Tanaka, J. Chem. Phys. **93**, 8138 (1990).

157. C. Zuhrt. L. Zülicke, F. Schneider, and X. Chapuisat, Laser Chem. **11**, 199 (1991).

158. J.T. Hougen and J.K.G. Watson, Can. J. Phys. **43**, 298 (1965).

159. E.J. Heller, J. Chem. Phys. **92**, 1718 (1990).

160. P.H. Turner, M.J. Corkill, and A.P. Cox, J. Phys. Chem. **83**, 1473 (1979).

161. P.N. Ghosh and H.H. Günthard, Spectrochimica Acta **37A**, 1055 (1981).

162. J.A. Darsey and D.L Thompson, Chem. Phys. Lett. **145**, 523 (1988).

163. W.D. Gwinn, R.J. Anderson, and D. Stelman, Bull. Am. Phys. Soc. **13**, 831 (1968).

164. J. Murto, M. Rasanen, A. Aspiala, and T. Lotta, J. Mol. Struct. **122**, 213 (1985).

165. O.E. Rössler, Z. Naturforsch. **31a**, 259 (1976).

166. See, for example, R.A. Schmitz, K.R. Graziani, and J.L. Hudson, J. Chem. Phys. **67**, 3040 (1977); D. Barkley, *ibid.* **89**, 5547 (1988); P. Ibison and S.K. Scott, J. Chem. Soc. Faraday Trans. **86**, 3695 (1990).

167. N.B. Slater, *Theory of Unimolecular Reactions* (Cornell, New York, 1959).

168. I. Ohmine, H. Tanaka, and P.G. Wolynes, J. Chem. Phys. **89**, 5852 (1988).

169. R.A. MacPhail and H.L. Strauss, J. Chem. Phys. **82**, 1156 (1985).

170. R.J. Sension and H.L. Strauss, J. Chem. Phys. **86**, 6665 (1987).

171. J.E. Anderson, in *Topics in Current Chemistry, Dynamic Chemistry*, edited by F. Boschke (Springer, New York, 1974).

172. E.P. Wallis and D.L. Thompson, Chem. Phys. Lett. **189**, 363 (1992).

173. Z. Iqbal, K. Suryananrayanan, S. Bulusu, and J.R. Autera, Army Technical Report 4401 (1972).

174. J.M. Coffin, S.Q. Newton, J.D. Ewbank, L. Schäfer, C.V. Alsenoy, and K. Siam, J. Molec. Struct. **251**, 219 (1991).

175. D. Habibollahzadeh, M. Grodzicki, J.M. Seminario, and P. Politzer, J. Phys. Chem. **95**, 7699 (1991).

176. D. Cremer and J.A. Pople J. Am. Chem. Soc. **97**, 1354 (1975).

177. E.P. Wallis and D.L. Thompson, J. Chem. Phys. **99**, 2661 (1993).

178. H.R. Dübal and M. Quack, Chem. Phys. Lett. **72**, 342 (1980).

179. B.N.J. Persson, J. Phys. Chem. **17**, 4741 (1984).

180. M. Hutchinson and T.F. George, Chem. Phys. Lett. **124**, 211 (1986).

181. Y. Li, M. Honigmann, G. Hirsch, and R.J. Buenker, Chem. Phys. Lett. **212**, 185 (1993).

182. (a) R.J. Duchovic, W.L. Hase, and H. Schlegel, J. Phys. Chem. **88**, 1339 (1984); (b) S.W. Cho, W.L. Hase, and K.N. Swamy, J. Phys. Chem. **94**, 7371 (1990); (c) S.R.V. Linde and W.L. Hase, J. Phys. Chem. **94**, 2778 (1990); (d) W.J. Lemon and W.L. Hase, J. Phys. Chem. **91**, 1596 (1987); (e) W.L. Hase, G. Mrowka, R.J. Brudzynski, and C.S. Sloane, J. Chem. Phys. **69**, 3548 (1978); (f) S.C. Tucker and D.G. Truhlar, J. Am. Chem. Soc. **112**, 3338 (1990).

183. S. Carter, I.M. Mills, and J.N. Murrell, Mol. Phys. **39**, 455 (1980); P.M. Agrawal, D.L. Thompson, and L.M. Raff, J. Chem. Phys. **92**, 1069 (1990).

184. C.F. Melius and J.S. Binkley, Twenty-first Symposium (International) on Combustion 1953 (1986).

185. R.C. Mowrey, M. Page, G.F. Adams and B.H. Lengsfield III, J. Chem. Phys.

93, 1857 (1990).

186. I.F. Shishkov, L.V. Vilkov, M. Kolonits and B. Rozsondai, Struct. Chem. **2**, 57 (1990).

187. B.M. Rice, C.F. Chabalowski, G.F. Adams, R.C. Mowrey, and M. Page, Chem. Phys. Lett. **184**, 335 (1991).

188. B.M. Rice, G.F. Adams, M. Page, and D.L. Thompson, in preparation.

189. R.A. Beyer and C.U. Morgan, Sixteenth JANNAF Combustion Meeting Proceedings 51 (1979).

190. J.N. Murrell, S. Carter, L.O. Halonen, J. Mol. Spectrosc. **93**, 307 (1982).

191. C.S. Choi and E. Prince, Acta Crystallogr. **B28**, 2857 (1972).

192. Yu.M. Burov and G.M. Nazin, Kinet. Kata **23**, 12 (1982); Yu.Ya. Maksimov, V.N. Apal'kova, O.V. Braverman, and A.I. Solov'ev, Zh. Fiz. Khim. **59**, 342 (1985).

193. Y. Oyumi, T.B. Brill, and A.L. Rheingold, J. Chem. Phys. **90**, 2526 (1986); Y. Oyumi and T.B. Brill, Conbust. and Flame **62**, 213 (1985).

194. R. Shaw and F.E. Walker, J. Phys. Chem. **81**, 2572 (1977).

195. H.H. Cady, A.C. Larson, and D.T. Cromer, Acta Cryst. **16**, 617 (1963).

196. F. Goetz and T.B. Brill, J. Phys. Chem. **83**, 340 (1979).

VITA

Candee Cae Chambers

Candidate for the Degree of

Doctor of Philosophy

Thesis: DYNAMICS OF POLYATOMIC MOLECULES
I. ENHANCEMENT OF VIBRATIONAL MODE MIXING DUE TO INTRAMOLECULAR CONVERSIONS II. CHEMICAL REACTIONS IN CYCLIC NITRAMINES

Major Field: Chemistry

Biographical:

Personal Data: Born in Fort Bragg, North Carolina, On August 10, 1968, the daughter of John A. and Wilma K. Chambers.

Education: Graduated from University High School, Normal, Illinois in May 1986; received Bachelor of Arts degree in Chemistry and Mathematics from Illinois College, Jacksonville, Illinois in May, 1990; completed requirements for Doctor of Philosophy Degree at Oklahoma State University in July, 1994.

Professional Experience: Teaching Assistant, Department of Chemistry, Oklahoma State University, August 1990 to May 1991 and August 1991 to December 1991; Graduate Research Assistant, Oklahoma State University, June 1990 to August 1990, May 1991 to August 1991, and January 1992 to July 1994.

Professional Memberships: Phi Lambda Upsilon (honorary chemical society), American Chemical Society, American Institute of Chemists.